Univerza v Ljubljani

Fakulteta za elektrotehniko

Matej Kranjc

Določanje porazdelitve električnega polja med elektroporacijo z magnetnoresonančno električnoimpedančno tomografijo

DOKTORSKA DISERTACIJA

Mentor: prof. dr. Damijan Miklavčič

Ljubljana, 2012

University of Ljubljana

Faculty of Electrical Engineering

Matej Kranjc

Feasibility of magnetic resonance electrical impedance tomography for monitoring electric field distribution during electroporation

DOCTORAL DISSERTATION

Mentor: prof. Damijan Miklavčič, Ph. D.

(University of Ljubljana, Slovenia)

Ljubljana, 2012

PREFACE

The present PhD thesis is a result of numerical modelling, algorithm development, phantoms and *ex vivo* research carried out during the PhD study period at the Laboratory of Biocybernetics, Faculty of Electrical Engineering, University of Ljubljana. The results of the performed work have been published (or are in press) in the following international journals:

Article 1: MAGNETIC RESONANCE ELECTRICAL IMPEDANCE TOMOGRAPHY FOR MONITORING ELECTRIC FIELD DISTRIBUTION DURING TISSUE ELECTROPORATION
KRANJC Matej, BAJD Franci, SERŠA Igor, MIKLAVČIČ Damijan
IEEE Transactions on Medical Imaging 30: 1771-1778, 2011.

Article 2: *EX VIVO* AND *IN SILICO* FEASIBILITY STUDY OF MONITORING ELECTRIC FIELD DISTRIBUTION IN TISSUE DURING ELECTROPORATION BASED TREATMENTS
KRANJC Matej, BAJD Franci, SERŠA Igor, WOO Eung Je, MIKLAVČIČ Damijan
PLoS ONE 7(9): e45737, 2012.

Article 3: ASSESSING HOW ELECTROPORATION AFFECTS THE EFFECTIVE CONDUCTIVITY TENSOR OF BIOLOGICAL TISSUES
MEZEME Melvin Essone, **KRANJC Matej**, BAJD Franci, SERŠA Igor, BROSSEAU Christian, MIKLAVČIČ Damijan
Applied Physics Letters: in press.

TABLE OF CONTENTS

ABSTRACT

Electroporation is a phenomenon caused by externally applied electric field of an adequate strength and duration to cells that results in increase of cell membrane permeability to various molecules which otherwise are deprived of transmembrane transport mechanism. Cells can be exposed to an electric field by applying electric pulses by electric pulse generator using electrodes. When electric parameters (number, shape, duration, repetition frequency of electric pulses and direction of electric field), electrodes geometry and electrode positions are appropriately chosen and consequently cells are exposed to adequate electric field, transient structural changes can be attained and the cell membrane reseals afterwards. Electroporation can thus be used to introduce various molecules into cells or to kill cells by using reversible or irreversible electroporation, respectively.

There are many clinical applications such as electrochemotherapy and non-thermal irreversible electroporation where electroporation was already successfully introduced. Electrochemotherapy and non-thermal irreversible electroporation are both potent procedures used in solid tumor treatment. Non-thermal irreversible electroporation is also promising ablation method for nonmalignant tissues. Both, electrochemotherapy and non-thermal irreversible electroporation rely on cell membrane electroporation. Electrochemotherapy combines electroporation with the use of chemotherapeutic drugs which exhibit higher cytotoxicity when they are combined. Electrochemotherapy has been successfully used for treatment of cutaneous and subcutaneous metastasis of various cancers achieving over 70 % complete responses on over 3000 treated patients in Europe since 2006. In non-thermal irreversible electroporation the extensive membrane electroporation alone leads to a loss of cell homeostasis and finally to cell death. Recently, electrochemotherapy and non-thermal irreversible electroporation have been also used in treatment of deep-seated tumors. In order to ensure adequate electric field coverage of the treated tissue, treatment planning using numerical modeling was introduced. It needs to be noted that cell membrane conductivity and consequently cell/tissue conductivity are increased after electroporation in a nonlinear way.

Unfortunately, this nonlinear tissue conductivity increase due to electroporation along with uncertainty of tissue conductivity determination makes treatment plan inaccurate and thus inherently unreliable. Another factor influencing success of the electroporation treatment is inaccuracy in electrode positioning with respect to the target tissue. It is therefore important to find efficient means of electroporation process monitoring on site.

Various methods of monitoring electroporation process were already suggested, particularly of irreversible electroporation where immediate changes of tissue properties can be detected. Main disadvantages of these methods are the incapability to monitor electroporation process during pulse delivery or that they are limited in observing solely irreversible electroporation. As the membrane electroporation is a consequence of an induced transmembrane potential which is directly proportional to the local electric field, we propose current density imaging and magnetic resonance electrical impedance tomography techniques to determine the electric field distribution during electroporation. Current density imaging is a magnetic resonance imaging method for acquiring current density distribution inside conductive samples by measuring magnetic field changes caused by applied current. Whereas tissue conductivity can be obtained by magnetic resonance electrical impedance tomography (MREIT), a technique used for reconstruction of electrical conductivity inside a tissue by means of current density As the measurement of current density and electrical conductivity is performed during electric pulse delivery determined electric field distribution takes into account all changes which occur in tissue due to electroporation.

Electroporation is used for therapeutic purposes and electric pulses can reach up to 3000 V and they can establish electric field distribution with strength up to 150 kVm^{-1} depending on electrodes geometry and distance between them. As current density imaging and magnetic resonance electrical impedance tomography have been developed for diagnostic purpose and there is a lack of reports where electric pulses that are normally used in electroporation applications would be used we demonstrated that both, current density imaging and magnetic resonance electrical impedance tomography, can be applied for obtaining electric field with such high field strength.

Determination of electric field distribution during tissue electroporation was demonstrated both experimentally and numerically on homogeneous and heterogeneous agar phantom with electrical properties similar to human tumor and surrounding tissue. A good agreement between experimental and numerical results was obtained for different pulse sequences, i.e. for different number and amplitude of pulses.

| ABSTRACT

Determination of electric field distribution during tissue electroporation was also successfully demonstrated on *ex vivo* chicken liver tissue, suggesting that current density imaging and magnetic resonance electrical impedance tomography can be used to determine the electric field during electric pulse delivery. Furthermore, experimental and numerical investigation on the anisotropy ratio of *ex vivo* tissue was also performed. Alteration of anisotropy ratio of the conductivity tensor was detected when reversible electroporation threshold was exceeded. Experimental results agreed with numerical and were also consistent with experimental investigations performed by other research groups.

A concern whether proposed method for determination of electric field distribution can be implemented in electroporation applications was addressed by a simulation in the case of a 3-D numerical model designed for the purpose of an electrochemotherapy treatment of deep-seated liver tumors. We demonstrated that it is possible to obtain sufficiently accurate information on electric field distribution in the targeted and surrounding tissue by measuring only one component of magnetic flux density and thus enable detection of areas with insufficient electric field coverage before the end of the treatment, thus increasing and assuring treatment effectiveness by implementing corrective steps.

As there is a lack of tissue specific experimental data on tissue properties for reliable numerical treatment planning and a great need for *in situ* determination of electric field distribution during electroporation pulse delivery, magnetic resonance electrical impedance tomography together with current density imaging could be of significant help in monitoring of future electroporation based applications. Before that, however, limited capability of magnetic resonance imaging scanners for their use in interventional procedures and frequency limitation of CDI algorithms need to be overcomed.

RAZŠIRJEN POVZETEK V SLOVENSKEM JEZIKU

UVOD

Če celico ali tkivo izpostavimo električnemu polju ustrezne jakosti in trajanja, pride do povečanja prepustnosti celične membrane. Večina teoretičnih študij predvideva, da je ta fenomen, imenovan elektroporacija (oziroma tudi elektropermeabilizacija), posledica strukturnih sprememb v obliki nastanka hidrofilnih por v celični membrani (Neumann *et al.*, 1989; Weaver in Chizmadzhev, 1996; Neu in Krassowska, 1999). Povečana prepustnost celične membrane omogoča vstop v celico različnim snovem, ki jih membrana v fizioloških pogojih ne prepušča (Neumann *et al.*, 1982; Orlowski *et al.*, 1988; Tsong, 1991; Serša *et al.*, 1995; Mir in Orlowski, 1999). Celico ali tkivo lahko izpostavimo električnemu polju tako, da preko elektrod dovedemo električne pulze. Ob ustrezni obliki in razporeditvi elektrod ter pravilni izbiri parametrov električnih pulzov (število, oblika, trajanje, ponavljalna frekvenca in smer) lahko dosežemo začasne strukturne spremembe celične membrane. Po prenehanju delovanja električnega polja se torej membrana povrne v prvotno stanje. Temu pojavu pravimo reverzibilna elektroporacija, saj celica ohrani zmožnost nadaljnjega obstoja (Neumann *et al.*, 1982; Zimmermann, 1982) – v nasprotju z ireverzibilno elektroporacijo, ki zaradi vzpostavitve premočnega električnega polja, ki celici onemogoči vzpostavitev prvotnega stanja, vodi v celično smrt. (Davalos *et al.*, 2005). Ustrezna izpostavljenost celice z dovolj močnim električnim poljem predstavlja enega izmed najpomembnejših pogojev za uspešno izvedbo elektroporacije (Miklavčič *et al.*, 1998; Miklavčič, Čorović, *et al.*, 2006).

Uporaba elektroporacije za elektrokemoterapijo (Marty *et al.*, 2006; Serša in Miklavčič, 2008), gensko elektrotransfekcijo (Andre *et al.*, 2008; Daud *et al.*, 2008; Heller in Heller, 2010), DNK vakcinacijo (Zhang *et al.*, 2004) in atermično ablacijo tkiva z ireverzibilno elektroporacijo (Rubinsky *et al.*, 2008; Garcia *et al.*, 2011) se uspešno vključuje v klinično prakso. Med najbolj uveljavljenimi *in vivo* aplikacijami elektroporacije je elektrokemoterapija. Gre za relativno nov postopek zdravljenja raka, ki z izpostavitvijo tumorja električnemu polju omogoči povečan vnos kemoterapevtika v celice tumorja. Navzočnost kemoterapevtika in ustrezna porazdelitev

električnega polja sta odločilna za uspeh terapije (Miklavčič *et al.*, 1998; Miklavčič, Čorović, *et al.*, 2006; Miklavčič *et al.*, 2010). Ustrezno porazdelitev polja zagotovimo z uporabo elektrod s fiksno geometrijo ali pa z uporabo numeričnih modelov in optimizacijskimi postopki v sklopu procesa načrtovanja elektrokemoterapije, v katerem na podlagi lastnosti in oblike tumorja določimo ustrezno amplitudo električnih pulzov in razporeditev elektrod. Zaradi nezanesljivih vrednosti električne prevodnosti tumorjev (Muftuler *et al.*, 2006), ki lahko privedejo do napačnih izračunov amplitud pulzov in razporeditve elektrod, je uporaba procesa načrtovanja elektrokemoterapije trenutno omejena. Pri procesu zdravljenja globje ležečih tumorjev z elektrokemoterapijo se soočamo tudi s težavo doseganja natančnosti vstavljanja elektrod med terapijo po navodilih oziroma rezultatih procesa načrtovanja (Kos *et al.*, 2010). Nenatančna postavitev elektrod pa lahko povzroči pokritost tumorja z neustreznim električnim poljem, kar lahko privede do neuspešne izvedbe terapije. Nova metoda spremljanja poteka elektroporacije z opazovanjem porazdelitve električnega polja bi imela velik pomen tako za elektrokemoterapijo kot tudi za ostale aplikacije elektroporacije, še posebno, če bi se metoda spremljanja lahko izvajala *in situ* med terapijo. Pomemben vidik spremljanja poteka elektroporacije je tudi v možnosti prilagajanja parametrov glede na napredek procesa elektroporacije, saj so se do zdaj parametri *in vivo* elektroporacije določili po terapiji z *in vivo* preizkusi permeabilizacije (Gehl in Mir, 1999) in z računanjem porazdelitve električnega polja z uporabo matematičnih modelov (Miklavčič *et al.*, 2000; Pavšelj in Miklavčič, 2008).

Nekateri avtorji so za spremljanje elektroporacije predlagali naslednje metode: merjenje električne prevodnosti z električno impedančno tomografijo (Davalos *et al.*, 2000, 2002, 2004; Granot *et al.*, 2009), opazovanje območij nastalih zaradi ireverzibilne elektroporacije z ultrazvokom (Lee *et al.*, 2007), spremljanje električnega toka in napetosti dovedenih pulzov (Cukjati *et al.*, 2007) ter slikanje z magnetno resonanco (Hjouj in Rubinsky, 2010; Zhang *et al.*, 2010; Mahmood *et al.*, 2011). Čeprav so omenjene metode merjenja zanimive, ima vsaka od njih svoje pomanjkljivosti. Težave, povezane z uporabo električne impedančne tomografije za namen spremljanja elektroporacije, so enake težavam električne impedančne tomografije v splošnem: številne dodatne elektrode, nizka občutljivost, majhna prostorska ločljivost in natančnost, medtem ko je šum visok. Magnetnoresonančni pristopi so omejeni na spremljanje ireverzibilne elektroporacije z zaznavanjem celične smrti na podlagi primerjav magnetnoresonančnih slik pridobljenih pred in po dovajanju elektroporacijskih pulzov. Podobno omejitev ima tudi ultrazvok, ki ga lahko uporabimo samo pri aplikacijah ireverzibilne elektroporacije. Glavna pomanjkljivost že predlaganih metod je v nezmožnosti spremljanja procesa elektroporacije med samim dovajanjem pulzov. To sicer ne velja za metodo spremljanja električnega toka in

napetosti dovedenih pulzov, vendar je merjenje pri tej metodi omejeno na samo en par elektrod, kar lahko ob heterogenosti merjenega tkiva privede do napačne interpretacije rezultatov.

Za učinkovitejše spremljanje procesa elektroporacije smo želeli razviti novo metodo, ki bo omogočala spremljanje porazdelitve električnega polja med dovajanjem pulzov za namen zgodnjega odkritja neustreznosti le-tega še pred koncem terapije in na ta način zagotoviti in omogočiti izvedbo popravkov ter tako izboljšati njeno učinkovitost. Ker se porazdelitve električnega polja znotraj tkiva ne da izmeriti neposredno, smo poiskali posredno rešitev. Z uporabo Ohmovega zakona lahko električno polje v vzorcu izračunamo na podlagi električne prevodnosti vzorca in gostote električnega toka, ki se vzpostavi v vzorcu ob dovajanju električnih pulzov. Gostoto električnega toka znotraj vzorca lahko določimo z uporabo magnetnoresonančne tehnike slikanja gostote toka (Joy *et al.*, 1989; Scott *et al.*, 1991; Serša *et al.*, 1994; Gamba in Delpy, 1998). Ena izmed mnogih aplikacij slikanja gostote električnega toka pa je magnetnoresonančna električnoimpedančna tomografija (MREIT), ki jo uporabljamo za rekonstrukcijo električne prevodnosti vzorca na podlagi gostote električnega toka (Woo *et al.*, 1994; Eyüboğlu *et al.*, 2001; Kwon, Lee, *et al.*, 2002; Kwon, Woo, *et al.*, 2002; Oh *et al.*, 2003; Seo, Yoon, *et al.*, 2003). Tehniki slikanja gostote električnega toka in MREIT so razvili v diagnostične namene, torej dovedeni električni tokovi ne presegajo vrednosti nekaj miliamperov, kar na merjenemu tkivu ne pušča posledic. Zelo malo je objavljenih študij, kjer bi za slikanje gostote električnega toka uporabili napetostne pulze višjih vrednosti – kot na primer slikanje gostote električnega toka v tumorju miši s 160V napetostnimi pulzi (Serša *et al.*, 1997). Pri elektrokemoterapiji in atermični ablaciji tkiva z ireverzibilno elektroporacijo uporabljamo napetostne pulze, ki lahko glede na geometrijo elektrod dosegajo vrednosti do 3000 V pri toku 50 A. Pred objavo rezultatov, ki so predstavljeni v tej disertaciji, v literaturi ni bilo poročil, v katerih bi za slikanje gostote električnega toka uporabili tako visoke pulze.

Cilj disertacije je bil raziskati metodo slikanja gostote električnega toka in magnetnoresonančne električnoimpedančne tomografije pri kratkih napetostnih pulzih s podobnimi amplitudami in smermi kot pri aplikacijah elektroporacije in raziskati možnost uporabe obeh metod za namen določanja porazdelitve električnega toka med elektroporacijo tkiv.

METODE

Evalvacija uporabe metod slikanja gostote električnega toka in magnetnoresonančne električnoimpedančne tomografije je bila izvedena na fantomih iz agarja in na tkivu piščančjih jeter. Električne prevodnosti raztopin agarja so bile podobne prevodnostim tumorja in okoliških tkiv. Fantomi so bili vstavljeni v posebej za ta namen narejeno posodo iz akrilnega stekla v obliki

valja (slika I), ki smo jo vstavili v odprtino magneta. Pokrov posode je imel štiri luknjice za vstavitev igelnih elektrod, preko katerih smo dovedli zaporedje električnih pulzov.
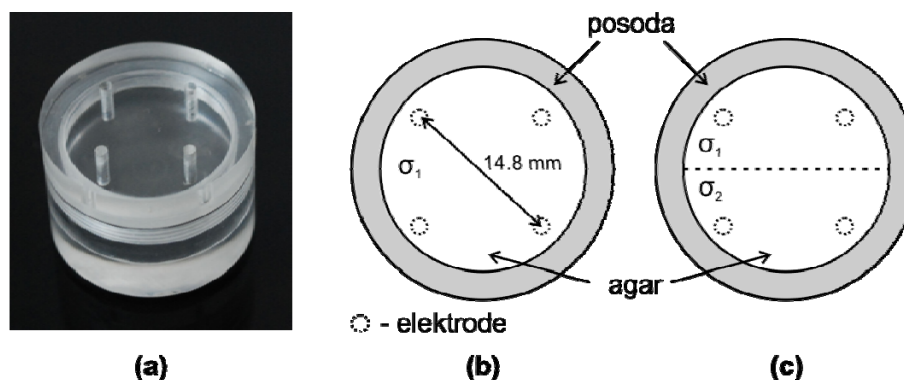
Slika I: Posoda, narejena iz akrilnega stekla, s štirimi luknjicami za elektrode (a). Fantomi s homogenimi (b) in heterogenimi (c) električnimi prevodnostmi so bili izdelani iz različnih raztopin agarja (σ_1 in σ_2).

Evalvacijo *ex vivo* opazovanja porazdelitve električnega polja smo izvedli na svežem tkivu piščančjih jeter. Jetra smo kupili v klavnici (Perutnina Ptuj, d. d., Ptuj, Slovenija), ki deluje v okviru slovenskih zakonov, proces zakola pa regulira Pravilnik za zaščito živali pri zakolu (Ur. l. RS, N. 5/2006). Temperatura jeter je bila do začetka poskusa vzdrževana na 4 °C. Tkivo smo razrezali na cilindrične kose in vstavili v isto posodo (slika Ia) kot pri evalvaciji z agarjem.

Fantome iz agarja in tkiva smo izpostavili posameznim zaporedjem električnih pulzov, ki jih uporabljamo pri aplikacijah elektroporacije. Električne pulze smo dovedli med diagonalnim parom skozi pokrov posode vstavljenih elektrod v zaporedjih, ki so sestavljena iz enega, dveh, štirih ali osmih 100 µs dolgih pulzov z amplitudami v območju od 1000 V do 3000 V v primeru fantomov iz agarja oziroma štirih 100 µs dolgih pulzov z amplitudami v območju od 1000 V do 1500 V v primeru tkiv. Za generiranje visokonapetostnih pulzov smo uporabili Cliniporator Vitae (IGEA, Carpi, Italija). Cliniporator Vitae je generator pulzov s šestimi neodvisnimi in električno izoliranimi izhodi, kjer je vsak izmed šestih izhodov zmožen generirati pravokotne napetostne pulze z amplitudo do 3000 V pri največjem električnem toku 50 A. Generator ima možnost merjenja izhodne napetosti s 3% natančnostjo. Štiri izmed šestih izhodov generatorja smo povezali s štirimi elektrodami, vstavljenimi v fantom. Dovedene pulze smo merili tudi z osciloskopom in tokovno sondo. Prožilni vhod generatorja smo povezali z magnetnoresonančno kontrolno enoto za sinhronizacijo s sekvenco pulzov tehnike slikanja gostote električnega toka.

Magnetnoresonančno slikanje gostote električnega toka smo izvedli s spektrometrom TecMag NMR, povezanim s horizontalnim superprevodnim magnetom Oxford 2.35 T na Institutu Jožef Stefan. Gostota električnega toka je bila v vseh fantomih slikana s *two-shot* slikovno sekvenco RARE - *Rapid Acquisition with Relaxation Enhancement* (hitro slikanje s poudarkom relaksacije) (Serša, 2008). Sekvenca je sestavljena iz dveh delov, tokovno kodiranega dela in slikovnega dela (Hennig *et al.*, 1986). Tokovno gostoto v fantomu smo izračunali z Amperovim zakonom

$$\mathbf{J} = \frac{1}{\mu_0} \nabla \times \mathbf{B} \qquad \text{(En. I)}$$

iz tokovno vzbujenih faznih zamikov φ, shranjenih v dobljeni magnetnoresonančni sliki

$$\varphi = \gamma T_c B_z, \qquad \text{(En. II)}$$

kjer je γ giromagnetno razmerje protona in T_c skupno trajanje dovedenih napetostnih pulzov. Zaradi geometrije fantoma smo pričakovali, da bo električni tok tekel pretežno v smeri pravokotno na elektrode. Gostota magnetnega pretoka je zato imela v središčni rezini komponento v smeri pravokotno na slikovno rezino – B_z različno od nič in zanemarljivo majhni komponenti v rezini (B_x, B_y). Pod temi pogoji smo lahko dobili gostoto električnega toka samo iz komponente, različne od nič, kar pomeni, da vzorca ni bilo treba obračati v vse tri pravokotne smeri, zato se enačba za izračun gostote električnega toka posploši na

$$\mathbf{J} = \frac{1}{\mu_0} \left(\frac{\partial B_z}{\partial y}, -\frac{\partial B_z}{\partial x}, 0 \right) \qquad \text{(En. III)}$$

Ali je ta posplošitev možna tudi v praktični uporabi elektroporacije, smo preverili z izračunom gostote električnega toka med elektroporacijo v tridimenzionalnem numeričnem modelu globoko ležečega tumorja v človeških jetrih, narejenega v procesu načrtovanja elektrokemoterapije (slika II), in sicer z uporabo samo ene komponente gostote magnetnega pretoka. Iz dobljenega toka smo nato izračunali še porazdelitev električnega polja z uporabo magnetnoresonačnega električnoimpedančnega algoritma, ki smo ga primerjali z dejansko porazdelitvijo električnega polja.
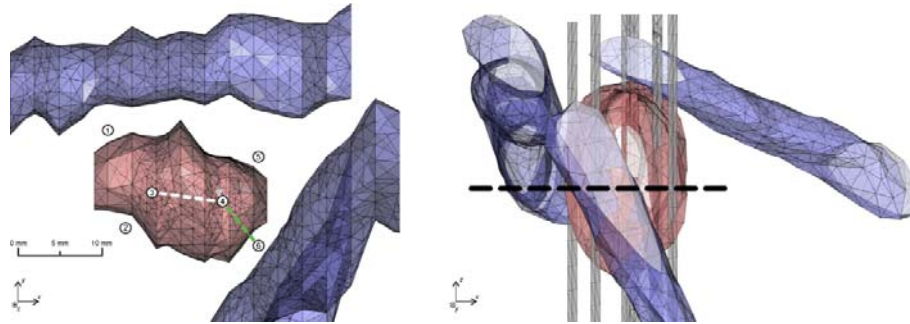
Slika II: Tridimenzionalen numerični model globoko ležega tumorja v človeških jetrih. Tumor (obarvan rdeče) je vmeščen med spodnjo veno kavo in srednjo hepatično veno (obarvani modro). Jetra niso prikazana zaradi lažje vizualizacije. Elektrode (obarvane sivo) so označene s številkami od 1 do 6. V xy ravnini na sredini tumorja (označena s črno črtkano črto) smo ovrednotili dve območji: območje tumorja (med elektrodama št. 3 in 4; označeno z belo črtkano črto) in območje, sestavljeno iz tumorja in jeter (med elektrodama št. 4 in 6; označeno z zeleno črtkano črto).

Rekonstrukcija porazdelitve električnega toka v fantomih iz agarja in tkiva ter v tridimenzionalnem numeričnem modelu globoko ležečega tumorja je temeljila na magnetnoresonačnih električnoimpedančnih algoritmih. Uporabili smo algoritem *J-substitution*, ki za izračun porazdelitve električne prevodnosti uporablja samo eno komponento gostote magnetnega pretoka (Seo, Yoon, *et al.*, 2003; Nam *et al.*, 2007; Park *et al.*, 2007). Algoritem *J-substitution* temelji na iterativnem reševanju Laplaceove enačbe

$$\nabla \cdot (\sigma^k \nabla u^k) = 0, \qquad \text{(En. IV)}$$

kjer je *u* porazdelitev električnega potenciala in *σ* porazdelitev električne prevodnosti, ki se z vsakim korakom iteracije (k + 1) poveča za

$$\sigma^{k+1} = \frac{|\mathbf{J}|}{|\nabla u^k|}, \qquad \text{(En. V)}$$

kjer je **J** gostota električnega toka, ki smo jo predhodno izmerili z metodo CDI.

Ko dobimo tako porazdelitev električne prevodnosti kot gostoto električnega toka **J**, lahko porazdelitev električnega polja **E** izračunamo po Ohmovem zakonu

$$\mathbf{E} = \frac{\mathbf{J}}{\sigma}. \qquad\qquad \text{(En. VI)}$$

Laplaceovo enačbo (En. IV) smo reševali z metodo končnih elementov, ki se je pri reševanju podobnih elektromagnetnih problemov že izkazala za zelo učinkovito (Miklavčič *et al.*, 2000; Pavšelj in Miklavčič, 2008). Z metodo končnih elementov parcialne diferencialne enačbe z določenimi robnimi in začetnimi pogoji znotraj kompleksnih struktur rešujemo tako, da model razdelimo na manjše sestavne dele – končne elemente, za katere predpostavimo, da lahko v njih iskane veličine opišemo s preprostimi funkcijami. Med prednostmi metode končnih elementov je zelo pomembno prilagajanje velikosti končnih elementov in s tem natančnosti rešitve na področjih, ki nas zanimajo. Računanje smo izvedli s programskim paketom, namenjenem reševanju problemov s končnimi elementi Comsol Multiphysics (Comsol AB, Stockholm, Švedska), v matematičnem okolju Matlab (Mathworks, Natick, ZDA), s pripadajočim dodatkom za reševanje parcialnih diferencialnih enačb.

REZULTATI

Rezultati našega dela kažejo, da magnetnoresonančno električnoimpedančno tomografijo lahko uporabimo za opazovanje porazdelitve električnega polja med elektroporacijo. V poskusih na fantomih iz agarja smo z uporabo tehnike slikanja gostote električnega toka uspešno izmerili porazdelitev gostote električnega toka in porazdelitev električnega polja z magnetnoresonančno električnoimpedančno tomografijo pri vseh uporabljenih napetostih in za različno število pulzov. Na sliki III so predstavljene z magnetnoresonančno električnoimpedančno tomografijo izmerjene porazdelitve električnega polja v homogenem agarju pri različnih napetostih štirih pulzov (1000, 1500 in 2000 V). Relativna napaka glede na numerični model je 6.4 % pri 1000 V, 7.1 % pri 1500 V in 8.0 % pri 2000 V.
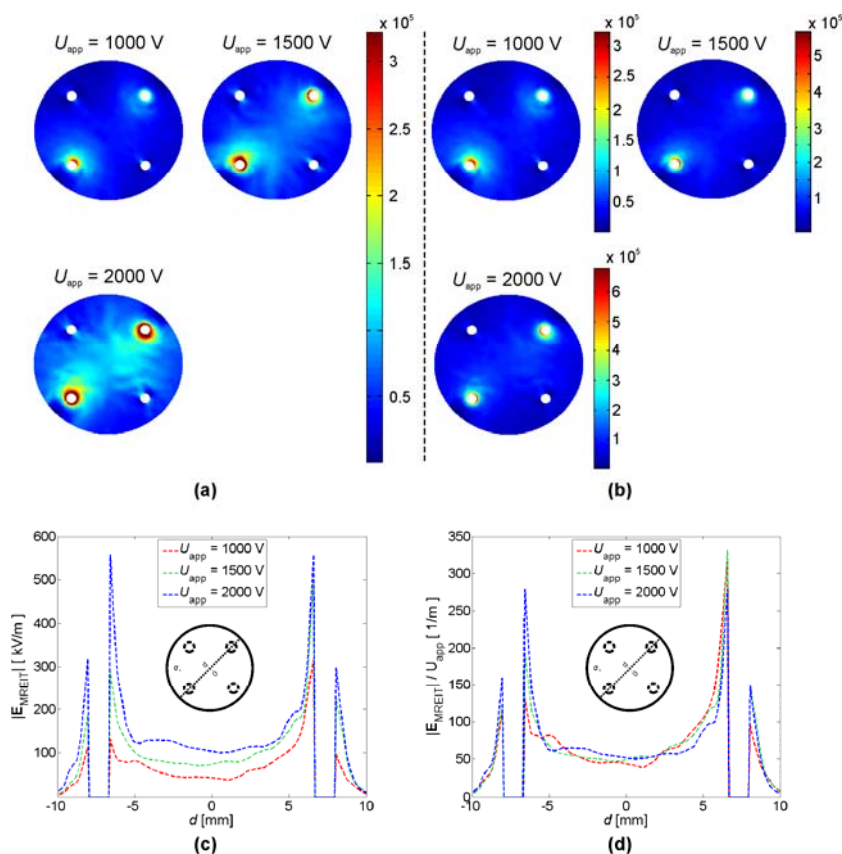
Slika III: Porazdelitev električnega polja (a, b) in potek električnega polja v diagonalni smeri (c) homogenega agarja, izpostavljenega različnim amplitudam pulzov. Vse tri porazdelitve polja v zgornjem levem delu slike (a) so prikazane na istem območju vrednosti polja, medtem ko imajo tri porazdelitve v zgornjem desnem delu slike (b) vsaka svoje območje vrednosti glede na svojo največjo in najmanjšo vrednost. Potek električnega polja v diagonalni smeri agarja je prikazan tudi v normalizirani obliki glede na amplitude pulzov (d).

Na sliki IV so predstavljene z magnetnoresonančno električnoimpedančno tomografijo izmerjene porazdelitve električnega polja v homogenem agarju, izpostavljenem različnemu številu napetostnih pulzov (1, 2, 4, 8).
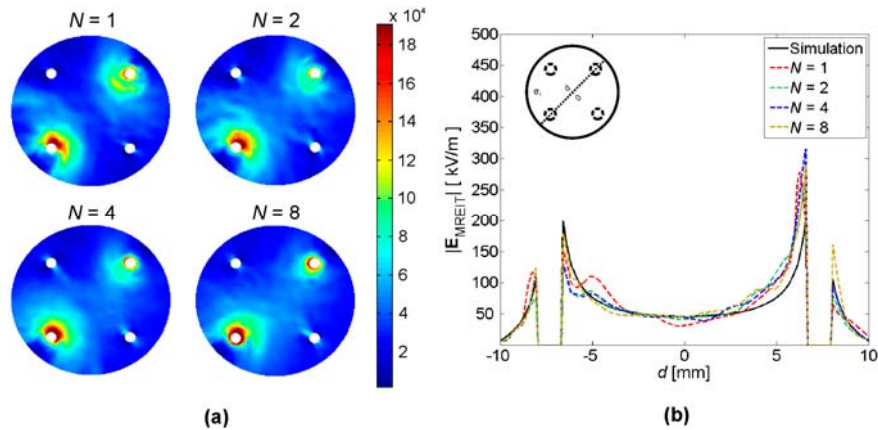
Slika IV: Porazdelitev električnega polja (a) in potek električnega polja v diagonalni smeri (b) homogenega agarja, izpostavljenega različnemu številu pulzov.

Primerjava poteka električnega polja, dobljenega z MREIT algoritmom, in poteka izračunanega polja iz numeričnega modela v diagonalni smeri heterogenega agarja je prikazana na sliki V. Največje neujemanje smo opazili v območju blizu elektrod, ki vnašajo motnje v magnetno polje in posledično povzročajo precejšnje artefakte na faznih slikah. To za spremljanje električnega polja med elektroporacijo ne predstavlja znatnih težav, ker se v splošnem območje, ki ga želimo izpostaviti željenemu električnemu polju, nahaja med elektrodama in tu je ujemanje dobro.
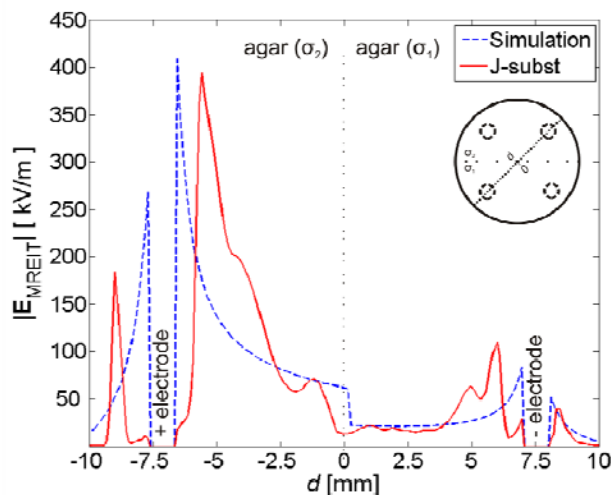
Slika V: Potek električnega polja, dobljenega z magnetnoresonančno električnoimpedančno tomografijo (označen s polno rdečo črto), in izračunanega polja iz numeričnega modela (označen s prekinjeno modro črto) v diagonalni smeri heterogenega agarja (označena s prekinjeno črno črto na zgornji desni sliki). Fantom je bil izpostavljen štirim pulzom z napetostjo 1000 V. Na osi x predstavlja d razdaljo od sredine proti robu fantoma.

Agar zaradi svoje strukture ne izkazuje odvisnosti med svojimi dielektričnimi lastnostmi in amplitudo dovedene napetosti. Naslednji niz poskusov merjenja električnega polja med elektroporacijo je zato potekal na piščančjih jetrih. Na sliki VI sta prikazana porazdelitev električne prevodnosti in vektorsko polje gostote električnega toka v piščančjih jetrih, izpostavljenih štirim 100 μs pulzom z amplitudami 1000 V in 1500 V. Pri napetosti 1000 V nismo opazili sprememb električne prevodnosti, razen ob robovih in neaktivnih elektrodah, kar je posledica motenj magnetnega polja in premajhnih vrednosti gostote električnega toka. Večje spremembe smo opazili pri napetosti 1500 V na območju med aktivnima elektrodama, kjer je tudi električno polje najmočnejše. Te spremembe električne prevodnosti so posledica lokalne elektroporacije tkiva oziroma dviga vzpostavljenega lokalnega električnega polja nad reverzibilni prag elektroporacije. Kot je razvidno iz slike vektorskega polja gostote električnega toka, je večji del električnega toka tekel ravno v območju, kjer je prišlo do elektroporacije oziroma povišanja električne prevodnosti. Do podobnih dognanj o spremembah prevodnosti v tkivu zaradi elektroporacije so prišli tudi v drugih študijah (Cukjati *et al.*, 2007; Ivorra *et al.*, 2009).
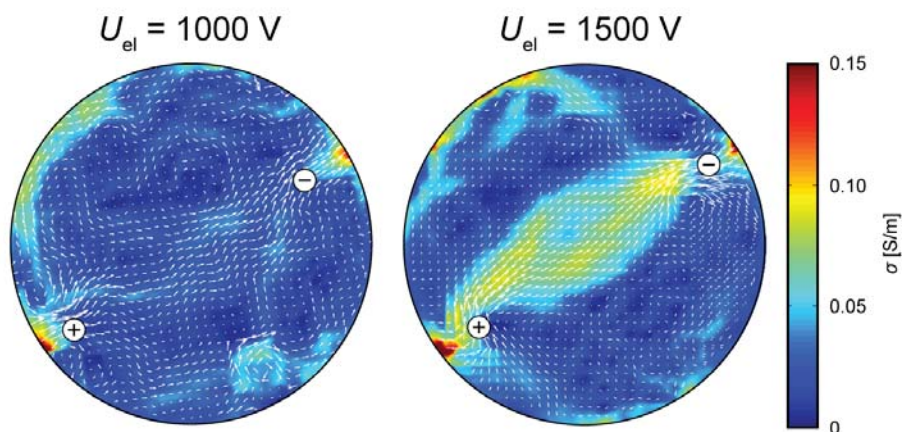
Slika VI: Porazdelitev električne prevodnosti in vektorsko polje gostote električnega toka (označeno z belimi puščicami) v piščančjih jetrih, izpostavljenih štirim 100 μs pulzom z amplitudam 1000 V (leva slika) in 1500 V (desna slika). Pulzi so bili dovedeni med diagonalnima elektrodama (označenima s + in –).

Rezultati ovrednotenja spremljanja porazdelitve električnega polja med aplikacijami elektroporacije, ki je bila izvedena na tridimenzionalnem numeričnem modelu globoko ležečega tumorja v človeških jetrih, narejenega v procesu načrtovanja elektrokemoterapije, so prikazani na sliki VII. Električno polje E$_{MREIT}$ smo izračunali na podlagi gostote električnega toka, ki je bila izračunana iz samo ene komponente gostote magnetnega pretoka po enačbi III. Kot je razvidno iz rezultatov, se električno polje tako v območju tumorja (slika VIIa) kot v območju sestavljenem iz tumorja in jeter (slika VIIb), dobro ujema z resničnim poljem E*.
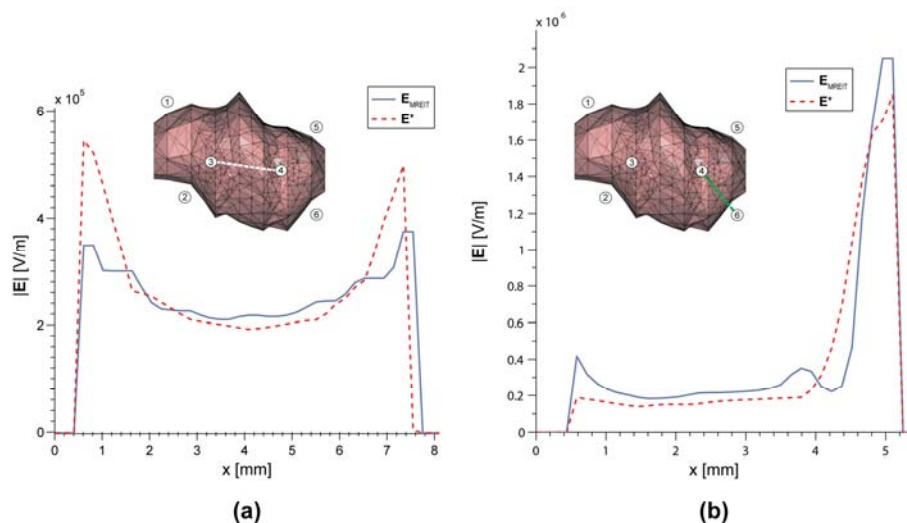
Slika VII: Električno polje v območju tumorja (a) in v območju, sestavljenem iz tumorja in jeter (b), izračunano na podlagi gostote električnega toka, ki je bila izračunana iz samo ene komponente gostote magnetnega pretoka (označeno s polno modro črto), in dejansko električno polje (označeno s prekinjeno rdečo črto). Med elektrodama 3 in 4 je bila vzpostavljena napetost 2100 V, medtem ko je bila med elektrodama 4 in 6 vzpostavljena napetost 1700 V.

ZAKLJUČKI

Glavni namen predstavljene disertacije je bil raziskati zmožnost uporabe magnetnoresonančne električnoimpedančne tomografije za opazovanje porazdelitve električnega polja med elektroporacijo. Eksperimentalno in numerično smo uspešno pokazali, da magnetnoresonančno električnoimpedančno tomografijo skupaj z metodo za slikanje gostote električnega toka lahko uporabimo za določitev porazdelitve električnega polja med dovajanjem elektroporacijskih pulzov.

Uporabo elektroporacije, kot sta na primer elektrokemoterapija in atermična ablacija z ireverzibilno elektroporacijo, lahko trenutno spremljamo ali z opazovanjem merljivih parametrov elektroporacijskih pulzov ali z izvedbo načrta zdravljenja pred samim postopkom aplikacij elektroporacije. Žal noben od omenjenih pristopov ne zagotavlja zanesljivega izida terapije. Ker je pokritost celic oziroma tkiva z ustreznim električnim poljem eden najpomembnejših pogojev za uspešno izvedbo elektroporacije, bi bila metoda za posredno merjenje porazdelitve električnega polja zelo pomembna za uspešnost terapij, ki temeljijo na

elektroporaciji. Predlagana metoda omogoča rekonstrukcijo porazdelitve električnega polja z uporabo osnovnega Ohmovega zakona in tehnik magnetne resonance: metode za merjenje gostote električnega toka in magnetnoresonančne električnoimpedančne tomografije.

Spremljanje porazdelitve električnega polja med elektroporacijo z uporabo metode za merjenje gostote električnega toka in magnetnoresonančne električnoimpedančne tomografije smo raziskali tako eksperimentalno kot numerično na homogenem in heterogenem fantomu iz agarja s podobnimi dielektričnimi lastnostmi kot v jetrih in tumorju. Sinhronizacija elektroporacijskih pulzov z metodo za slikanje gostote električnega toka nam je omogočila uspešno slikanje gostote električnega toka med elektroporacijo. Temu je sledil izračun porazdelitve električnega polja z uporabo električnoimpedančnega magnetnoresonačnega algoritma *J-substitution*, ki temelji samo na eni komponenti gostote magnetnega pretoka. Ker smo izmerili dobro ujemanje eksperimentalnih in numeričnih rezultatov, lahko sklepamo, da sta metoda merjenja gostote električnega toka in magnetnoresonančna električnoimpedančna tomografija uporabni za določanje porazdelitve električnega polja med dovajanjem elektroporacijskih pulzov. To smo tudi potrdili z eksperimentom na piščančjih jetrih, kjer smo zaznali spremembo električne prevodnosti tkiva kot posledico elektroporacije. Poleg tega smo na območjih, kjer je električno polje preseglo reverzibilni prag elektroporacije, zaznali spremembe anizotropnih lastnosti jeter.

Prav tako smo uspešno pokazali, da je predlagano metodo za spremljanje električnega polja možno uporabiti tudi med aplikacijami elektroporacije z izvedbo numerične simulacije na tridimenzionalnem numeričnem modelu globoko ležečega tumorja v človeških jetrih. Pokazali smo namreč, da lahko dovolj dobro izmerimo porazdelitev električnega polja v tumorju in okoliških tkivih z uporabo samo ene komponente gostote magnetnega pretoka. Tako bi lahko z uporabo predlagane metode določanja porazdelitve električnega polja detektirali nezadostne pokritosti električnega polja še pred koncem terapije in zagotovili večjo učinkovitost s korekcijo amplitude, števila ali trajanja pulzov ali z razmestitvijo elektrod. Pred implementacijo predlagane metode v aplikacije elektroporacije bo treba rešiti še nekaj težav, kot sta omejena zmožnost uporabe magnetnoresonačnih tomografov med intervencijskimi posegi in frekvenčna omejitev tehnike slikanja gostote električnega toka.

Zaradi pomanjkanja podatkov o dielektričnih lastnosti posameznih tkiv pri izvedbi zanesljivega načrta zdravljenja in neustreznih metod za opazovanje porazdelitve električnega polja med elektroporacijo bi lahko bila v bližnji prihodnosti magnetnoresonančna električnoimpedančna tomografija skupaj s tehniko za slikanje gostote električnega toka pomembna pridobitev za spremljanje poteka izvedbe elektroporacije in zagotavljanje njene učinkovitosti.

IZVIRNI PRISPEVKI K ZNANOSTI

RAZVOJ METODE ZA DOLOČITEV ELEKTRIČNEGA POLJA MED ELEKTROPORACIJO NA OSNOVI MAGNETNORESONANČNE ELEKTRIČNOIMPEDANČNE TOMOGRAFIJE

Ustrezna pokritost celice z dovolj močnim električnim poljem predstavlja enega izmed najpomembnejših pogojev za uspešno izvedbo elektroporacije. Pokazali smo, da magnetnoresonančno električnoimpedančno tomografijo skupaj z metodo za slikanje gostote električnega toka lahko uporabimo za določitev porazdelitve električnega polja. Spremljanje porazdelitve električnega polja med elektroporacijo smo raziskali tako eksperimentalno kot numerično na homogenem in heterogenem fantomu iz agarja s podobnimi dielektričnimi lastnostmi kot v jetrih in tumorju. Poleg tega smo porazdelitev električnega polja med elektroporacijo določili tudi na piščančjih jetrih.

OVREDNOTENJE METODE IN POTRDITEV OBSTOJA Z ELEKTROPORACIJO POVZROČENE ANIZOTROPIJE ELEKTRIČNE PREVODNOSTI V BIOLOŠKIH TKIVIH

Elektroporacija je terapevtska metoda, kjer se uporablja napetostne pulze z amplitudo do 3000 V, ki lahko vzpostavijo električna polja vrednosti do 150 kVm^{-1} glede na geometrijo in razdaljo med elektrodami. Ker sta bili tehniki slikanja gostote električnega toka in magnetnoresonančne električnoimpedančne tomografije razviti z namenom diagnosticiranja, je objavljenih zelo malo študij na temo uporabe obeh metod z napetostnimi pulzi, katerih vrednost je podobna tistim, ki se uporabljajo pri elektroporaciji. Na fantomu iz agarja in piščančjih jetrih smo pri različnih amplitudah in različnem številu električnih pulzov uspešno pokazali, da lahko tako metodo slikanja gostote električnega toka kot magnetnoresonančno električnoimpedančno tomografijo uporabimo za določitev porazdelitve električnega polja. Poleg tega smo na območjih, kjer je električno polje preseglo reverzibilni prag elektroporacije, zaznali spremembe anizotropnih lastnosti jeter.

Uspešno smo tudi pokazali, da je predlagano metodo za spremljanje električnega polja možno uporabiti tudi med aplikacijami elektroporacije z izvedbo numerične simulacije na tridimenzionalnem numeričnem modelu globoko ležečega tumorja v človeških jetrih.

INTRODUCTION

First reports on the effect of biological cell exposure to externally applied electric field date from almost six decades ago (Stämpfli, 1958; Hamilton and Sale, 1967; Sale and Hamilton, 1967, 1968; Neumann and Rosenheck, 1972; Zimmermann et al., 1974). Since then, most theoretical studies predict that this phenomenon, termed electroporation (sometimes also electropermeabilization), results in structural changes which occur in the membrane in the form of hydrophilic pores (Neumann et al., 1982, 1989; Weaver and Chizmadzhev, 1996; Neu and Krassowska, 1999), allowing various normally nonpermeant molecules to enter the cell by crossing the membrane (Neumann et al., 1982; Orlowski et al., 1988; Tsong, 1991; Serša et al., 1995; Mir and Orlowski, 1999; Kotnik et al., 2012). The cell or tissue can be exposed to an electric field by applying electric pulses by electric pulse generator via electrodes as shown in Figure 1. When electric parameters (number, shape, duration and repetition frequency of electric pulses, direction of electric field), electrodes geometry, and electrode positions are appropriately chosen and consequently the cell is exposed to adequate electric field, transient structural changes can be attained and the cell membrane reseals afterwards. This is termed reversible electroporation as cell preserves its viability (Neumann *et al.*, 1982; Zimmermann, 1982). On the contrary, irreversible electroporation leads to cell death as the applied electric field is too strong and the cell does not regain its integrity (Davalos *et al.*, 2005). An accurate coverage of the cell with sufficiently large electric field presents one of the most important conditions for successful electroporation (Miklavčič *et al.*, 1998; Miklavčič, Čorović, *et al.*, 2006).
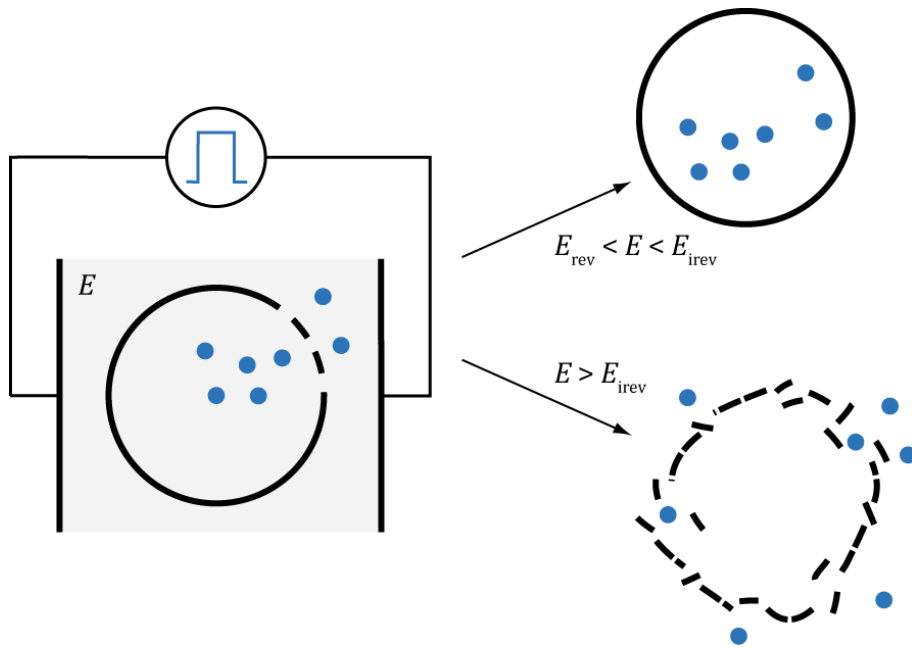
Figure 1: Reversible and irreversible cell electroporation. Reversible electroporation occurs when a cell is exposed to electric field between reversible E_{rev} and irreversible threshold E_{irev}, and molecules can enter the cell by crossing the membrane which reseals afterwards. On the contrary, irreversible electroporation occurs when applied electric field is too strong, i.e. above E_{irev}, and the cell does not regain its integrity.

Applications of electroporation such as electrochemotherapy (ECT) (Marty *et al.*, 2006; Serša and Miklavčič, 2008), electroporation based gene transfer for gene therapy (Andre *et al.*, 2008; Daud *et al.*, 2008; Heller and Heller, 2010), DNA vaccination (Zhang *et al.*, 2004) and non-thermal irreversible electroporation ablation (N-TIRE) (Rubinsky *et al.*, 2008; Garcia *et al.*, 2011) are being successfully introduced into clinical practice. Electrochemotherapy, a relatively new approach to cancer treatment and the most established *in vivo* application of electroporation, treats tumors by increasing the uptake of chemotherapeutic drugs into tumor cells by exposing it to the electric field. Presence of chemotherapeutic drug and adequate local electric field distribution are crucial for therapy's success (Miklavčič *et al.*, 1998; Miklavčič, Čorović, *et al.*, 2006; Miklavčič *et al.*, 2010). Electric field distribution is governed by electrode positioning and applied voltage at given pulse parameters, both obtained by treatment planning for electrochemotherapy, which already proved to have a great potential in clinical use (Miklavčič et al., 2010; Edhemović et al., 2011). Its applicability, however, is currently limited due to uncertain conductivity values of the treated tissue, especially within the tumor where

heterogeneous conductivity was already observed (Muftuler *et al.*, 2006), resulting in obtaining inappropriate electrodes position, electric pulse parameters and consequently insufficient electric field coverage of the tumor. Another concern is the electrode positioning during the electrochemotherapy treatment procedure. Namely, it is relatively difficult to insert electrodes precisely according to the treatment plan (Kos *et al.*, 2010). Imprecise placement of the electrodes and inaccurate conductivity values can thus result in an inadequate electric field coverage of the target area and hence treatment failure (Pavliha *et al.*, 2012).

A method that would allow determination of the electric field strength within tissue would thus be of great importance for electrochemotherapy as well as for other electroporation based applications. As the electric field distribution inside the observed tissue cannot be measured directly, an indirect approach of obtaining it needs to be evaluated. By means of Ohm's law, the electric field distribution can be determined when an electric current density and an electrical conductivity of the tissue are obtained. The electric current density inside a conductive tissue can be obtained by magnetic resonance imaging (MRI) using current density imaging technique (CDI) by measuring magnetic field changes caused by applied current (Joy *et al.*, 1989; Scott *et al.*, 1991; Serša *et al.*, 1994; Gamba and Delpy, 1998). Whereas tissue conductivity can be obtained by magnetic resonance electrical impedance tomography (MREIT), a technique used for reconstruction of electrical conductivity inside a tissue by means of current density (Woo *et al.*, 1994; Eyüboğlu *et al.*, 2001; Kwon, Lee, *et al.*, 2002; Kwon, Woo, *et al.*, 2002; Oh *et al.*, 2003; Seo, Yoon, *et al.*, 2003).

The goal of this dissertation is to investigate current density imaging and magnetic resonance electrical impedance tomography using short intense pulses of similar amplitudes and directions as used in electroporation based clinical applications and to investigate feasibility of both methods to determine electric field distribution during tissue electroporation.

BASIC PRINCIPLES OF ELECTROPORATION

Electroporation (or electropermeabilization) is a biological phenomenon of transient permeabilizing of the cell membrane by exposing it to electric field (Hamilton and Sale, 1967; Mir *et al.*, 1988; Neumann *et al.*, 1989; Rols and Teissié, 1989, 1990; Miklavčič *et al.*, 2000). The cell can be exposed to the electric field by an application of electric pulses which establish an induced potential difference across the cell membrane which is added to the resting membrane potential. The cell membrane becomes permeable when the total transmembrane potential, a sum of induced potential difference and resting membrane potential, exceeds the critical value (Kotnik *et al.*, 2010).

The standard model of electroporation or model of pore formation describes electroporation phenomenon as a formation of aqueous pores due to applied transmembrane voltage (Weaver and Chizmadzhev, 1996; Kotnik et al., 2012). Aqueous pores are established after transition from the hydrophobic to the hydrophilic state which are then stable due to a local minimum of free energy. This state is reversible until applied voltage remains under critical value. When this value is exceeded an irreversible breakdown of the membrane occurs (Kotnik *et al.*, 1997). Successful electroporation occurs when transmembrane voltage potential reaches threshold values from 200 mV to 1 V (Neumann *et al.*, 1982, 1989; Zimmermann, 1982; Weaver and Chizmadzhev, 1996; Miklavčič *et al.*, 2000).

Herman P. Schwan defined the induced transmembrane potential difference ΔV for a spherical cell (Schwan and Kay, 1957):

$$\Delta V = 1.5rE \cos \left(\varphi \right) \tag{Eq. 1}$$

where *r* is the radius of the cell, *E* is externally applied electric field and φ is the angle between the direction of the electric field and the selected point on the cell surface (Figure 2a). When geometrical shape of the cell is either spheroid (Kotnik and Miklavčič, 2000) or cylinder the transmembrane potential can be derived analytically. In case of more complex cell geometries numerical methods have to be introduced (Pucihar *et al.*, 2006).

(a)   (b)
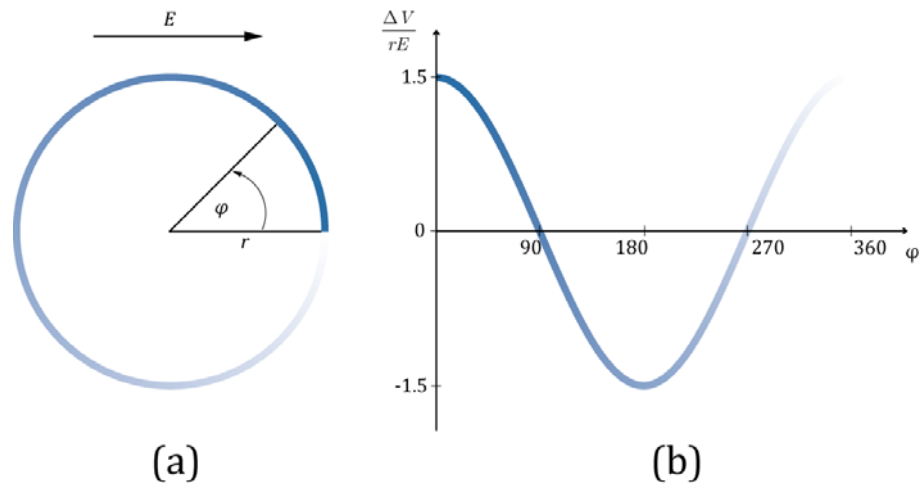
Figure 2: The model of spherical cell (a) and the dependence of the membrane potential on the position of the cell membrane according to Schwan equation (Eq. 1) *.*

The Schwan equation describes transmembrane voltage dependency on the position on the cell membrane as illustrated in Figure 2b. Nevertheless, (Eq. 1) can lead to significant errors when extracellular conductivity is very low and original equation has to be applied where all three conductivities (extracellular conductivity, membrane conductivity, cytoplasmic conductivity) are taken into account (Kotnik *et al.*, 1997). Experiments *in vitro* on Chinese hamster ovary (CHO) cells confirmed that the membrane breakdown first occurs at the anodic hemisphere (Sixou and Teissié, 1993) due to induced transmembrane voltage superimposed to resting potential (Gabriel and Teissié, 1997).

PARAMETERS FOR EFFECTIVE ELECTROPORATION

Numerous factors control the effectiveness of cell and tissue electroporation such as biological and physical parameters of the cell and the parameters of the applied electric pulses. Influence on the transmembrane voltage induced by an external electric field is strongly dependent on cell density, cell shape, size and orientation with respect to the field (Susil *et al.*, 1998; Valič *et al.*, 2003), the cytoskeleton structure of the cells, the membrane composition, and the extracellular environment (Rols and Teissié, 1992; Sukhorukov *et al.*, 2005; Kanthou *et al.*, 2006). Different electric pulse parameters are needed for the electroporation of different cell lines (Čemažar *et al.*, 1998) and for specific application of electroporation. The electric pulse parameters are the amplitude, duration, number of pulses and pulse repetition frequency and each of them has its own role in the electroporation process (Canatella *et al.*, 2001; Maček-Lebar and Miklavčič,

2001; Maček-Lebar *et al.*, 2002). The amplitude mostly affects the induced transmembrane potential and consequently the area of permeabilized membrane. The number of pulses and their duration is correlated with the extent of membrane electroporation, i.e. the number and the size of formed pores (Gabriel and Teissié, 1997; Krassowska and Filev, 2007). Pulse repetition frequency does not have large effect on a single cell as it has on tissues by reducing the muscle contractions and associated unpleasant sensations for patients involved in electrochemotherapy (Pucihar *et al.*, 2002; Miklavčič *et al.*, 2005). It was also demonstrated that the change in the value of a specific pulse parameter can be compensated by carefully selected value of other parameter (Miklavčič and Towhidi, 2010; Pucihar *et al.*, 2011).

FROM CELLS TOWARDS TISSUE ELECTROPORATION

In dense cell suspension and in tissues cells are positioned much closer together and therefore each of the cell is not exposed to the same electric field as it is in the case of the low density cell suspension (Susil *et al.*, 1998; Pavlin *et al.*, 2002). Structure of tissues is usually not homogeneous but rather heterogeneous as tissues consist of cells of different sizes, shapes and orientations. In addition, cells in tissues are distributed in different densities (Miklavčič, Pavšelj, *et al.*, 2006) and are connected to each other through gap junctions and extracellular matrix that can additionally influence the process of electroporation (Pucihar *et al.*, 2007). Furthermore, the local electric field in tissues is affected by applied electroporation pulses which depends on local electrical conductivity and *vice versa*, electroporation increases the conductivity and consequently alters the electric field distribution (Šel et al., 2005; Pavšelj et al., 2005; Cukjati et al., 2007; Ivorra and Rubinsky, 2007; Essone Mezeme et al., 2012; Neal et al., 2012).

Taking all of the above into consideration, it is somehow understandable that numerical modelling of the electroporation process for predicting electroporation outcomes is a daunting task. Even though, numerical modelling has been quite successful in characterizing the electroporation process either on a single cell level using computational demanding molecular dynamics simulations (Tieleman *et al.*, 2003; Tieleman, 2004; Tarek, 2005; Delemotte and Tarek, 2012) or on bulk tissue using finite element method (Šemrov and Miklavčič, 1998; Miklavčič *et al.*, 1998). Finite element modelling has advanced rapidly in the last decade and models are now able to predict alteration of conductivity due to electroporation (Šel *et al.*, 2005; Pavšelj *et al.*, 2005), they are successfully used in optimization tasks (Čorović *et al.*, 2008; Županic *et al.*, 2010) and for the purpose of treatment planning (Županič, 2010; Kos *et al.*, 2010; Miklavčič *et al.*, 2010).

APPLICATIONS OF ELECTROPORATION

There are many applications of electroporation which are being successfully introduced into clinical practice such as electrochemotherapy (ECT) (Marty *et al.*, 2006; Serša and Miklavčič, 2008), electroporation based gene transfer for gene therapy (Andre *et al.*, 2008; Daud *et al.*, 2008; Heller and Heller, 2010), DNA vaccination (Zhang *et al.*, 2004; Luxembourg *et al.*, 2007) and non-thermal irreversible electroporation ablation (N-TIRE) (Rubinsky *et al.*, 2008; Garcia *et al.*, 2011). ECT and N-TIRE, both potent procedures used in solid tumor treatment, are two most advanced applications of electroporation that would benefit the most from a monitoring method by detection of areas with insufficient electric field coverage before the end of the treatment. However, ECT could benefit more from it as there are other approaches being investigated for detecting irreversibly electroporated areas.

ELECTROCHEMOTHERAPY (ECT)

ECT combines electroporation with the use of chemotherapeutic drugs, which exhibit higher cytotoxicity when they are combined (Orlowski *et al.*, 1988; Serša *et al.*, 1995; Marty *et al.*, 2006; Serša and Miklavčič, 2008). In comparison to classical protocols of chemotherapy it requires lower drug doses and provides localized treatment. Bleomycin and cisplatin, both otherwise poorly permeant anticancer drugs, were found to be the most appropriate candidates for combined use with electric pulses (Serša *et al.*, 1995; Mir and Orlowski, 1999). First ECT experiments date back to eighties of the previous century (Okino and Mohri, 1987; Mir *et al.*, 1988). Successful application of ECT to mice and rats for variety of tumors followed. Clinical trials in humans have demonstrated excellent results in antitumor therapy, especially for adenocarcinoma, basal cell carcinoma, treatment of head and neck squamous and melanoma (Serša *et al.*, 1995, 2003; Heller *et al.*, 1998, 1999; Gehl, 2003). Until now, ECT as a standard clinical procedure has been successfully used for treatment of cutaneous and subcutaneous metastasis of various cancers achieving over 70 % complete responses (Marty *et al.*, 2006) on over 3000 treated patients in Europe since 2006 (Serša *et al.*, 2012). Recently, ECT in treatment of deep-seated tumors has been introduced (Miklavčič *et al.*, 2010; Edhemović *et al.*, 2011; Thomson *et al.*, 2011).

Presence of chemotherapeutic drug and adequate local electric field distribution are crucial for therapy's success (Miklavčič *et al.*, 1998; Miklavčič, Čorović, *et al.*, 2006). Electric field distribution in the tissue is determined by electrode positioning and applied pulse parameters, both obtained by treatment planning for the ECT, which already proved to have a great potential in clinical use (Miklavčič *et al.*, 2010; Pavliha *et al.*, 2012). Its applicability however is currently limited due to uncertain conductivity values of tissues, especially within the tumor where heterogeneous conductivity was already observed (Muftuler *et al.*, 2006). Uncertain conductivity

values can result in obtaining inappropriate electrodes position, electric pulse parameters and consequently insufficient electric field coverage of the tumor. Another concern is the electrode positioning during the ECT treatment procedure. Namely, it is relatively difficult to insert electrodes precisely according to the anatomy-based numerical treatment plan (Kos *et al.*, 2010). An imprecise placement of the electrodes can also result in an inadequate electric field coverage of the target area and therefore treatment failure. A new electroporation monitoring method that would allow determination of the electric field strength within the sample would be of great importance for ECT, especially if the method could be performed *in situ* during the treatment.

Non-thermal irreversible electroporation ablation (N-TIRE)

N-TIRE is also effective application of electroporation for tumor treatment although it does not require chemotherapeutic drugs to kill tumor cells (Rubinsky *et al.*, 2007). Here, solely electric field above the irreversible threshold is used to achieve death of all targeted cells. N-TIRE is a prime candidate for tissue ablation as it can be applied without introducing significant thermal effects (Davalos *et al.*, 2005; Miller *et al.*, 2005; Edd *et al.*, 2006; Al-Sakere *et al.*, 2007). Its unique advantages over thermal focal therapies and surgical resections are preserving the extracellular matrix, major vascular and other sensitive structures while facilitating rapid lesion resolution which results in minimal scarring (Onik *et al.*, 2007; Neal *et al.*, 2012). It was tested as an ablation modality in various medical applications: ablation of cancer (Onik *et al.*, 2007; Rubinsky *et al.*, 2008), kidney ablation (Leveillee *et al.*, 2009), intracranial ablation (Garcia *et al.*, 2009), epicardial ablation (Lavee *et al.*, 2007) and prevention of restenosis after angioplasty (Maor *et al.*, 2008). As in ECT, treatment planning was also introduced for N-TIRE in order to guarantee no thermal effects are involved during the treatment and to define treated and untreated areas (Nemkov and Goldstein, 2003; Garcia *et al.*, 2009; Neal *et al.*, 2011, 2012; Golberg and Rubinsky, 2012). Unlike in ECT, the effects can be monitored immediately after the application of pulses due to immediate changes in tissue structure (Lee *et al.*, 2007; Rubinsky *et al.*, 2007).

MONITORING OF TISSUE ELECTROPORATION

Various methods of monitoring electroporation process were already suggested, particularly of irreversible electroporation where immediate changes of tissue properties can be detected. The damage to the cellular membrane due to the irreversible electroporation and the consequent release of intracellular content can be detected by comparing MRI images of different modalities (T_1-, T_2-weighted, FLAIR or STIR, DW-MRI) acquired before and after the application of N-TIRE pulses (Hjouj and Rubinsky, 2010; Mahmood *et al.*, 2011). Similar method of comparing MRI images of different modalities was used to observe irreversible electroporation of liver tissues by detecting local fluid accumulation due to transient permeabilization of blood vessels as suggested by authors (Zhang *et al.*, 2010). Ultrasound can also be applied for observation of ablation zones during irreversible electroporation by detecting a spherical hypoechoic areas (Lee *et al.*, 2007). Electrical impedance tomography (EIT) was suggested for imaging irreversible electroporation by reconstructing conductivity distribution of the targeted tissue during the treatment (Davalos *et al.*, 2000, 2002, 2004; Granot *et al.*, 2009).

Monitoring of reversible electroporation is however more demanding task since there are almost no immediate visible physical changes in treated tissue. One of the few proposed methods is based on real time electroporation control for in vivo non-viral gene therapy by adjusting measured voltage and current during application of electroporation pulses (Cukjati *et al.*, 2007). However, this method inherits the main restraint of conductivity evaluation methods that are based on voltage/current measurements. Monitoring of voltage and current between only one pair of electrodes at a time can led to false conductivity and to an inaccurate electric field distribution calculation due to lack of information on tissue heterogeneity between the electrodes.

Practical and reliable method of monitoring electroporation process is needed. A method capable of determining electric field distribution during the pulse delivery seems to be useful as electroporation depends on local electric field. This would enable detection of insufficient electric field coverage before the end of the treatment, thus increasing and assuring its effectiveness. As the electric field distribution inside the observed sample cannot be measured directly, an indirect approach of obtaining it needs to be evaluated. By means of Ohm's law, the electric field distribution $\mathbf{E}$ can be calculated when an electric current density $\mathbf{J}$ and an electrical conductivity of the tissue σ are obtained.

$$\mathbf{E} = \frac{\mathbf{J}}{\sigma}$$

(Eq. 2)

The electric current density inside a conductive tissue can be obtained by MRI using current density imaging technique (CDI) by measuring magnetic field changes caused by applied current (Joy *et al.*, 1989; Scott *et al.*, 1991; Serša *et al.*, 1994; Gamba and Delpy, 1998). Whereas tissue conductivity can be obtained by magnetic resonance electrical impedance tomography (MREIT), a technique used for reconstruction of electrical conductivity inside a tissue by means of current density (Woo *et al.*, 1994; Eyüboğlu *et al.*, 2001; Kwon, Lee, *et al.*, 2002; Kwon, Woo, *et al.*, 2002; Oh *et al.*, 2003; Seo, Yoon, *et al.*, 2003).

CURRENT DENSITY IMAGING (CDI)

Current density imaging (CDI) is an MRI method for acquiring current density distribution inside conductive samples during the application of electric pulses. The method is based on detecting magnetic field changes caused by applied current (Figure 3). When magnetic field changes are obtained by means of MRI, current density distribution can be calculated using Ampere's law (Maxwell, 1865). Magnetic field changes are proportional to the frequency shift so they can be acquired by chemical shift imaging methods (Manassen *et al.*, 1988). Usually electric pulses are applied in synchronization with the imaging sequence and the magnetic field change is proportional to the phase shift (Joy *et al.*, 1989). CDI methods that are based on current detections by magnetic field change can be further divided into direct current density imaging methods (DC-CDI) (Joy *et al.*, 1989; Serša *et al.*, 1994), alternating current density imaging methods (AC-CDI) (Mikac *et al.*, 2001) and radiofrequency current density imaging methods (RF-CDI) (Scott *et al.*, 1992).
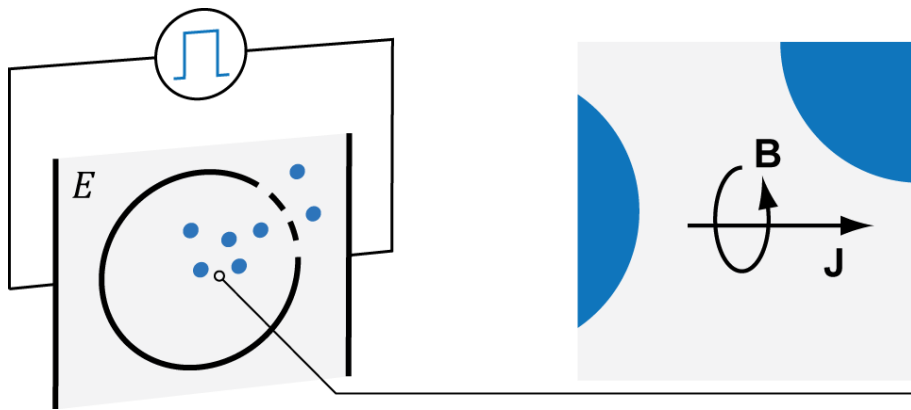
*Figure 3: When an electric pulse is injected into electrically conducting body an induced magnetic flux density **B** and an electric current density **J** are established. **B** is proportional to the current induced phase shifts stored in the images acquired by MRI.*

There are many applications of CDI, e.g., studying electric currents in models of porous materials (Weber and Kimmich, 2002), following electro-osmotic flow (Buhai *et al.*, 2007), monitoring chemical reactions that release ions (Mikac *et al.*, 2007), studying electrically induced skin burns (Patriciu *et al.*, 2005), specific radiofrequency absorption rate distribution measurements (Beravs *et al.*, 2000), studying brain conductivity changes during transcranial stimulation (Joy *et al.*, 1999) and others. CDI was also applied for mapping spatial distribution of electric current through mice tumors during application of electroporation pulses (Serša *et al.*, 1997). It should be noted however that at that time, 256 applications of electric pulses were needed in order to obtain a map of current density distribution of the tumor.

At the moment, a two-shot RARE (Rapid Acquisition with Relaxation Enhancement) current density magnetic resonance imaging sequence is more appropriate for mapping current density distributions during electroporation as it allows faster magnetic field change mapping than the standard spin-echo based CDI (Serša, 2008). It consists of two parts, the current encoding part and the imaging part based on the RARE MRI sequence (Hennig *et al.*, 1986). During the current encoding part, which is essentially a conventional spin-echo sequence with superimposed electric pulses, the electroporation train of high-voltage electric pulses is executed in the interval between the excitation 90° RF pulse and the refocusing 180° RF pulse. The electric pulses induce a phase shift in the NMR signal that is proportional to the time integral of the applied electric pulses. The phase shift is preserved during the imaging part of the sequence and stored in the phase of the MR image. This is achieved in the two-shot RARE CDI sequence by signal co-addition of two RARE sequences having phases of the refocusing RF pulses 90° apart.

MAGNETIC RESONANCE ELECTRICAL IMPEDANCE TOMOGRAPHY (MREIT)

Conductivity and permittivity distributions inside the human body is an emerging topic as these distributions deliver better differentiation of organs and tissues, enabling improved diagnosis or treatment of various diseases. For this purpose, electrical impedance tomography (EIT) was introduced almost 30 years ago, although it still has not reached the stage of clinical applications due to methodological limitations in terms of practical feasibility (Webster, 1990; Holder, 2004).

MREIT is relatively new medical imaging modality based on CDI for visualizing electrical conductivity distribution inside a conductive sample. While EIT is limited on a set of voltage data obtained on a portion of the imaging object boundary by means of limited number of surface electrodes, MREIT relies on a set of inner data, i.e. current density distribution, obtained by CDI using MRI. Typical MREIT generator for applying electric pulses to establish a current density inside an imaging object is based on a current source (Woo and Seo, 2008). Surface electrodes made out of nonmagnetic conductive materials such as copper, silver or carbon, are usually used

for delivering electric pulses to the imaging object. For avoiding artefacts due to shielding of RF signals a recessed electrode which has a gap of a moderately conductive gel between the object's surface and a cooper electrode was introduced (Lee *et al.*, 2006). Lately, flexible carbon-hydrogel electrodes with conductive adhesive are being applied in *in vivo* animal and human experiments (Jeong *et al.*, 2008; Kim *et al.*, 2008). It should be noted that the described MREIT setup for delivering electric pulses differs greatly from the typical electroporation setup which employs voltage sources and sometimes even needle electrodes if required (Figure 4).
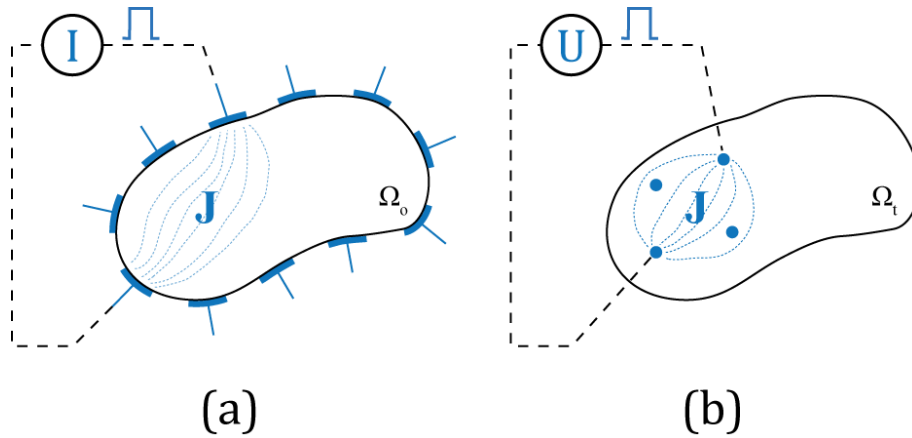
Figure 4: MREIT setup for establishing current density distribution in the imaging object Ω_o using current source and surface electrodes (a). Electroporation setup for delivering electric pulses in treated tissue Ω_t using voltage source and needle electrodes (b).

Early MREIT algorithms such as *J*-substitution algorithm (Khang *et al.*, 2002; Kwon, Woo, *et al.*, 2002), the current constrained voltage scaled reconstruction algorithm (Birgül *et al.*, 2003) and equipotential line methods (Kwon, Lee, *et al.*, 2002; Ider *et al.*, 2003) required mechanical rotations of the imaging sample within MRI scanner as all three components of magnetic flux density were needed to obtain conductivity distribution. In order to avoid object rotation harmonic B_z algorithm was introduced which uses only one magnetic flux density component (Oh *et al.*, 2003, 2005; Seo, Kwon, *et al.*, 2003; Seo, Yoon, *et al.*, 2003). There are also special MREIT algorithms, such as projected current density algorithm which is positioned between *J*-substitution and harmonic B_z algorithm as it applies *J*-substitution algorithm to reconstruct a conductivity image and uses only one magnetic flux density component for computation of current density distribution (Seo, Yoon, *et al.*, 2003; Nam *et al.*, 2007; Park *et al.*, 2007). This

algorithm can be successfully applied when a current flow in the sample is confined within the plane perpendicular to the measured component of magnetic flux density.

The use of MREIT for conductivity imaging has advanced rapidly in the last decade and has now reached the stage of *in vivo* animal and human imaging experiments (Park, Kwon, *et al.*, 2004; Park, Park, *et al.*, 2004; Kwon *et al.*, 2005; Oh *et al.*, 2005; Kim *et al.*, 2008, 2009). Technical development in MREIT has demonstrated that high-resolution conductivity imaging is feasible by examining biological tissues by means of applying electrical pulses and obtaining induced magnetic flux densities using MRI scanner. As the method does not present additional cost to the conventional MRI procedure it could become a part of an MRI system and provide additional and valuable contrast information (Woo and Seo, 2008). Electroporation applications such as ECT and N-TIRE would also greatly benefit from high-resolution conductivity imaging method such as MREIT. Tissue conductivity change due to electroporation and heterogeneity of tumors represent open and demanding challenges in patient specific treatment planning for ECT (Pavliha *et al.*, 2012). Reconstruction of electrical conductivity during electroporation pulse delivery together with measuring current density distribution using MREIT and CDI, respectively, would enable much needed *in situ* determination of electric field distribution thus increasing and assuring the effectiveness of the electroporation based treatments.

AIMS OF THE DOCTORAL THESIS

The appropriate local electric field distribution in the treated tissue is one of the most important conditions for successful cell membrane electroporation. A new electroporation monitoring method that would allow determination of the electric field strength during the pulse delivery in order to detect insufficient electric field coverage before the end of the treatment would be of great importance for electroporation applications. As the electric field distribution inside the observed sample cannot be measured directly, an indirect approach based on Ohm's law using current density imaging and magnetic resonance electrical impedance tomography is proposed and evaluated. By means of Ohm's law, the electric field distribution can be calculated when an electric current density and an electrical conductivity of the tissue are obtained. The electric current density inside a tissue can be acquired by magnetic resonance imaging using current density imaging technique while electrical conductivity can be reconstructed using magnetic resonance electrical impedance tomography. As both, current density imaging and magnetic resonance electrical impedance tomography have been developed for diagnostic purposes there is a lack of reports on application of electric pulses of parameters that are normally used in electroporation.

The goal of this dissertation was to investigate current density imaging and magnetic resonance electrical impedance tomography using short intense pulses of similar amplitudes and directions as used in electroporation based clinical applications and to investigate feasibility of both methods to determine electric field distribution during tissue electroporation.

SCIENTIFIC ARTICLES

MAGNETIC RESONANCE ELECTRICAL IMPEDANCE TOMOGRAPHY FOR MONITORING ELECTRIC FIELD DISTRIBUTION DURING TISSUE ELECTROPORATION
KRANJC Matej, BAJD Franci, SERŠA Igor, MIKLAVČIČ Damijan
IEEE Transactions on Medical Imaging 30: 1771-1778, 2011.

***EX VIVO* AND *IN SILICO* FEASIBILITY STUDY OF MONITORING ELECTRIC FIELD DISTRIBUTION IN TISSUE DURING ELECTROPORATION BASED TREATMENTS**
KRANJC Matej, BAJD Franci, SERŠA Igor, WOO Eung Je, MIKLAVČIČ Damijan
PLoS ONE: PLoS ONE 7(9): e45737, 2012.

ASSESSING HOW ELECTROPORATION AFFECTS THE EFFECTIVE CONDUCTIVITY TENSOR OF BIOLOGICAL TISSUES
MEZEME Melvin Essone, KRANJC Matej, BAJD Franci, SERŠA Igor, BROSSEAU Christian, MIKLAVČIČ Damijan
Applied Physics Letters: in press.

ARTICLE 1

Title: Magnetic resonance electrical impedance tomography for monitoring electric field distribution during tissue electroporation

Authors: KRANJC Matej, BAJD Franci, SERŠA Igor, MIKLAVČIČ Damijan

Publication: IEEE Transactions on Medical Imaging

DOI: 10.1109/TMI.2011.2147328

Year: 2011

Volume: 30

Number: 10

Pages: 1771 - 1778

Impact factor: 3.643

Ranking:

Category name	Total journals in category	Journal rank in category	Quartile in category
computer science, interdisciplinary applications	99	4	Q1
engineering, biomedical	72	7	Q1
engineering, electrical & electronic	244	12	Q1
imaging science & photographic technology	21	3	Q1
radiology, nuclear medicine & medical imaging	116	17	Q1

Magnetic Resonance Electrical Impedance Tomography for Monitoring Electric Field Distribution During Tissue Electroporation

M. Kranjc, F. Bajd, I. Serša, and D. Miklavčič*

Abstract—**Electroporation is a phenomenon caused by externally applied electric field of an adequate strength and duration to cells that results in the increase of cell membrane permeability to various molecules, which otherwise are deprived of transport mechanism. As accurate coverage of the tissue with a sufficiently large electric field presents one of the most important conditions for successful electroporation, applications based on electroporation would greatly benefit with a method of monitoring the electric field, especially if it could be done during the treatment. As the membrane electroporation is a consequence of an induced transmembrane potential which is directly proportional to the local electric field, we propose current density imaging (CDI) and magnetic resonance electrical impedance tomography (MREIT) techniques to measure the electric field distribution during electroporation. The experimental part of the study employs CDI with short high-voltage pulses, while the theoretical part of the study is based on numerical simulations of MREIT. A good agreement between experimental and numerical results was obtained, suggesting that CDI and MREIT can be used to determine the electric field during electric pulse delivery and that both of the methods can be of significant help in planning and monitoring of future electroporation based clinical applications.**

Index Terms—**Current density imaging (CDI), electroporation, magnetic resonance imaging (MRI), magnetic resonance impedance tomography (MREIT).**

I. INTRODUCTION

$\mathbf{A}$N exposure of a cell or tissue to an electric field of an adequate strength and duration leads to an increased cell membrane permeability. This phenomenon, termed electroporation, allows various otherwise nonpermeant molecules to cross the membrane and enter the cell [1]–[4].

When the strength of the applied electric field is below the irreversible electroporation threshold only transient structural changes can be attained and the cell membrane will reseal afterwards. This is termed reversible electroporation as cell preserves its viability [5]. On the contrary, irreversible electroporation leads to a cell death as the applied electric field is above

M. Kranjc is with the Faculty of Electrical Engineering, University of Ljubljana, SI-1000 Ljubljana, Slovenia (e-mail: matej.kranjc@fe.uni-lj.si).
F. Bajd and I. Serša are with the Institut "Jožef Stefan", Jamova cesta 39, SI-1000 Ljubljana, Slovenia and with the EN-FIST Centre of Excellence, SI-1000 Ljubljana, Slovenia (e-mail: franci.bajd@ijs.si; igor.sersa@ijs.si).
*D. Miklavčič is with the Faculty of Electrical Engineering, University of Ljubljana, SI-1000 Ljubljana, Slovenia (e-mail: damijan.miklavcic@fe.uni-lj.si).
Digital Object Identifier 10.1109/TMI.2011.2147328

the irreversible electroporation threshold and the cell does not regain its integrity [6]. An accurate coverage of the cell with a sufficiently large electric field therefore presents one of the most important conditions for successful electroporation [7], [8].

Applications such as electrochemotherapy (ECT) [9], [10], electroporation based gene transfer for gene therapy [11]–[13], DNA vaccination [14] and nonthermal irreversible electroporation ablation (NTIRE) [15], [16] are being successfully introduced into clinical practice. A new electroporation monitoring method that would allow direct measurement of the electric field strength within the sample would be of great importance for these applications. If possible the method should be performed *in situ* during the treatment. Another important aspect of the electroporation monitoring process is a possibility of input electroporation parameter adjustments according to the progress of the electroporation treatment as for now, optimal parameters for *in vivo* electroporation are determined using *in vivo* tests of permeabilization after the treatment [17] and by a mathematical modeling to determine the electric field distribution [18], [19]. Various methods of monitoring electroporation process were already suggested: electrical conductivity measurement by electrical impedance tomography (EIT) [20], [21], current and voltage measurements of delivered pulses [22] and recently magnetic resonance imaging (MRI) [23], [24]. Although these approaches, if further developed, might be interesting, they are either unable to monitor the process during pulse delivery in case of EIT and MRI approach or they can deliver false results due to lack of measurements in case of current and voltage measurements of delivered pulses.

Tissue is an electrically conducting material and it can be exposed to an electric field by injecting electric current by an electric pulse generator via electrodes. When an electric current is injected into an electrically conductive body such as a tissue, the magnetic field density $\mathbf{B} = (B_x, B_y, B_z)$ and the electric current density $\mathbf{J} = (J_x, J_y, J_z)$ are established inside this body. The electric current density inside conductive watery samples can be obtained using current density imaging technique (CDI) by measuring magnetic field density $\mathbf{B}$ with MRI and solving Ampere's law equation $\mathbf{J} = (1)/(\mu_0)\nabla \times \mathbf{B}$ [25]–[27]. One of many CDI applications is also magnetic resonance electrical impedance tomography (MREIT), a technique used for reconstruction of electrical conductivity inside a conducting body by means of current density ($\mathbf{J}$-based MREIT) [28]–[31] or one component of magnetic flux density—B_z (B_z-based MREIT) [32], [33]. The main problem of $\mathbf{J}$-based MREIT is in a difficulty to image the sample in different perpendicular orientations in order to obtain all three components of $\mathbf{B}$ and $\mathbf{J}$. MRI namely allows measurement of only one $\mathbf{B}$ component at a time,

i.e., the component in the direction of the main magnetic field. The sample reorientation may result in a pixel misalignments and a sample deformation. For this reason most *in vivo* studies [34]–[36] have been usually done with B_z-based MREIT in which conductivity distribution is obtained without the sample rotation. When both, the electrical conductivity and the current density are obtained, the electric field distribution inside the sample can be calculated using Ohm's law. As the membrane electroporation is a consequence of an induced transmembrane potential which is directly proportional to the local electric field [8], [37], CDI and MREIT techniques could be useful techniques to monitor the electroporation process by measuring the electric field distribution during electroporation.

CDI and MREIT were designed for diagnostic purposes in which the injected current is not producing any significant effect on the tissue. For that reason the injected current is limited to a few milliampere or even less, which corresponds to voltage pulses of only few volts. There are few reports published where in CDI voltage pluses of higher amplitudes were used; for example in CDI of mice tumors 160 V electric pulses were used [38], however, there is no report on CDI where electric pulses of voltages that are normally used in electroporation would be used. In electrochemotherapy and non-thermal irreversible electroporation ablation the electric pulses can be up to 3000 V depending on electrodes geometry and a distance between the electrodes.

The aim of this work was to study feasibility of MREIT to monitor electric field distribution during tissue electroporation. The experimental part of the study employs CDI with short high-voltage pulses, as are normally used in electroporation based clinical applications such as electrochemotherapy and nonthermal irreversible electroporation ablation, while the theoretical part of the study is based on numerical simulations of MREIT. All experiments were performed on two different phantoms, a homogeneous and a heterogeneous phantom. The homogeneous phantom was made of agar with a single electrical conductivity, which resembled the conductivity of a typical tumor, while the heterogeneous phantom was made of two agars, with two different electrical conductivities; one resembling the conductivity of a tumor and the other resembling the conductivity of a liver. They were exposed to different electroporation pulse sequences with different number of pulses of different amplitudes. The current density distribution inside the phantoms was measured by CDI and the electric field distribution inside the phantom was calculated by the MREIT algorithm. For comparison with the experimental results a numerical model of the phantom was constructed using the finite element method.

II. Materials and Methods

A. Experimental Setup

Cylindrically shaped homogeneous and heterogeneous phantoms measuring 21 mm in radius and 2 mm in height made of an agar mixture were placed in the acrylic glass container as shown in Fig. 1. The agar mixture was made of agar powder (Kemika, Zagreb, Croatia), 0.9% NaCl saline solution (B. Braun, Melsungen, Germany), and distilled deionized water (B. Braun, Melsungen, Germany). The homogeneous phantom
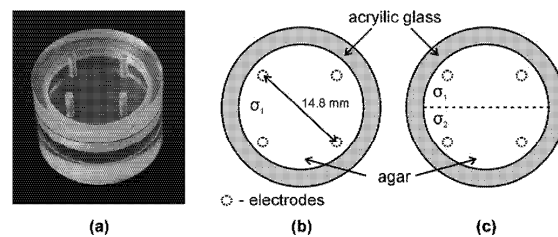
Fig. 1. Phantom used in the study was made of the acrylic glass container with four holes for electrodes (a). The phantom was used in two different arrangements: in the homogeneous arrangement (b) it was filled with one agar type having homogeneous electrical conductivity, while in the heterogeneous arrangement (c) it was filled with two agar types with two different electrical conductivities, each filing half of the cylinder.

was made of a single cylindrically shaped agar mixture with electrical conductivity ($\sigma_1 = 0.23$ S/m) as shown in Fig. 1(b), while the heterogeneous phantom was made of two half cylindrically shaped agar mixtures—each of them with its own electrical conductivity ($\sigma_1 = 0.23$ S/m and $\sigma_2 = 0.05$ S/m) as shown in Fig. 1(c). The first conductivity resembles a tumor conductivity and the second conductivity resembles a liver conductivity [39]–[41]. Electrical conductivity of agar mixtures was measured by Conductivity meter MA 5950 (Metrel, Horjul, Slovenia). Four cylindrically shaped electrodes—needles measuring 1 mm in radius made of platinum-iridium alloy were inserted through the cover of the acrylic glass container into the phantom as shown in Fig. 1(a). Distance between the diagonal electrodes from the center to the center was 14.8 mm.

Electric pulse generator used for delivering electroporation pulses into the phantom was customized Cliniporator Vitae (IGEA, Carpi, Italy). The Cliniporator Vitae device is a pulse generator with six independently controlled and electrically insulated outputs each providing rectangular pulses with amplitudes up to 3000 V and 50 A maximum current. The generator is also capable of measuring the output voltage at 3% precision. Four of the outputs were connected to four electrodes inserted in the phantom. The outputs were also measured with an oscilloscope (WavePro 7300A, LeCroy, Chestnut Ridge, NY) and current probe (AP015, LeCroy, Chestnut Ridge, NY) to obtain the current amplitude of the delivered pulses (I_{OSC}). The trigger input of the generator was connected to the MRI control unit and synchronized with the CDI pulse sequence.

Homogenous and heterogeneous phantoms were exposed to sequences of electric pulses, which are commonly used in electroporation applications [42]. The electric pulses were delivered between the diagonal electrodes of the sample in sequences of either one, two, four, or eight 100-μs-long pulses separated by 100 μs intervals. Every sequence of pulses was delivered three times, each time with a different pulse amplitude (U_{app}). In experiments on homogeneous phantoms, voltage amplitudes of the applied pulses were $U_{app} = 1000$ V, 1500 V, and 2000 V, while in experiments on heterogeneous phantoms the amplitudes were somewhat higher $U_{app} = 1000$ V, 2000 V, and 3000 V due to its lower electrical conductivity compared to the homogeneous phantom. All experiments were repeated three times.

B. Current Density Imaging

Electric current distribution in all the phantoms was imaged by the two-shot RARE current density magnetic resonance imaging sequence [43]. The sequence consists of two parts, the current encoding part and the imaging part based on the RARE MRI sequence [44]. During the current encoding part, which is essentially the conventional spin-echo sequence with superimposed electric pulses, the electroporation train of high-voltage electric pulses was executed in the interval between the excitation 90° RF pulse and the refocusing 180° RF pulse. The electric pulses induced a phase shift in the nuclear magnetic resonance (NMR) signal that is proportional to the time integral of the applied electric pulses. The phase shift must be preserved during the imaging part of the sequence and stored in the phase of the MR image. This is in the two-shot RARE CDI sequence achieved by signal co-addition of two RARE sequences having phases of the refocusing RF pulses 90° apart. Current density in the phantom was calculated using the Ampere law

$$\mathbf{J} = \frac{1}{\mu_0} \nabla \times \mathbf{B} \qquad (1)$$

from current induced phase shifts φ stored in the acquired images

$$\varphi = \gamma t_c B_z. \qquad (2)$$

Here γ is the proton gyromagnetic ratio and t_c is the total duration of the applied electric pulses. In the presented experiments the phantom geometry was such that currents were flowing predominately in the direction perpendicular to the electrodes. Therefore, the magnetic field in the central axial slice through the phantom had nonzero component in the direction perpendicular to the imaging slice, i.e., B_z, and negligible in-slice components (B_x, B_y). Under these conditions current density calculation simplifies to

$$\mathbf{J} = \frac{1}{\mu_0} \left(\frac{\partial B_z}{\partial y}, -\frac{\partial B_z}{\partial x}, 0 \right). \qquad (3)$$

It should be noted here that such slice/sample/electrode arrangement does not require sample reorientation to perpendicular orientations that is usually inevitable for other arrangements in order to acquire other components of current induced magnetic field changes.

MR imaging was performed on a TecMag NMR spectrometer connected to an Oxford 2.35T horizontal bore superconducting magnet. The MRI system was equipped with Bruker microimaging accessories with maximum gradients of 250 mT/m. The phantoms were inserted in the 25 mm RF probe and connected to the electric pulse generator using cables including low-pass filters to avoid possible RF disturbances in the NMR signal. MR images of current induced magnetic field changes were acquired using the two-shot RARE CDI sequence as shown in Fig. 2 with parameters: field of view (FOV) 30 mm, imaging matrix 64×64, inter-echo delay 2.64 ms, echo time of the current encoding period 20 ms and the time interval between the two RARE signal acquisitions was 10 s. As the phantom
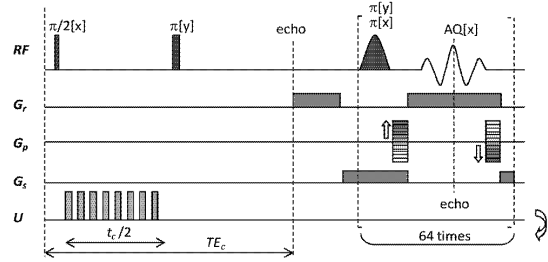
Fig. 2. Two-shot RARE CDI sequence that was used to acquire images of current induced magnetic field changes.

was flat, i.e., in a form of an excited slice, slice excitation RF pulses were not needed and they were replaced by nonselective RF pulses that excited the entire phantom, while the imaging plane coincided with the "phantom slice."

C. Electric Field Reconstruction

Electric field was reconstructed by means of $\mathbf{J}$ obtained with CDI method, application of the $\mathbf{J}$-substitution algorithm for reconstruction of conductivity distribution [28], [32], [45], [46] and Ohm's law for calculation of electric field distribution. A mathematical model of the phantom body $\Omega_{\mathbf{p}}$ surrounded with the outer boundary $\partial\Omega_{\mathbf{p\_o}}$ was build. Four electrodes were modeled as four inner boundaries $\partial\Omega_{\mathbf{p\_e}}$ inside the body $\Omega_{\mathbf{p}}$.

The Corresponding voltage u satisfies the boundary value problem in any given conductivity σ of the model

$$\nabla \cdot (\sigma \nabla u) = 0 \quad \text{in } \Omega_{\mathbf{p}} \qquad (4)$$

with the corresponding Neumann boundary condition on the phantom outer boundary $\partial\Omega_{\mathbf{p\_o}}$

$$\sigma \frac{\partial u}{\partial n_{\mathbf{p}}} = 0 \quad \text{on } \partial\Omega_{\mathbf{p\_o}} \qquad (5)$$

where $n_{\mathbf{p}}$ denotes the exterior normal vector to the boundary $\partial\Omega_{\mathbf{p\_o}}$ and Dirichlet boundary condition on the inner—electrodes boundary $\partial\Omega_{\mathbf{p\_e}}$

$$u = V \quad \text{on } \partial\Omega_{\mathbf{p\_e}} \qquad (6)$$

where V is the voltage on the electrodes measured by the generator.

Both voltage u and electrical conductivity σ in (4) are unknown variables. Equations (4), (5), and (6) are solved by the iterative scheme yielding the correct value of σ

$$\nabla \cdot (\sigma^k \nabla u^k) = 0 \quad \text{in } \Omega_{\mathbf{p}} \qquad (7)$$

$$\sigma^k \frac{\partial u^k}{\partial n_{\mathbf{p}}} = 0 \quad \text{on } \partial\Omega_{\mathbf{p\_o}} \qquad (8)$$

$$u^k = V \quad \text{on } \partial\Omega_{\mathbf{p\_e}}. \qquad (9)$$

All iterative schemes in this study started with $\sigma^0 = 1 (k = 0)$. After solving (7), (8), and (9) the solution u^k was used in

$$\sigma^{k+1} = \frac{|\mathbf{J}_{\text{CDI}}|}{|\nabla u^k|} \qquad (10)$$

where σ^{k+1} is the new conductivity and $\mathbf{J}_{\mathbf{CDI}}$ is the current density obtained by the CDI method. The iterative scheme lasts until the relative difference between two successive σ falls below ε (in our study ε had value of 0.01)

$$\frac{\|\sigma^k - \sigma^{k-1}\|}{\|\sigma^k\|} < \varepsilon. \tag{11}$$

Electric field distribution $\mathbf{E}_{\mathbf{MREIT}}$ can then be calculated using Ohm's law

$$\mathbf{E}_{\mathbf{MREIT}} = \frac{\mathbf{J}_{\mathbf{CDI}}}{\sigma^k}. \tag{12}$$

Relative error e of the obtained electric field distribution was calculated using

$$e = \frac{|\mathbf{E}_{\mathbf{num}} - \mathbf{E}_{\mathbf{MREIT}}|}{|\mathbf{E}_{\mathbf{num}}|} \tag{13}$$

where $\mathbf{E}_{\mathbf{num}}$ is the electric field distribution obtained by solving the numerical model.

It should be noted that different conductivity distributions may correspond to the same current density distribution in a heterogeneous sample due to nonuniqueness [47]. For this reason, the heterogeneous phantom was measured with two different sequences of electric pulses that satisfy the condition

$$|\mathbf{J}_{\mathbf{CDI\_1}} \times \mathbf{J}_{\mathbf{CDI\_2}}| \neq 0 \tag{14}$$

here $\mathbf{J}_{\mathbf{CDI\_1}}$ and $\mathbf{J}_{\mathbf{CDI\_2}}$ are the two current density distributions that result from the two different pulse sequences. Therefore pulse sequences were delivered between both diagonal pairs of electrodes.

The finite element method was used to solve the problem in (7), (8), and (9). All calculations of the mathematical model were performed with the numerical computational environment Matlab 2010a (Mathworks, Natick, MA) and its Partial Differential Equation Toolbox on a desktop PC (Windows 7, 2.66 GHz, 4 GB RAM). The calculations took on average only a few seconds.

D. Numerical Model

Experimental results obtained by CDI and MREIT were compared also to two numerical models: one for the homogeneous and the other for the heterogeneous phantom. The electric field distribution ($\mathbf{E}_{\mathbf{num}}$), corresponding current density distribution ($\mathbf{J}_{\mathbf{num}}$) and its spatial integral, i.e., the net electric current ($I_{\mathbf{num}}$) in numerical models were obtained by solving (4), (5), and (6) using known conductivities of the homogeneous (σ_1) and heterogeneous phantoms (σ_1 and σ_2). The numerical model was solved using a finite element method with the commercial finite element software package COMSOL Multiphysics 3.5a (COMSOL AB, Stockholm, Sweden) running on the same desktop PC as noted previously. The mesh of the numerical model consisted of 6 752 triangular elements.

III. RESULTS

When the phantom was exposed to electroporation pulses an electric current density and electric field were established inside the phantom. The former was successfully measured by
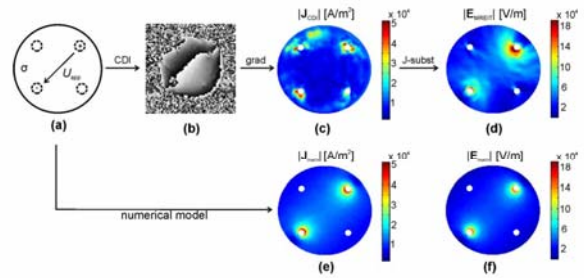
Fig. 3. Homogeneous phantom exposed to four high voltage pulses of 1000 V delivered between diagonal electrodes (a). The initial phase image (b) was acquired by the two-shot RARE based CDI sequence. The current density distribution (c) in the phantom was calculated from the phase image using (3). Finally, the electric field distribution (d) was calculated using J-substitution algorithm from the current density distribution. Numerical model results of current density distribution (e) and electric field distribution (f) in the phantom are shown below the corresponding experimental results.

CDI method, while the later was calculated from the CDI data using the MREIT J-substitution algorithm. Both results are presented in Fig. 3, which corresponds to the experiment on the homogeneous phantom exposed to four electroporation pulses of 1000 V. Current densities and electric field distributions in the homogeneous phantom were also successfully and reproducibly obtained for other pulse parameters (data not shown). Fig. 3 includes also results of the numerical model for the same phantom. The numerical results are in a good agreement with the experimental results as we obtained 7.8% relative error for homogeneous phantoms when we compared experimental with numerical results.

Current densities and electric field distribution obtained by CDI and MREIT in the heterogeneous phantom exposed to four electric pulses of 1000 V are shown in Fig. 4 along with the numerical model results. Current densities and electric field distributions in the heterogeneous phantoms were also successfully and reproducibly obtained for other pulse parameters (data not shown). When we compared experimental with numerical results, we obtained 9.2% and 22% relative error for more conductive half (σ_1) and less conductive half (σ_2) of the phantoms, respectively.

Measured electric currents during applied electric pulses by a current probe and by CDI are presented in Table I for the homogeneous and heterogeneous phantom together with the numerical model results.

In order to evaluate electric field distribution obtained with J-substitution, electric field diagonally across the phantom was compared with the electric field obtained by solving numerical model as shown in Fig. 5 for heterogeneous phantom.

Phantoms were exposed to different sequences of electric pulses which differed in number of applied electric pulses and by their amplitudes. Electric field distributions for the homogeneous phantom exposed to different number of pulses ($N = 1, 2, 4, 8$) with the amplitude of 1000 V are shown in Fig. 6. When we compared experimental with numerical results, we obtained an average relative error of 9.7%, 7.9%, 7.3%, and 6.2% for N = 1, 2, 4, and 8, respectively.

Electric field distributions in the homogeneous phantom for different amplitudes pulses ($U_{\mathbf{app}} = 1000, 1500, 2000$ V) of
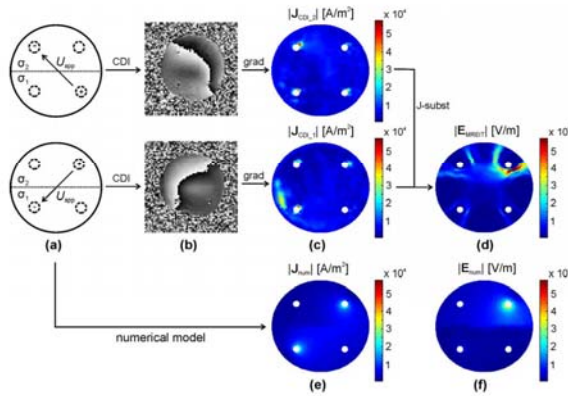
Fig. 4.   Heterogeneous phantom exposed to four electric pulses of 1000 V delivered between diagonal electrodes (a). Initial phase images (b) were acquired by the two-shot RARE CDI sequence. Current density distributions (c) in the phantom were obtained by applying (3) to phase images. Finally, the electric field distribution (d) was calculated using the J-substitution algorithm from both current density distributions. Due to heterogeneous electrical conductivity of the phantom two different current density distributions were needed to obtain a unique conductivity distribution. Corresponding numerical model results of current density distribution (e) and of electric field (f) distribution in the phantom are shown below experimental.

TABLE I
COMPARISON OF TWO EXPERIMENTAL (I_{osc} AND I_{int}) AND ONE NUMERICAL (I_{num}) APPROACH IN ASSESSMENT OF ELECTRIC CURRENTS IN ELECTROPORATION. I_{osc} PRESENTS ELECTRIC CURRENT MEASURED WITH THE OSCILLOSCOPE DURING PULSE DELIVERY, I_{int} IS A SOLUTION OF SURFACE INTEGRAL OVER MEASURED CURRENT DENSITY OBTAINED BY CDI AND I_{num} IS A SOLUTION OF THE NUMERICAL MODEL. RESULTS OF THREE EXPERIMENTS ARE PRESENTED AS MEANS $\pm$ STANDARD DEVIATION

	Homogeneous phantom			Heterogeneous phantom		
	U_{app} [V]			U_{app} [V]		
	1000	1500	2000	1000	2000	3000
I_{osc} [A]	3.3 ± 0.1	5.0 ± 0.2	8.9 ± 1.1	1.1 ± 0.1	2.1 ± 0.1	4.0 ± 0.6
I_{int} [A]	2.9 ± 0.3	4.6 ± 0.3	7.2 ± 1.8	1.5 ± 0.1	2.6 ± 0.2	3.8 ± 0.5
I_{num} [A]	3.2	4.9	6.5	1.2	2.3	3.5

four electric are shown in Fig. 7. When we compared experimental with numerical results, we obtained an average relative error of 6.4%, 7.1%, and 8.0% for $U_{app} = 1000$ V, 1500 V, and 2000 V, respectively.

IV.   DISCUSSION

The aim of our study was to investigate CDI and MREIT techniques for its feasibility to monitor the process of electroporation by measuring electric field distribution during electroporation. Experiments on homogeneous and heterogeneous phantoms were performed and compared to the results of the numerical model. Different number of pulses and of their amplitudes were used in separate experiments to evaluate feasibility of the methods to determine electric field distribution during the electroporation. Electric current flowing between
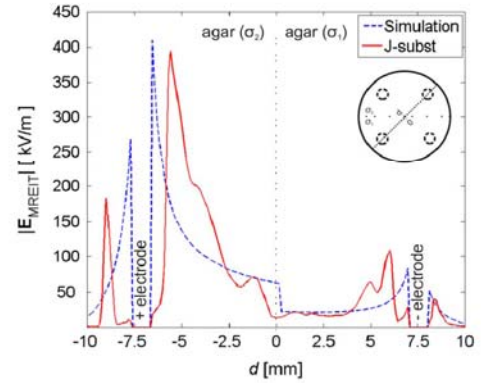
Fig. 5.   Electric field diagonally across the heterogeneous phantom (see dashed line in the right insert of the figure) calculated with the J-substitution algorithm (solid red line) and electric field calculated by the numerical model (blue dashed line). The phantom was exposed to four pulses of 1000 V. On the x axis d presents distance from the center to the border of the phantom.
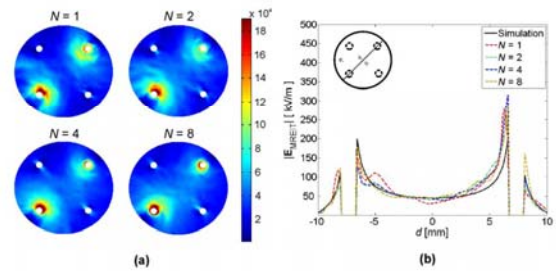
Fig. 6.   Electric field distribution (a) and electric field diagonally across the homogeneous phantom (b) for different number of electric pulses. The phantoms were exposed to one, two, four, or eight pulses of 1000 V.

the electrodes during pulse sequences was obtained with three different approaches, two experimental and one numerical. Results presented in Table I confirm good agreement between the approaches in both phantoms used and for most of the applied voltages. A minor discrepancy was observed between the homogeneous phantom exposed to pulses of 2000 V and the heterogeneous phantom exposed to pulses of 3000 V due to exceedingly high current in agar of the phantoms, resulting in its deterioration due to excessive heating and consequently in higher electrical conductivity. As shown in Fig. 5, experimentally and numerically obtained electric field profiles diagonally across the phantoms are in a good agreement. The largest disagreement between experimental and numerical results was observed in areas close to electrodes. Electrodes manly cause large distortions in the magnetic field and significant susceptibility artifacts. *Magnetic field distortion around electrodes* does not represent considerable problem to monitor electric field distribution during electroporation as the area between the electrodes is more important for efficient electroporation. CDI and MREIT allowed determination of the electric field distribution for all pulse sequences used in our study. The experiments showed that the electric field intensity and its distribution are independent of the number of electric pulses (Fig. 6) while solely its distribution is independent of their amplitude (Fig. 7).
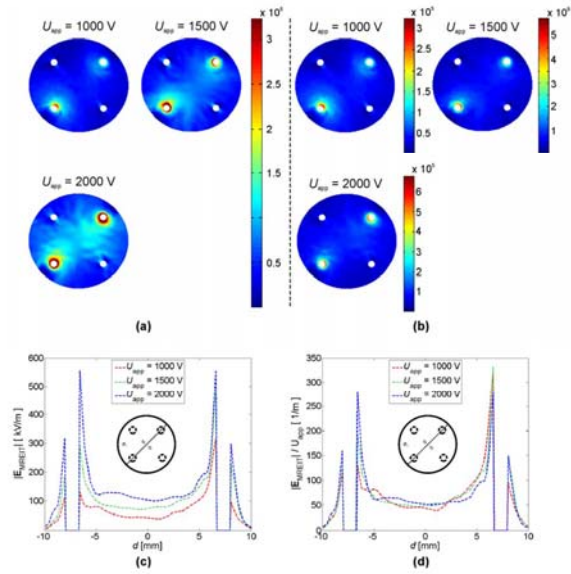
Fig. 7. Electric field distributions (a), (b) and electric fields diagonally across the phantoms (c) with homogenous electrical conductivity exposed to sequences of four electric pulses of different amplitudes (U_{app} = 1000 V, 1500 V, 2000 V). Electric field distributions on the upper left (a) are scaled to the same range while three distributions on the upper right (b) are scaled according to their maximum and minimum value of each distribution. Electric fields diagonally across the phantoms normalized to the amplitude of applied pulses ($|\mathbf{E}_{MREIT}|/U_{app}$) are also presented (d).

As already mentioned in the introduction, different attempts to monitor electroporation process were already proposed. Similar to MREIT, EIT is used for reconstruction of conductivity images only that voltage and current measurements of the EIT are limited to the boundaries of the object. Difficulties associated with the use of EIT to monitor electroporation process [20] are identical to those of using EIT to image tissue in general; numerous additional electrodes are required, sensitivity, spatial resolution and accuracy are low, while noise is high. Recent published report on MRI of nonthermal irreversible electroporation in vegetable tissue is limited in observation of only irreversible electroporation where the damage to the cellular membrane and the consequent release of intracellular content can be detected by comparing MRI images of different modalities (T_1-, T_2-weighted, FLAIR or STIR) acquired before and after the application of NTIRE pulses [23]. Similar method of comparing MRI images of different modalities was used to observe irreversible electroporation of liver tissues by detecting local fluid accumulation owing to transient permeabilization of blood vessels, as suggested by authors [24]. Main disadvantage of all of the above mentioned methods is the incapability to monitor electroporation during pulse delivery. This does not apply to the method of current and voltage measurement of delivered pulses described in [22], although this method inherits the main restraint of conductivity evaluation methods that are based on voltage/current measurements. Monitoring of voltage and current between only one pair of electrodes at a time can led to false conductivity and to an inaccurate electric field distribution

calculation due to lack of information on tissue heterogeneity between the electrodes. More accurate monitoring of electroporation during pulse delivery can be accomplished with acquiring current density information during pulse delivery and its transformation to the electric field distribution by means of proposed CDI and MREIT methods. As single two-shot RARE CDI sequence used in this study takes about 20 s and MREIT J-substitution algorithm additional few seconds, the electric field distribution can then be obtained in less than a minute after the beginning of pulse delivery in case of heterogeneous tissues. This time could be additionally reduced in future by means of faster CDI sequences.

The main limitation of our study lies in the phantom substance—agar, which became deteriorated after long exposure to high-voltage pulses resulting in measurement failure. A technical limitation of the MREIT algorithm used in this study is also inability of anisotropic conductivity measurement. For that reason implementation of more advanced MREIT methods [48] will be examined in our future studies. The difficulty of using MREIT to monitor electric field distribution during electroporation in a clinical environment is associated with the limited capability of MRI scanners for their use in interventional procedures, although recently a report on MREIT with an open magnet systems was published [49]. A question that needs answering in the near future is whether it is possible to obtain an accurate current density distribution in CDI from only one $\mathbf{B}$ component. However, it was already reported that longitudinal current density component J_z in a transversal imaging slice (xy-plane) can be successfully measured when current flows mainly in the transversal direction, i.e., the case when longitudinal electrodes, similar those used in ECT and NTIRE experiments, are used [50], [51].

NTIRE and ECT treatments are two electroporation applications that would probably benefit most with the implementation of CDI and MREIT. NTIRE is a new minimally invasive surgical technique for tissue ablation in which electroporation pulses form nanoscale defects in the cell membrane that lead to cell death, while ECT, a relatively new approach to cancer treatment and the most established in vivo application of electroporation, treats tumors by increasing the uptake of chemotherapeutic drugs into the tumor cells by exposing it to the electric field. Adequate local electric field distribution is crucial for success of both therapies. The treatment planning for ECT already proved to have a great potential in clinical use of ECT in treatment of tumors [52]. However, its applicability is currently limited due to uncertain conductivity values of treated areas, especially within the tumor where heterogeneous conductivity was already observed [53], resulting in obtaining inappropriate electrodes position and electric pulse parameters. Another concern is electrodes positioning during the ECT treatment procedure. Namely, it is difficult to insert electrodes precisely according to the treatment plan [54]. An imprecise placement of the electrodes can thus result in an inadequate electric field coverage of the treated area and therefore a treatment failure. Monitoring of the electric field distribution during ECT and NTIRE would enable detection of an insufficient electric field coverage before the end of the treatment, thus increasing and assuring the effectiveness of both methods.

V. CONCLUSION

Monitoring electric field distribution during tissue electroporation by means of CDI and MREIT is described and investigated both experimentally and numerically on homogeneous and heterogeneous phantom with electric properties similar to a liver and a tumor. Synchronization of electroporation pulses with the CDI sequence enabled imaging of current densities during electroporation. This was followed by calculation of the electric field distribution using the MREIT J-substitution method. A good agreement between experimental and numerical results was obtained, suggesting that CDI and MREIT can be used to determine the electric field during electric pulse delivery and that both of the methods can be of significant help in planning and monitoring of future electroporation based clinical applications such as electrochemotherapy, nonthermal irreversible electroporation ablation and electroporation based gene transfer for gene therapy.

ACKNOWLEDGMENT

REFERENCES

[1] L. M. Mir and S. Orlowski, "Mechanisms of electrochemotherapy," *Adv. Drug Delivery Rev.*, vol. 35, no. 1, pp. 107–118, 1999.
[2] E. Neumann, M. Schaeferridder, Y. Wang, and P. Hofschneider, "Gene-transfer into mouse lyoma cells by electroporation in high electric-fields," *EMBO J.*, vol. 1, no. 7, pp. 841–845, 1982.
[3] S. Orlowski, J. Belehradek, C. Paoletti, and L. M. Mir, "Transient electropermeabilization of cells in culture. Increase of the cytotoxicity of anticancer drugs," *Biochem. Pharmacol.*, vol. 37, no. 24, pp. 4727–4733, 1988.
[4] G. Serša, M. Čemažar, and D. Miklavčič, "Antitumor effectiveness of electrochemotherapy with cis-diamminedichloroplatinum(II) in mice," *Cancer Res.*, vol. 55, no. 15, pp. 3450–3455, 1995.
[5] A. M. Lebar, G. Sersa, S. Kranjc, A. Groselj, and D. Miklavcic, "Optimisation of pulse parameters in vitro for in vivo electrochemotherapy," *Anticancer Res.*, vol. 22, no. 3, pp. 1731–1736, 2002.
[6] R. V. Davalos, I. L. M. Mir, and B. Rubinsky, "Tissue ablation with irreversible electroporation," *Ann. Biomed. Eng.*, vol. 33, no. 2, pp. 223 231, 2005.
[7] D. Miklavcic, S. Corovic, G. Pucihar, and N. Pavselj, "Importance of tumour coverage by sufficiently high local electric field for effective electrochemotherapy," *Eur. J. Cancer Suppl.*, vol. 4, no. 11, pp. 45–51, 2006.
[8] D. Miklavcic, K. Beravs, D. Semrov, M. Cemazar, F. Demsar, and G. Sersa, "The importance of electric field distribution for effective in vivo electroporation of tissues," *Biophys. J.*, vol. 74, no. 5, pp. 2152–2158, 1998.
[9] M. Marty *et al.*, "Electrochemotherapy—An easy, highly effective and safe treatment of cutaneous and subcutaneous metastases: Results of ESOPE study," *Eur. J. Cancer Suppl.*, vol. 4, no. 11, pp. 3–13, 2006.
[10] G. Sersa and D. Miklavcic, "Electrochemotherapy of tumours," *J. Vis. Experiments*, no. 22, 2008.
[11] F. Andre *et al.*, "Efficiency of high- and low-voltage pulse combinations for gene electrotransfer in muscle, liver, tumor, and skin," *Human Gene Therapy*, vol. 19, no. 11, pp. 1261–1271, 2008.
[12] L. Heller and R. Heller, "Electroporation gene therapy preclinical and clinical trials for melanoma," *Current Gene Therapy*, vol. 10, no. 4, pp. 312–317, 2010.
[13] A. I. Daud *et al.*, "Phase I trial of interleukin-12 plasmid electroporation in patients with metastatic melanoma," *J. Clin. Oncol.*, vol. 26, no. 36, pp. 5896–5903, 2008.
[14] L. Zhang, G. Widera, and D. Rabussay, "Enhancement of the effectiveness of electroporation-augmented cutaneous DNA vaccination by a particulate adjuvant," in *Bioelectrochemistry*, Amsterdam, The Netherlands, 2004, vol. 63, no. 1–2, pp. 369–373.

[15] P. A. Garcia *et al.*, "Non-thermal irreversible electroporation (N-TIRE) and adjuvant fractionated radiotherapeutic multimodal therapy for intracranial malignant glioma in a canine patient," *Technol. Cancer Res. Treatment*, vol. 10, no. 1, pp. 73–83, 2011.
[16] J. Rubinsky, G. Onik, P. Mikus, and B. Rubinsky, "Optimal parameters for the destruction of prostate cancer using irreversible electroporation," *J. Urol.*, vol. 180, no. 6, pp. 2668–2674, 2008.
[17] J. Gehl and L. M. Mir, "Determination of optimal parameters for in vivo gene transfer by electroporation, using a rapid in vivo test for cell permeabilization," *Biochem. Biophys. Res. Commun.*, vol. 261, no. 2, pp. 377–380, 1999.
[18] D. Miklavcic, D. Semrov, H. Mekid, and L. M. Mir, "A validated model of in vivo electric field distribution in tissues for electrochemotherapy and for DNA electrotransfer for gene therapy," *Biochimica Et Biophysica Acta*, vol. 1523, no. 1, pp. 73–83, Sept. 2000.
[19] N. Pavšelj and D. Miklavčič, "Numerical modeling in electroporation-based biomedical applications," *Radiol. Oncol.*, vol. 42, no. 3, pp. 159–168, 2008.
[20] R. V. Davalos, D. M. Otten, L. M. Mir, and B. Rubinsky, "Electrical impedance tomography for imaging tissue electroporation," *IEEE Trans. Biomed. Eng.*, vol. 51, no. 5, pp. 761–767, May 2004.
[21] Y. Granot, A. Ivorra, E. Maor, and B. Rubinsky, "In vivo imaging of irreversible electroporation by means of electrical impedance tomography," *Phys. Med. Biol.*, vol. 54, no. 16, pp. 4927–4943, 2009.
[22] D. Cukjati, D. Batiuskaite, F. André, D. Miklavcic, and L. M. Mir, "Real time electroporation control for accurate and safe in vivo non-viral gene therapy," *Bioelectrochemistry*, vol. 70, no. 2, pp. 501–507, 2007.
[23] M. Hjouj and B. Rubinsky, "Magnetic resonance imaging characteristics of nonthermal irreversible electroporation in vegetable tissue," *J. Membrane Biol.*, vol. 236, no. 1, pp. 137–146, 2010.
[24] Y. Zhang *et al.*, "MR imaging to assess immediate response to irreversible electroporation for targeted ablation of liver tissues: Preclinical feasibility studies in a rodent model," *Radiology*, vol. 256, no. 2, pp. 424–432, 2010.
[25] H. Gamba and D. Delpy, "Measurement of electrical current density distribution within the tissues of the head by magnetic resonance imaging," *Med. Biol. Eng. Comput.*, vol. 36, no. 2, pp. 165–170, 1998.
[26] M. Joy, G. Scott, and M. Henkelman, "Invivo detection of applied electric currents by magnetic-resonance imaging," *Magn. Reson. Imag.*, vol. 7, no. 1, pp. 89–94, 1989.
[27] G. Scott, M. Joy, R. Armstrong, and R. Henkelman, "Measurement of nonuniform current-density by magnetic-resonance," *IEEE Trans. Med. Imag.*, vol. 10, no. 3, pp. 362–374, Sep. 1991.
[28] O. Kwon, E. Woo, J. Yoon, and J. Seo, "Magnetic resonance electrical impedance tomography (MREIT): Simulation study of J-substitution algorithm," *IEEE Trans. Biomed. Eng.*, vol. 49, no. 2, pp. 160–167, Feb. 2002.
[29] E. J. Woo, S. Y. Lee, and C. W. Mun, "Impedance tomography using internal current density distribution measured by nuclear magnetic resonance," in *Proc. SPIE*, 1994, pp. 377–385.
[30] M. Eyuboglu, O. Birgul, and Y. Z. Ider, "A dual modality system for high resolution—True conductivity imaging," in *Proc. XI Int. Conf. Elec. Bioimpedance (ICEBI)*, 2001, pp. 409–13.
[31] O. Kwon, J. Lee, and J. Yoon, "Equipotential line method for magnetic resonance electrical impedance tomography," *Inverse Problems*, vol. 18, no. 4, pp. 1089–1100, 2002.
[32] J. K. Seo, J.-R. Yoon, E. J. Woo, and O. Kwon, "Reconstruction of conductivity and current density images using only one component of magnetic field measurements," *IEEE Trans. Biomed. Eng.*, vol. 50, no. 9, pp. 1121–1124, Sep. 2003.
[33] S. H. Oh *et al.*, "Conductivity and current density image reconstruction using harmonic Bz algorithm in magnetic resonance electrical impedance tomography," *Phys. Med. Biol.*, vol. 48, no. 19, pp. 3101–3116, 2003.
[34] H. J. Kim *et al.*, "In vivo high-resolution conductivity imaging of the human leg using MREIT: The first human experiment," *IEEE Trans. Med. Imag.*, vol. 28, no. 11, pp. 1681–1687, Nov. 2009.
[35] H. J. Kim *et al.*, "In vivo electrical conductivity imaging of a canine brain using a 3 T MREIT system," *Physiol. Measurement*, vol. 29, no. 10, pp. 1145–1155, 2008.
[36] E. J. Woo, H. J. Kim, A. S. Minhas, Y. T. Kim, W. C. Jeong, and O. Kwon, "Electrical conductivity imaging of lower extremities using MREIT: Postmortem swine and in vivo human experiments," in *Proc. Annu. Int. Conf. IEEE Eng. Med. Biol. Soc. Conf.*, 2008, pp. 5830–5833.

[37] T. Kotnik, G. Pucihar, and D. Miklavčič, "Induced transmembrane voltage and its correlation with electroporation-mediated molecular transport," *J. Membrane Biol.*, vol. 236, no. 1, pp. 3–13, 2010.

[38] I. Sersa, K. Beravs, N. J. Dodd, S. Zhao, D. Miklavcic, and F. Demsar, "Electric current density imaging of mice tumors," *Magn. Reson. Med.*, vol. 37, no. 3, pp. 404–409, 1997.

[39] D. Haemmerich, D. J. Schutt, A. W. Wright, J. G. Webster, and D. M. Mahvi, "Electrical conductivity measurement of excised human metastatic liver tumours before and after thermal ablation," *Physiol. Measurement*, vol. 30, no. 5, pp. 459–466, 2009.

[40] S. Gabriel, R. W. Lau, and C. Gabriel, "The dielectric properties of biological tissues: II. Measurements in the frequency range 10 Hz to 20 GHz," *Phys. Med. Biol.*, vol. 41, no. 11, pp. 2251–2269, 1996.

[41] S. Laufer, A. Ivorra, V. E. Reuter, B. Rubinsky, and S. B. Solomon, "Electrical impedance characterization of normal and cancerous human hepatic tissue," *Physiol. Measurement*, vol. 31, no. 7, pp. 995–1009, 2010.

[42] L. M. Mir, J. Gehl, and G. Sersa, "Standard operating procedures of the electrochemotherapy: Instructions for the use of bleomycin or cisplatin administered either systemically or local," *Eur. J. Cancer (Suppl.)*, no. 4, pp. 14–25, 2006.

[43] I. Sersa, "Auxiliary phase encoding in multi spin-echo sequences: Application to rapid current density imaging," *J. Magn. Reson.*, vol. 190, no. 1, pp. 86–94, 2008.

[44] J. Hennig, A. Nauerth, and H. Friedburg, "RARE imaging: A fast imaging method for clinical MR," *Magn. Reson. Med.*, vol. 3, no. 6, pp. 823–833, 1986.

[45] H. Khang *et al.*, "J-substitution algorithm in magnetic resonance electrical impedance tomography (MREIT): Phantom experiments for static resistivity images," *IEEE Trans. Med. Imag.*, vol. 21, no. 6, pp. 695–702, Jun. 2002.

[46] H. S. Nam, B. I. Lee, J. Choi, C. Park, and O. I. Kwon, "Conductivity imaging with low level current injection using transversal J-substitution algorithm in MREIT," *Phys. Med. Biol.*, vol. 52, no. 22, pp. 6717–6730, 2007.

[47] S. Kim, O. Kwon, J. Seo, and J. Yoon, "On a nonlinear partial differential equation arising in magnetic resonance electrical impedance tomography," *SIAM J. Math. Anal.*, vol. 34, no. 3, pp. 511–526, 2003.

[48] H. S. Nam and O. I. Kwon, "Axial anisotropic conductivity imaging based on projected current density in MREIT," *IEEE Trans. Med. Imag.*, vol. 29, no. 3, pp. 781–789, Mar. 2010.

[49] H. Wang, Y. Wang, W. Yang, Z. Wang, and L. Hu, "Conductivity image reconstruction of oblique slice with c-shaped open permanent magnet MRI systems," *IEEE Trans. Appl. Supercond.*, vol. 20, no. 3, pp. 814–817, 2010.

[50] C. Park, B. I. Lee, and O. I. Kwon, "Analysis of recoverable current from one component of magnetic flux density in MREIT and MRCDI," *Phys. Med. Biol.*, vol. 52, no. 11, pp. 3001–3013, 2007.

[51] J. Seo, O. Kwon, B. Lee, and E. Woo, "Reconstruction of current density distributions in axially symmetric cylindrical sections using one component of magnetic flux density: Computer simulation study," *Physiol. Measurement*, vol. 24, no. 2, pp. 565–577, 2003.

[52] D. Miklavcic *et al.*, "Towards treatment planning and treatment of deep-seated solid tumors by electrochemotherapy," *Biomed. Eng. OnLine*, vol. 9, no. 1, p. 10, 2010.

[53] L. Muftuler, M. Hamamura, O. Birgul, and O. Nalcioglu, "In vivo MRI electrical impedance tomography (MREIT) of tumors," *Technol. Cancer Res. Treatment*, vol. 5, no. 4, pp. 381–387, 2006.

[54] B. Kos, A. Zupanic, T. Kotnik, M. Snoj, G. Sersa, and D. Miklavcic, "Robustness of treatment planning for electrochemotherapy of deep-seated tumors," *J. Membrane Biol.*, vol. 236, no. 1, pp. 147–153, 2010.

ARTICLE 2

Title: *Ex vivo* and *in silico* feasibility study of monitoring electric field distribution in tissue during electroporation based treatments

Authors: KRANJC Matej, BAJD Franci, SERŠA Igor, WOO Eung Je, MIKLAVČIČ Damijan

Publication: PLoS ONE

DOI: 10.1371/journal.pone.0045737

Year: 2012

Volume: 7

Number: 9

Pages: e45737

Impact factor: 4.092

Ranking:

Category name	Total journals in category	Journal rank in category	Quartile in category
biology	84	12	Q1

PLOS | ONE

Ex Vivo and *In Silico* Feasibility Study of Monitoring Electric Field Distribution in Tissue during Electroporation Based Treatments

Matej Kranjc[1], Franci Bajd[2], Igor Sersa[2], Eung Je Woo[3], Damijan Miklavcic[1]*

1 Faculty of Electrical Engineering, University of Ljubljana, Ljubljana, Slovenia, 2 Institut Jozef Stefan, Ljubljana, Slovenia, 3 Department of Biomedical Engineering, Kyung Hee University, Seoul, Republic of Korea

Abstract

Magnetic resonance electrical impedance tomography (MREIT) was recently proposed for determining electric field distribution during electroporation in which cell membrane permeability is temporary increased by application of an external high electric field. The method was already successfully applied for reconstruction of electric field distribution in agar phantoms. Before the next step towards *in vivo* experiments is taken, monitoring of electric field distribution during electroporation of *ex vivo* tissue *ex vivo* and feasibility for its use in electroporation based treatments needed to be evaluated. Sequences of high voltage pulses were applied to chicken liver tissue in order to expose it to electric field which was measured by means of MREIT. MREIT was also evaluated for its use in electroporation based treatments by calculating electric field distribution for two regions, the tumor and the tumor-liver region, in a numerical model based on data obtained from clinical study on electrochemotherapy treatment of deep-seated tumors. Electric field distribution inside tissue was successfully measured *ex vivo* using MREIT and significant changes of tissue electrical conductivity were observed in the region of the highest electric field. A good agreement was obtained between the electric field distribution obtained by MREIT and the actual electric field distribution in evaluated regions of a numerical model, suggesting that implementation of MREIT could thus enable efficient detection of areas with insufficient electric field coverage during electroporation based treatments, thus assuring the effectiveness of the treatment.

Introduction

Electrochemotherapy (ECT) and nonthermal irreversible electroporation ablation (NTIRE) are potent procedures used in solid tumor treatment. In addition, NTIRE is also promising ablation method for nonmalignant tissues. Both, ECT and NTIRE, rely on cell membrane electroporation, a process which increases cell membrane permeability due to externally applied electric field [1–3]. ECT combines electroporation with the use of chemotherapeutic drugs, which exhibit higher cytotoxicity when they are combined [4–7]. ECT has been successfully used for treatment of cutaneous and subcutaneous metastasis of various cancers achieving over 70% complete responses [6] on over 3000 treated patients in Europe since 2006 [8]. In NTIRE the extensive membrane electroporation alone leads to a loss of cell homeostasis and finally to cell death [9,10].

Recently, ECT and NTIRE have been also used in treatment of deep-seated tumors [11,12]. Electroporation based treatments efficiency is correlated to electric field distribution [13]. More specifically, at a given number and duration of pulses, the local electric field is the critical factor determining tissue electroporation. In order to ensure adequate electric field coverage of the treated tissue treatment, planning using numerical modeling was

introduced [14,15]. It also needs to be noted that cell membrane conductivity and consequently cell/tissue conductivity are increased after electroporation in a nonlinear way [16,17]. Unfortunately, this nonlinear tissue conductivity increase due to electroporation along with uncertainty of tissue conductivity determination makes treatment plan inaccurate and thus inherently unreliable. Another factor influencing success of the electroporation treatment is inaccuracy in electrode positioning with respect to the target tissue [14,18]. Both, tissue conductivity and electrode positioning were also highlighted as major unknowns in a recent publication on patient specific treatment planning for electroporation based therapies [19]. It is therefore important to find efficient means of electroporation process monitoring on site. Two promising methods for monitoring electroporation are electrical impedance tomography (EIT) and magnetic resonance imaging (MRI). EIT was already successfully applied in vivo [20,21] however it introduces demanding implementation of additional electrodes and solving the mathematically ill-posed problem of determining conductivity from boundary voltage measurements. MRI was also used to detect electroporated tissue regions, however not *in situ* and only for irreversible electroporation based treatments such as NTIRE [22,23]. Recently, a method based on magnetic resonance

electrical impedance tomography (MREIT) was suggested for monitoring an electric field distribution during irreversible and also reversible electroporation based treatments such as ECT [24]. MREIT would namely allow determination of electric field distribution *in situ* thus taking into account actual tissue conductivity and electrodes position. Since electric field distribution is available immediately after the delivery of electric pulses also corrective intervention would be possible.

The aim of this study was to investigate whether electric field distribution during electroporation of *ex vivo* liver tissue can be efficiently monitored by MREIT. In addition, feasibility of using MREIT to monitor electric field distribution during electroporation based treatments was evaluated *in silico* on a recently reported case [11].

Materials and Methods

Preparation of ex vivo Tissue Sample

Chicken liver primarily intended for human consumption were obtained from a slaughterhouse (Perutnina Ptuj, d.d., Ptuj, Slovenia) which operates in accordance to Slovenian law. Experiments were in compliance with the slaughterhouse as all of their goods are produced strictly for human consumption. The process of slaughtering is regulated by Rules on animal protection and welfare at slaughter (Ur.l. RS, N. 5/2006) which ensures ethical standards of slaughtering procedure and is in compliance with European Union Council directive on the protection of animals at the time of slaughter or killing (93/119/EC). Temperature of the tissue was maintained at 4°C before the beginning of experiment when they were allowed to heat up to the room temperature. Tissues were sectioned in flat and cylindrical shaped samples with a diameter of 20 mm and placed in an acrylic glass container (see Fig. 1). Four cylindrically shaped platinium-iridium electrodes with a diameter of 1 mm were placed inside. Samples were then inserted in the 25 mm RF probe and connected to the electric pulse generator using cables including a low-pass filter to avoid possible RF disturbances in the NMR signal. The sequence of four high voltage electric pulses with an amplitude U_{el} of either 1000 V or 1500 V and a duration of 100 μs were delivered between electrode pairs 1–2 and 1–3 by an electric pulse generator Cliniporator Vitae (IGEA, Carpi, Italy) to establish electric field distribution below and above reversible electroporation threshold value in the case of U_{el} = 1000 V and U_{el} = 1500 V, respectively. Electroporation threshold values were already determined in previous study [25] and were adjusted to our pulse parameters [26]. The current and voltage of electric pulses were also measured with an oscilloscope (WavePro 7300A, LeCroy, USA) using current probe (AP015, LeCroy, USA) and high-voltage probe (PPE2KV, LeCroy, USA). All experiments were repeated three times for each electrode/voltage arrangement. The sample was replaced with a fresh one after each electroporation pulse delivery to ensure identical initial conditions in all electroporation experiments.

Magnetic Resonance Electrical Impedance Tomography

MREIT algorithms are in general used for reconstruction of conductivity distribution inside samples [27,28], although they can also be applied for reconstruction of electric field. MREIT is based on current density imaging (CDI) which is an MRI method for acquiring current density distribution inside samples. Briefly, in CDI, maps of image signal phase shift are acquired after application of electric current pulses to the sample [29]. The phase shift is proportional to the average magnetic field change in the sample (in the direction of the static magnetic field) caused by
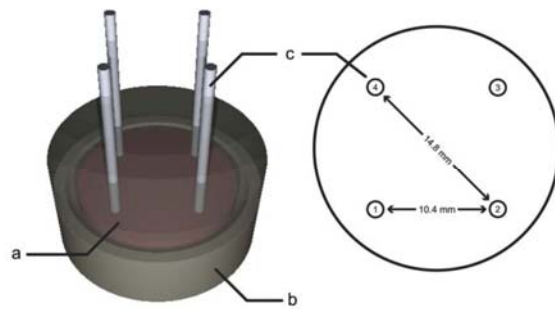
Figure 1. Liver sample with inserted electrodes placed in an acrylic glass container. A liver sample (a) was placed in an acrylic glass container (b). Four needle electrodes (c) were inserted in the sample through predesigned holes in the container. Sequences of electric pulses were delivered between electrode pairs 1–2 and 1–3. doi:10.1371/journal.pone.0045737.g001

currents flowing through the sample. By rotating sample along with the electrodes to different perpendicular orientations, different vector components of electric current induced magnetic field change can be obtained from current induced phase shift φ stored in acquired images

$$\varphi_{x/y/z} = \gamma t_c B_{x/y/z}. \tag{1}$$

where γ is the proton gyromagnetic ratio and t_c is the total duration of the applied electric pulses. Once these are known, electric current density in the sample $\mathbf{J} = (\mathcal{J}_x, \mathcal{J}_y, \mathcal{J}_z)$ can be calculated from the current induced magnetic field change vector $\mathbf{B}_c = (B_x, B_y, B_z)$ using Ampere's law

$$\mathbf{J} = \frac{1}{\mu_0} \nabla \times \mathbf{B}_c. \tag{2}$$

As rotating of the sample to different orientations can cause unwanted pixel misalignments and sample deformation, geometry of *ex vivo* tissue presented in this study was such that currents were flowing predominantly in the plane perpendicular to the electrodes. This allowed a simpler current distribution reconstruction by disregarding two negligible in-slice magnetic field change components (B_x, B_y) and using only the nonzero component in direction parallel to the imaging slice, i.e. B_z, for calculation of the current density $\mathbf{J}_{CDI} = (\mathcal{J}_x, \mathcal{J}_y)$

$$\mathbf{J}_{CDI} = \frac{1}{\mu_0} \left(\frac{\partial B_z}{\partial y}, -\frac{\partial B_z}{\partial x} \right). \tag{3}$$

MR images of current induced magnetic field changes were obtained by means of two-shot RARE CDI sequence [30] as shown in Fig. 2 with parameters: imaging matrix 64×64, field of view 30 mm, inter-echo delay 2.64 mm, echo time of the current encoding period 20 ms and the time interval between two RARE signal acquisitions was 10 s. MR imaging was performed on a TecMag NMR spectrometer connected to an Oxford 2.35 T horizontal bore superconducting magnet. The MRI system was equipped with Bruker microimaging accessories with maximum gradients of 250 mT/m.
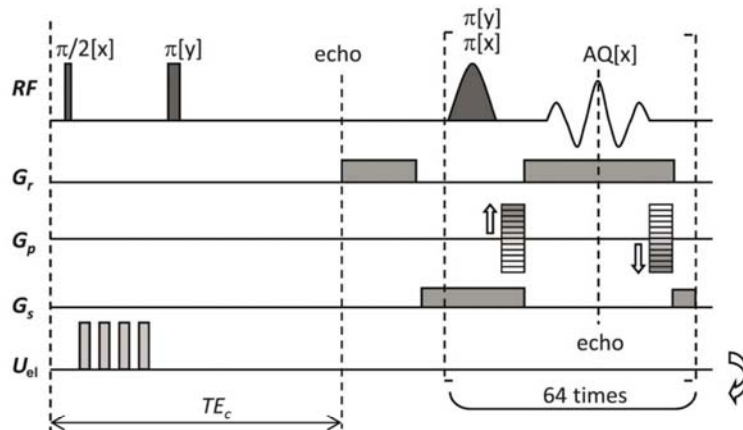
Figure 2. Two-shot RARE CDI sequence.
doi:10.1371/journal.pone.0045737.g002

After current density inside the sample was obtained, the MREIT J-substitution algorithm was applied. The algorithm is based on iteratively solving of Laplace's equation:

$$\nabla \cdot \left(\sigma^k \nabla u^k \right) = 0 \text{ in } \Omega \tag{4}$$

where u satisfies the following boundary conditions:

$$\sigma^k \frac{\partial u^k}{\partial n} = 0 \text{ on } \Omega \tag{5}$$

$$u^k = U_{el} \text{ on } \Omega_e \tag{6}$$

where Ω is the sample body, Ω_e is the boundary of the electrodes, n denotes normal vector to the boundary, U_{el} is the voltage on the electrodes measured by the generator, σ is unknown electrical conductivity of the sample and k denotes a number of current iteration. Electrical conductivity was updated after each iteration $(k+1)$

$$\sigma^{k+1} = \frac{|\mathbf{J}_{CDI}|}{|\nabla u^k|} \tag{7}$$

where $\mathbf{J}_{CDI}$ is current density obtained by CDI method. When difference between two successive conductivities σ falls below 0.01 electric field distribution E can be calculated using Ohm's law

$$\mathbf{E} = \frac{\mathbf{J}_{CDI}}{\sigma}. \tag{8}$$

Calculations were performed with the numerical computational environment Matlab 2011a (Mathworks, Natick, MA) on a desktop PC (Windows 7, 2.66 GHz, 4 GB RAM) using a finite element method.

3-D Numerical Model

In order to evaluate the proposed MREIT algorithm used to acquire the current and electric field distribution during electro-poration based treatments without rotating the subject, i.e. using only one **B** component, we performed a simulation in the case of a 3-D numerical model designed for the purpose of an electro-chemotherapy treatment of deep-seated liver tumors. The treatment was done as part of an on-going Phase I/II clinical study (EudraCT number 2008-008290-54; clinicaltrials.org – NCT01264952). The study was approved by Institutional Medical Board and Ethical Committee of the Republic of Slovenia. A report of the treatment was published by Edhemovic *et al*, where all details about the treatment procedure can be found [11].

Briefly, a model of a patient with a metastasis located between the inferior vena cava (IVC) and the main hepatic veins was studied. The model included a 3-D geometry of the metastasis that was built by means of segmented MRI images of the patient [31]. The numerical model distinguishes between three tissues as shown in Fig. 3: liver, tumor and blood vessels. Six electrodes were inserted in a configuration as obtained after genetic algorithm optimization [32]. For the purpose of *in silico* MREIT evaluation we focused on two regions between two pairs of electrodes where electroporation occurs due to the highest electric field. The first region or the tumor region was situated between the electrode pair 3–4. The tumor had a homogeneous electrical conductivity $\sigma_T = 0.4$ S/m. The second region or the tumor-liver region was situated between the electrode pair 4–6. The region consisted of tumor and liver tissues, each with its own electrical conductivity. The liver had a homogeneous electrical conductivity $\sigma_L = 0.05$ S/m. On the border between tumor and liver tissue we applied gradual change of electrical conductivity using sigmoid curve.

The magnetic field density $\mathbf{B}^* = (B_x, B_y, B_z)$ and the electric field distribution $\mathbf{E}^* = (E_x, E_y, E_z)$ were calculated for two regions – the tumor and the tumor-liver region by applying electric pulses with amplitudes of $U_{app} = 1700$ V and $U_{app} = 2100$ V between each pair of electrodes (3–4 and 4–6, respectively). The obtained electric field distribution $\mathbf{E}^*$ can be considered as an actual electric field distribution. It was used as a reference in evaluation of MREIT results using only one $\mathbf{B}^*$ component, i.e. B_z, established during application of pulses in one direction (either between electrodes pair 3–4 or 4–6). These calculations were done by solving the 3-D numerical model using the finite element method with the commercial finite element software package COMSOL Multiphysics 3.5a (COMSOL AB, Stockholm, Sweden). The current density distribution $\mathbf{J}_{CDI} = (J_x, J_y)$ was calculated using Eq.
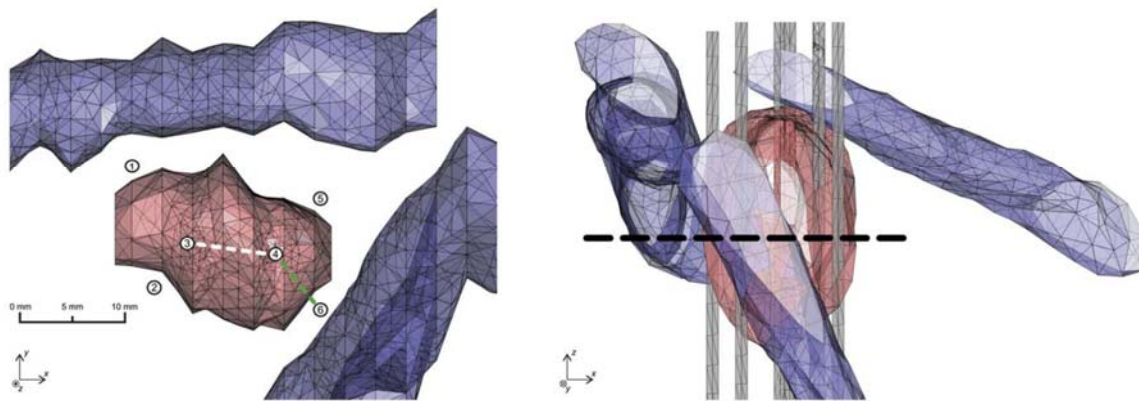
Figure 3. 3-D numerical model of a deep-seated tumor in a liver. A 3-D numerical model of a deep-seated tumor in a liver observed from two different viewing angles. The tumor (in red) was located between the IVC and main hepatic veins (all in blue). The liver tissue, surrounding the tumor and veins, is not shown for the purpose of visualization. Electrodes (in grey) are labeled with numbers from 1 to 6. Two regions in an xy-plane in the middle of the tumor (black dashed line) were evaluated: the tumor region (between electrodes no. 3 and 4; white dashed line) and the region consisted of a tumor and a liver tissue (between electrodes no. 4 and 6; green dashed line).
doi:10.1371/journal.pone.0045737.g003

(3) by means of only the component B_z in an xy-plane positioned across the middle of the tumor (see Fig. 3). Electric field distribution $\mathbf{E}_{\mathrm{MREIT}} = (\tilde{E}_x, \tilde{E}_y)$ within the xy-plane was calculated using Ohm's law

$$\mathbf{E}_{\mathrm{MREIT}} = \frac{\mathbf{J}_{\mathrm{CDI}}}{\sigma_{\mathrm{MREIT}}}, \qquad (9)$$

where σ_{MREIT} is electrical conductivity distribution of liver and tumor obtained by the J-substitution algorithm as described in [24].

Results

When a tissue sample is exposed to electroporation pulses an electric current density and electric field are established inside the tissue. The former was successfully measured by the CDI method using only the B_z component, while the later was obtained from the CDI data using the MREIT J-substitution algorithm. Electrical conductivities, calculated using the MREIT algorithm, are presented together with current densities in Fig. 4, which correspond to the experiment on the liver tissues exposed to four 100 µs long electroporation pulses with different amplitudes ($U_{\mathrm{el}} = 1000$ V and $U_{\mathrm{el}} = 1500$ V). When tissue was exposed to electric pulses with an amplitude of $U_{\mathrm{el}} = 1000$ V no significant alteration of electrical conductivity was measured except near boundaries and in the region of inactive electrode. On contrary, major changes of conductivity were observed in the region between the electrodes compared to the rest of the tissue when it was exposed to pulses with $U_{\mathrm{el}} = 1500$ V. Current density was at both applied amplitudes the highest near the active electrodes and in the region of increased conductivity in the case of $U_{\mathrm{el}} = 1500$ V.

Measured electric current and voltage for liver tissues exposed to four 100 µs long electroporation pulses with different amplitudes ($U_{\mathrm{el}} = 1000$ V and $U_{\mathrm{el}} = 1500$ V) are presented in Fig. 5.

Electric field distributions in the liver tissue for electric pulses with different amplitudes ($U_{\mathrm{el}} = 1000$ V and $U_{\mathrm{el}} = 1500$ V) delivered between the electrode pairs 1–2 and 1–3 are shown in Fig. 6. As expected, the electric field was the highest around electrodes and was larger in $U_{\mathrm{el}} = 1500$ V case than in $U_{\mathrm{el}} = 1000$

V, as well as higher in case when pulses were delivered between electrodes pair 1–2 than between 1–3. Results were successfully and reproducibly obtained in all treated liver tissues.

Evaluation results of MREIT to monitor electric field distribution during electroporation based treatments are presented in Fig. 7. An electric field distribution across the tumor region and in the tumor-liver region obtained by means of the MREIT algorithm using only the B_z component is compared with the corresponding true electric field calculated by the 3-D numerical model of a deep-seated tumor in liver.

Discussion

The aim of this study was to investigate feasibility of the MREIT technique to monitor electric field distribution during tissue electroporation by means of an *ex vivo* liver tissue experiment. Feasibility of MREIT to use in electroporation based treatments such as electrochemotherapy and nonthermal irreversible electroporation ablation was evaluated also using numerical modeling on a recently reported case.

As shown in Figs. 4 and 6, electric field and electric conductivity distributions within liver tissue during application of electroporation pulses were successfully obtained. When examining results and comparing them to our previous findings on agar phantoms, considerable differences were however observed [24]. While dielectric properties of agar remained unchanged in spite of applied high electric field, presumably due absence of a cell structure in an agar gel [33], significant changes of the liver tissue electrical conductivity were observed when tissue was exposed to pulses with an amplitude of $U_{\mathrm{el}} = 1500$ V (Fig. 4). The region with a higher electrical conductivity between electrodes was established as a consequence of tissue changes associated to a high electric field in the region. Such changes were not detected in tissue exposed to pulses with an amplitude of $U_{\mathrm{el}} = 1000$ V due to lower electric field. Observed tissue changes are a consequence of local tissue electroporation as electric field in the region between electrodes exceeded reversible threshold value in the case of $U_{\mathrm{el}} = 1500$ V whereas most of this region remained under the threshold value in the case of $U_{\mathrm{el}} = 1000$ V. Comparison of electric current (Fig. 5) also confirms increment of electrical conductivity
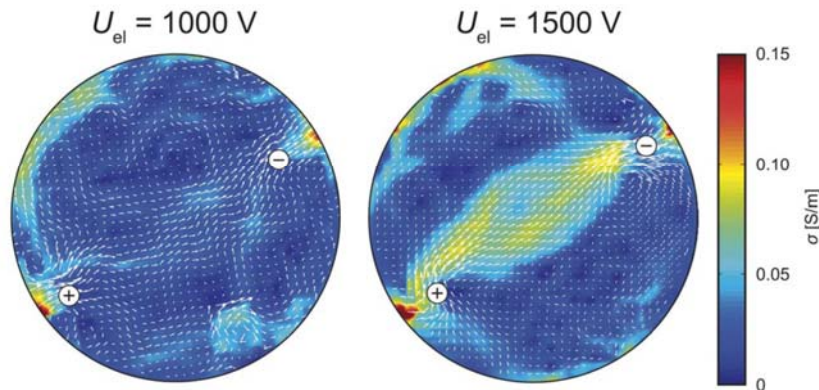
Figure 4. Electrical conductivitiy of a liver tissue obtained by MREIT. An electrical conductivity of a liver tissue obtained by MREIT. Tissues were exposed to four 100 µs long electric pulses with an amplitude of U_{el} = 1000 V (left figure) and 1500 V (right figure). Pulses were delivered between two needle electrodes (marked with + and −). The corresponding electric current densities are presented as a vector field (white arrows). A length of arrows corresponds to current density magnitude.
doi:10.1371/journal.pone.0045737.g004

as amplitudes value of electric current in liver tissue approximately doubled (from 320 mA to 670 mA) when the voltage was increased for only half of its value (from 1000 V to 1500 V). Similar changes of tissue conductivity after electroporation were already observed and have been reported previously [17,34]. It also needs to be noted that local alterations of conductivity near the boundary of the container and in the region of inactive electrode in Fig. 4 are measurement errors due to distortions of magnetic field caused by electrodes and due to noise near the boundary where the lower limit of sensitivity in CDI is met.

Implementation of MREIT during electroporation pulse delivery could significantly improve electroporation procedures in clinical applications such as ECT and NTIRE. Adequate electric field distribution and sufficiently high local electric field are two of the most important conditions for successful realization of both therapies. Even though the treatment planning for ECT already proved in clinical treatment of deep-seated tumors [14], its

applicability is limited for now due to conductivity values of treated tissues which were determined with high uncertainty. As a consequence treatment plan can yield inappropriate electric pulse parameters and electrode configuration. Another concern is electrodes positioning during the treatment procedure as it is difficult to place electrodes accurately according to the treatment plan [18]. An imprecise insertion of the electrodes can establish inadequate electric field coverage of the treated tissue which can lead to a treatment failure. Monitoring of the electric field distribution during ECT and NTIRE by means of MREIT would thus enable detection of insufficient electric field coverage before potential treatment failure, hence assuring and increasing the effectiveness of both methods. Some previously reported difficulties associated with the use of MREIT [24] have been addressed as part of this study. We have successfully evaluated a major concern of the MREIT use, namely, whether it is possible to obtain an accurate electric field distribution from only one **B** component
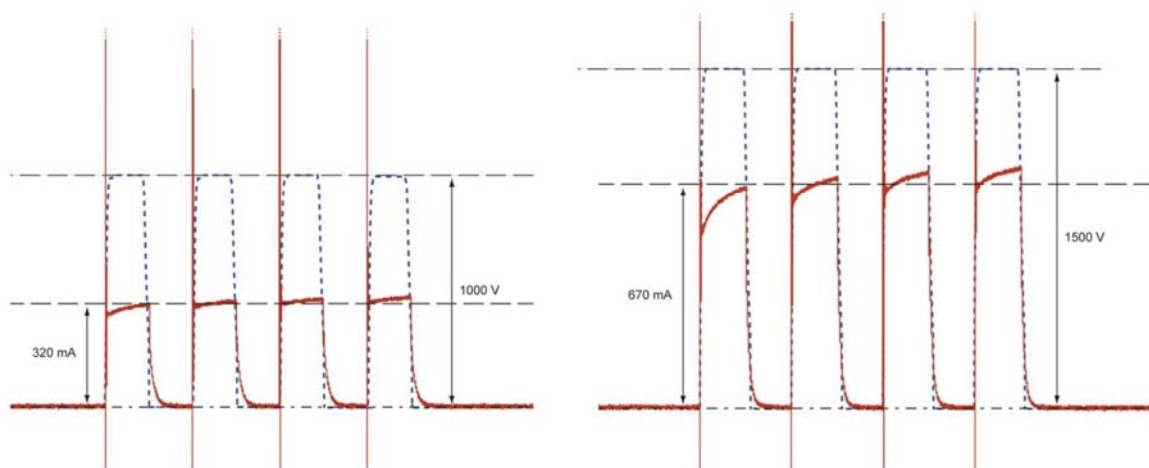
Figure 5. Electric current and voltage in liver tissue. Electric current (red solid line) and voltage (blue dashed line) in liver tissue exposed to four 100 µs long electric pulses with an amplitude of U_{el} = 1000 V (left figure) and 1500 V (right figure).
doi:10.1371/journal.pone.0045737.g005
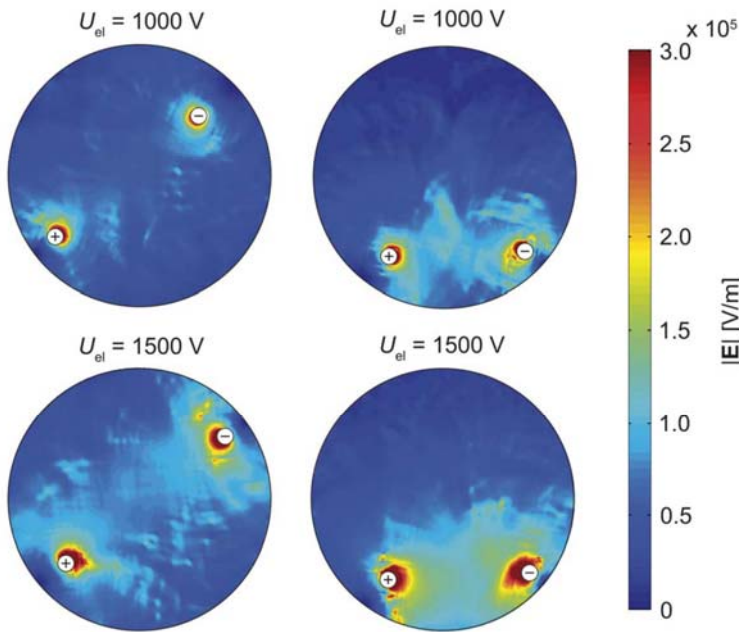
Figure 6. Electric field distribution in the liver tissue obtained by MREIT. Electric field distribution in the liver tissue exposed to the sequence of four electric pulses of different amplitudes (U_{el} = 1000, 1500 V). All four distributions are scaled to the same range for easier comparison.
doi:10.1371/journal.pone.0045737.g006
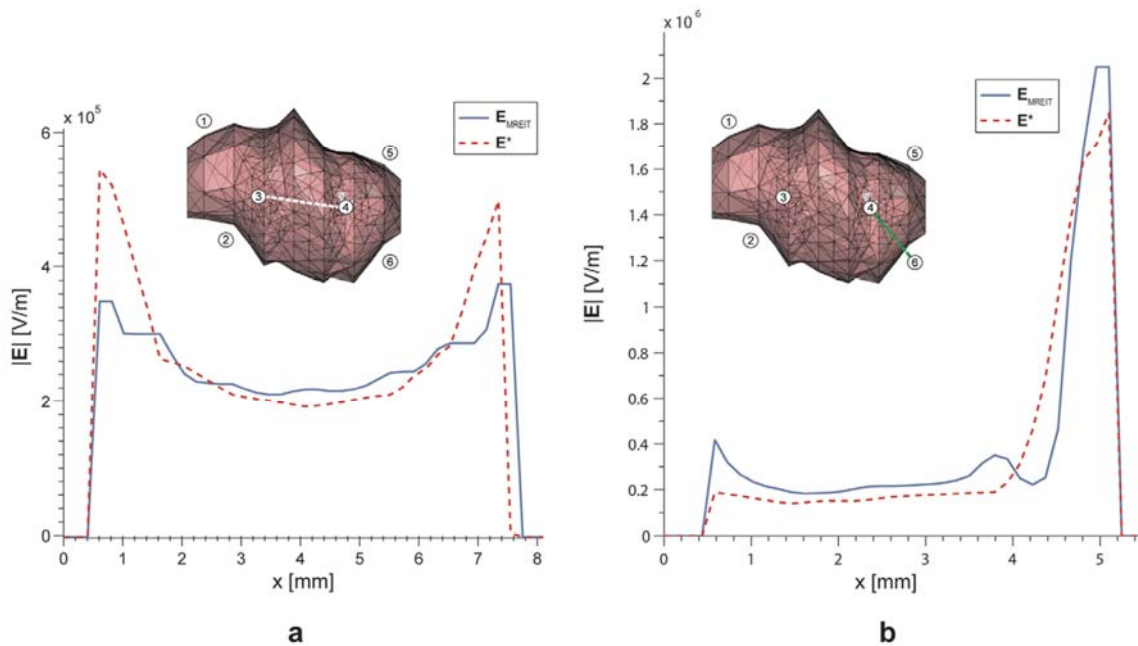
Figure 7. Electric field distribution in the 3-D numerical model obtained by MREIT. An electric field distribution across the tumor region (a) and in the tumor-liver region (b) obtained by means of the MREIT algorithm using only the B_z component (blue solid line) and the corresponding true electric field calculated by the numerical model (red dashed line). Evaluations regions are presented as white and green dashed line in the inserts of figure. Voltage of 1700 V and 2100 V was applied between the electrode pair 3–4 and 4–6, respectively. Note that scales in a and b are different.
doi:10.1371/journal.pone.0045737.g007

using a 3-D numerical model built for the purpose of electro-chemotherapy treatment of deep-seated tumors in liver. An electric field was successfully obtained in both regions, i.e. in the tumor region and in the tumor-liver region. As shown in Fig. 7a and 7b, a good agreement was obtained in both regions. It should be noted that regions with tissues of different conductivities correspond in MREIT to only one current density distribution due to non-uniqueness [35]. This necessitates application of more than one sequence of pulses in at least two directions in order to calculate conductivity and electric field distributions more accurately. This approach is usually done in regular MREIT for diagnostic cases where injected currents are of the order of few mA and dielectric properties of the observed tissue remain intact [36]. However, this cannot be done in treatment cases, such as electroporation, where high electric currents affect electrical conductivity of the tissue after each pulse sequence [17,34]. Even though, results obtained by means of using only one pulse sequence seem sufficiently accurate to enable monitoring of electric field and consequently assume tissue electroporation in the target tissue.

In this study new potential in monitoring electric field distribution by means of MREIT were examined. Electric field distribution in tissue samples *ex vivo* was measured during electroporation by applying electrical pulses in one direction only. As expected, alteration of tissue conductivity distribution caused by applied high voltage pulses was detected. Conductivity changes that occur during the pulse [21] are at the moment too demanding

to assess with MREIT as a function of time. Even though, it is important to be aware that with the CDI technique the accumulative effect of electric current on the MRI signal phase is measured. Therefore, this technique yields a current density distribution, which is a time average of its altering time course so that all the consequences of conductivity alteration, which affect electric current, are not neglected within this distribution. It was also shown that it is possible to obtain a corresponding electric field distribution in electroporation based treatments using numerical model based on a clinical case of the ECT treatment. Our results show that MREIT would confirm delivery of sufficiently high electric field in the whole target tissue and thus enable detection of areas with insufficient electric field coverage during electroporation based treatments like electrochemotherapy and nonthermal irreversible electroporation ablation. This essential near real time information could then be used to improve the electroporation treatment by setting new amplitudes of electric pulses, changing their duration or number or by electrode repositioning, thus increasing effectiveness of electroporation based clinical procedures.

Author Contributions

References

1. Mir LM, Orlowski S (1999) Mechanisms of electrochemotherapy. Adv Drug Deliv Rev 35: 107–118.
2. Neumann E, Schaeferridder M, Wang Y, Hofschneider P (1982) Gene-Transfer into Mouse Lyoma Cells by Electroporation in High Electric-Fields. EMBO J 1: 841–845.
3. Kotnik T, Pucihar G, Miklavcic D (2010) Induced Transmembrane Voltage and Its Correlation with Electroporation-Mediated Molecular Transport. J Membrane Biol 236: 3–13.
4. Orlowski S, Belehradek J, Paoletti C, Mir LM (1988) Transient electropermeabilization of cells in culture. Increase of the cytotoxicity of anticancer drugs. Biochem Pharmacol 37: 4727–4733.
5. Sersa G, Cemazar M, Miklavcic D (1995) Antitumor Effectiveness of Electrochemotherapy with cis-Diamminedichloroplatinum(II) in Mice. Cancer Res 55: 3450–3455.
6. Marty M, Sersa G, Garbay JR, Gehl J, Collins CG, et al. (2006) Electrochemotherapy - An easy, highly effective and safe treatment of cutaneous and subcutaneous metastases: Results of ESOPE (European Standard Operating Procedures of Electrochemotherapy) study. EJC Suppl 4: 3–13.
7. Sersa G, Miklavcic D (2008) Electrochemotherapy of Tumours. JoVE. Available: http://www.jove.com/index/Details.stp?ID = 1038.
8. Sersa G, Cufer T, Paulin SM, Cemazar M, Snoj M (2012) Electrochemotherapy of chest wall breast cancer recurrence. Cancer Treat Rev 5: 379–386.
9. Garcia PA, Pancotto T, Rossmeisl JH, Henao-Guerrero N, Gustafson NR, et al. (2011) Non-Thermal Irreversible Electroporation (N-TIRE) and Adjuvant Fractionated Radiotherapeutic Multimodal Therapy for Intracranial Malignant Glioma in a Canine Patient. Technol Cancer Res Treat 10: 73–83.
10. Rubinsky J, Onik G, Mikus P, Rubinsky B (2008) Optimal parameters for the destruction of prostate cancer using irreversible electroporation. J Urol 180: 2668–2674.
11. Edhemovic I, Gadzijev EM, Brecelj E, Miklavcic D, Kos B, et al. (2011) Electrochemotherapy: a new technological approach in treatment of metastases in the liver. Technol Cancer Res Treat 10: 475–485.
12. Thomson KR, Cheung W, Ellis SJ, Federman D, Kavnoudias H, et al. (2011) Investigation of the safety of irreversible electroporation in humans. J Vasc Interv Radiol 22: 611–621.
13. Miklavcic D, Beravs K, Semrov D, Cemazar M, Demsar F, et al. (1998) The Importance of Electric Field Distribution for Effective in Vivo Electroporation of Tissues. Biophys J 74: 2152–2158.
14. Miklavcic D, Snoj M, Zupanic A, Kos B, Cemazar M, et al. (2010) Towards treatment planning and treatment of deep-seated solid tumors by electrochemotherapy. Biomed Eng Online 9: 10.
15. Zupanic A, Kos B, Miklavcic D (2012) Treatment planning of electroporation-based medical interventions: electrochemotherapy, gene electrotransfer and irreversible electroporation. Physics in Medicine and Biology 57: 5425–5440. doi:10.1088/0031-9155/57/17/5425.

16. Pavlin M, Kanduser M, Rebersek M, Pucihar G, Hart FX, et al. (2005) Effect of cell electroporation on the conductivity of a cell suspension. Biophys J 88: 4378–4390. doi:10.1529/biophysj.104.048975.
17. Cukjati D, Batiuskaite D, André F, Miklavcic D, Mir LM (2007) Real time electroporation control for accurate and safe in vivo non-viral gene therapy. Bioelectrochemistry 70: 501–507. doi:10.1016/j.bioelechem.2006.11.001.
18. Kos B, Zupanic A, Kotnik T, Snoj M, Sersa G, et al. (2010) Robustness of Treatment Planning for Electrochemotherapy of Deep-Seated Tumors. J Membrane Biol 236: 147–153.
19. Pavliha D, Kos B, Zupanic A, Marcan M, Sersa G, et al. (2012) Patient-specific treatment planning of electrochemotherapy: Procedure design and possible pitfalls. Bioelectrochemistry: In press. doi:10.1016/j.bioelechem.2012.01.007.
20. Granot Y, Ivorra A, Maor E, Rubinsky B (2009) In vivo imaging of irreversible electroporation by means of electrical impedance tomography. Phys Med Biol 54: 4927–4943. doi:10.1088/0031-9155/54/16/006.
21. Ivorra A, Rubinsky B (2007) In vivo electrical impedance measurements during and after electroporation of rat liver. Bioelectrochemistry 70: 287–295. doi:10.1016/j.bioelechem.2006.10.005.
22. Zhang Y, Guo Y, Ragin AB, Lewandowski RJ, Yang G-Y, et al. (2010) MR Imaging to Assess Immediate Response to Irreversible Electroporation for Targeted Ablation of Liver Tissues: Preclinical Feasibility Studies in a Rodent Model1. Radiology 256: 424–432. doi:10.1148/radiol.10091955.
23. Lee EW, Chen C, Prieto VE, Dry SM, Loh CT, et al. (2010) Advanced Hepatic Ablation Technique for Creating Complete Cell Death: Irreversible Electroporation. Radiology 255: 426 433. doi:10.1148/radiol.10090337.
24. Kranjc M, Bajd F, Sersa I, Miklavcic D (2011) Magnetic Resonance Electrical Impedance Tomography for Monitoring Electric Field Distribution During Tissue Electroporation. IEEE Trans Med Imaging 30: 1771–1778.
25. Miklavcic D, Semrov D, Mekid H, Mir LM (2000) A validated model of in vivo electric field distribution in tissues for electrochemotherapy and for DNA electrotransfer for gene therapy. Biochim Biophys Acta 1523: 73–83.
26. Pucihar G, Krmelj J, Rebersek M, Napotnik TB, Miklavcic D (2011) Equivalent pulse parameters for electroporation. IEEE Trans Biomed Eng 58: 3279–3288. doi:10.1109/TBME.2011.2167232.
27. Khang HS, Lee BI, Oh SH, Woo EJ, Lee SY, et al. (2002) J-substitution algorithm in Magnetic Resonance Electrical Impedance Tomography (MREIT): Phantom experiments for static resistivity images. IEEE Trans Med Imaging 21: 695–702.
28. Kwon O, Woo E, Yoon J, Seo J (2002) Magnetic resonance electrical impedance tomography (MREIT): Simulation study of J-substitution algorithm. IEEE Trans Biomed Eng 49: 160–167.
29. Sersa I, Jarh O, Demsar F (1994) Magnetic Resonance Microscopy of Electric Currents. J Magn Reson 111: 93–99. doi:10.1006/jmra.1994.1230.

30. Sersa I (2008) Auxiliary phase encoding in multi spin-echo sequences: application to rapid current density imaging. J Magn Reson 190: 86–94. doi:10.1016/j.jmr.2007.10.009.

31. Sel D, Cukjati D, Batiuskaite D, Slivnik T, Mir LM, et al. (2005) Sequential finite element model of tissue electropermeabilization. IEEE Trans Biomed Eng 52: 816–827. doi:10.1109/TBME.2005.845212.

32. Corovic S, Zupanic A, Miklavcic D (2008) Numerical Modeling and Optimization of Electric Field Distribution in Subcutaneous Tumor Treated With Electrochemotherapy Using Needle Electrodes. IEEE Trans Plasma Sci IEEE Nucl Plasma Sci Soc 36: 1665–1672. doi:10.1109/TPS.2008.2000996.

33. Essone Mezeme M, Pucihar G, Pavlin M, Brosseau C, Miklavcic D (2012) A numerical analysis of multicellular environment for modeling tissue electroporation. Appl Phys Lett 100: 143701.

34. Ivorra A, Al-Sakere B, Rubinsky B, Mir LM (2009) In vivo electrical conductivity measurements during and after tumor electroporation: conductivity changes reflect the treatment outcome. Phys Med Biol 54: 5949–5963.

35. Kim S, Kwon O, Seo J, Yoon J (2003) On a nonlinear partial differential equation arising in magnetic resonance electrical impedance tomography. SIAM J Appl Math 34: 511–526.

36. Seo JK, Woo EJ (2011) Magnetic Resonance Electrical Impedance Tomography (MREIT). SIAM Rev 53: 40.

| 38

ARTICLE 3

Title: Assessing how electroporation affects the effective conductivity tensor of biological tissues

Authors: MEZEME Melvin Essone, KRANJC Matej, BAJD Franci, SERŠA Igor, BROSSEAU Christian,

MIKLAVČIČ Damijan

Publication: Applied Physics Letters[1]

DOI: /

Year: /

Volume: /

Number: /

Pages: /

Impact factor: 4.092

Ranking:

Category name	Total journals in category	Journal rank in category	Quartile in category
physics, applied	125	17	Q1

---

[1] At the time of writting, the manuscript has been in press.

Abstract

We report calculations of the anisotropy ratio of the electrical conductivity of a simple model of a loose connective biological tissue described as a random assembly of multiscale undeformable core-shell and controlled polydisperse spherical structures. One can estimate a 10 % increase in the anisotropy ratio due to the application of electric field (duration 100 μm) above the electroporation threshold (40 kVm^{-1}) up to 120 kVm^{-1}. These findings are consistent with the experimental data on the field-induced anisotropy dependence of the electrical conductivity due to cell membrane electroporation.

The Article

There has been a long-standing difficulty to model the interaction of large electric fields with biological tissues [1-3]. The reason is that treating all degrees of freedom in these multiscale systems with strongly correlated cells is a daunting task. In a previous Letter, we have shown by computational means that despite differences in length scales and density, random ternary core-shell sphere packings with different spatial scales can provide a basis for detailed analysis of the electroporation (EP) of tissues [4]. A particularly interesting feature of this method is that it allows for efficient evaluation of temporal evolution of the electrical conductivity of these packings during application of an electric field with magnitude either below or above the value leading to cell membrane EP. It has been pointed out that it predicts a sigmoidal electric field-dependent fraction of electroporated cells which is consistent with what is observed experimentally.

So far, the bulk of theoretical and experimental efforts along these lines have focused on using scalar permittivity and electrical conductivity. Very little is known at this point about the anisotropy properties of biological tissues. The number of reported experimental studies of permittivity and electrical tensors of biological tissues is not large, e.g. see Refs. [5-7]. Much attention has been focused on high-resolution microelectrode arrays that allow electrical characterization of tissues noninvasively with large spatiotemporal resolution [7]. Tuch and co-workers [8] showed how the electrical conductivity tensor of tissue can be quantitatively inferred from the water self-diffusion tensor as measured by diffusion tensor magnetic resonance imaging (MRI). Recent advances in transport measurements, coupled to the development of models, revealed the existence of a small anisotropy in the conductivity above a threshold value of the induced transmembrane voltage (ITV$_{th}$). In fact, the authors reporting conductivity anisotropy results noted a $\approx$ 10 % difference between two perpendicular electric field orientations [5-6].

The aim of the simulations described in this Letter was to search for estimating the anisotropy ratio of the conductivity tensors of such biological materials. As well as being important in their own right, our analysis also provides a useful testbed for identifying important features of EP, determining what causes it, and finding the range of parameters over which it applies.

We performed a set of numerical experiments based on the asymptotic DeBruin-Krassowska (DBK) model of EP for a single cell based on the Smoluchowski equation [6,9]. Though we lack a general microscopic theory linking transport properties and the hierarchy of the cell's microstructure, this approach not only has the virtue of being very general but is also able to describe the electric shock-induced changes in transmembrane potential, which is of crucial importance for EP. Here and throughout the Letter, we will restrict attention to undeformable spherical cells modelled as a core-shell (CS) structure. Schwan [10] laid the groundwork in understanding the properties of such CS models of cells with known size, shape, and distribution of charges. Representative values for the primary parameters defining the assembly of CS structures and the cell and tissue EP are identical to those of Table I in [11]. The geometry we consider is depicted schematically in Fig. 1 (a). The self-consistent method we use to characterize transport properties has been extensively described in the literature (see, e.g., Refs. [2-4] and references therein) and details will not be given here, except where crucial. We consider the case where a uniform external electric field pulse (100 μs), with magnitude E and rise time t_r=0.1 μs, is applied along the x-axis. Since the conductivity $\bar{\bar{\sigma}}$ tensor is independent of the precise boundary conditions imposed on the electrical potential, we can choose those conditions such that $\bar{\bar{\sigma}} = \begin{bmatrix} \sigma_{xx} & 0 & 0 \\ 0 & \sigma_{yy} & 0 \\ 0 & 0 & \sigma_{yy} \end{bmatrix}$, in the Cartesian coordinate system defined by the dielectric axis. We have performed finite element simulations of the σ_{xx}, and σ_{yy} components of $\bar{\bar{\sigma}}$. To obtain σ_{yy} a perpendicular electric field pulse (100 μs) in the y direction is superimposed to the field in the x direction. Typical results of these simulations are shown in Figs. 2-3. To be specific, the cell is modelled by using a simple CS structure with membrane thickness of 5 nm, membrane conductivity of 5×10^{-7} $\Omega^{-1}\text{m}^{-1}$, intracellular conductivity of 0.2 $\Omega^{-1}\text{m}^{-1}$, and extracellular conductivity of 0.127 $\Omega^{-1}\text{m}^{-1}$. These numbers are comparable to related theoretical calculations [2-4,6,9-10]. To model simply a tissue as a random assembly of multiscale CS spherical structures, we have considered three cell radii 8, 10, and 12 μm. These values are consistent with the cell size distribution observed in reflectance in biological tissues [12]. The cubic computational domain (condenser) is filled by a homogeneous medium (whose dielectric properties are assimilated to water) in which nonoverlapping spherical cells are distributed randomly but uniformly. In the actual numerical calculations, the volume fraction of

cell is held constant and is set to 33 vol.%. Because of the large computational effort for modelling three dimensional heterostructures we limit ourselves to study five realizations of the random assembly of cells. The average computational time of a typical simulation of the multicellular tissue model shown in Fig. 1 (b) is about 1 hour. Most computational parameters are the same as those used in our earlier work [4]. As long as the quasistatic approximation is valid, all of the tensor components are calculable in this continuous effective medium approach. We use finite element as implemented in COMSOL MULTIPHYSICS [13], using a $80 \times 80 \times 80$ µm³ computational domain with electrically insulated boundary conditions for the *x-y* and *x-z* planes (conservation of the electric current density). The average cell number is 82 for the 5 realizations of the model and the density is 1.6 10^{14} cells/m³.
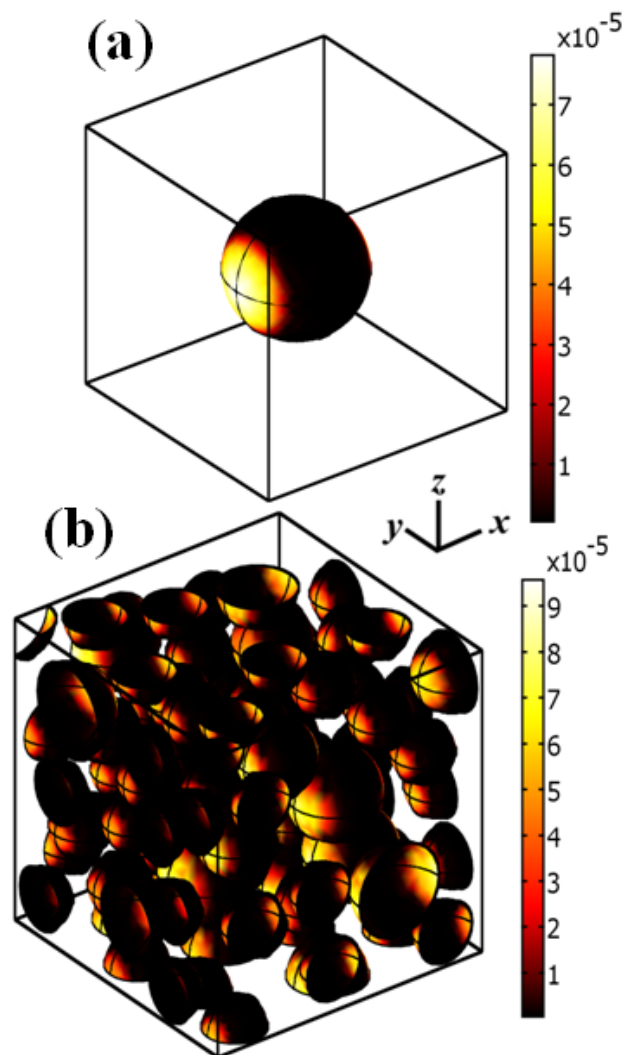
Fig.1 : (a) A single cell in the computational domain. (b) Illustrating the random ternary CS sphere packings studied, with three cell radii 8, 10, and 12 µm, corresponding to a volume fraction of cell inside the computational domain set to 33 vol.%.

Experimental measurement of the anisotropy ratio of the conductivity tensor using magnetic resonance electrical impedance tomography (MREIT) was also performed. MREIT is based on reconstructing images of true conductivity with high spatial resolution by obtaining current density information using magnetic resonance imaging (MRI) and measuring surface voltage potential [14-16]. Even though reconstructed conductivity images are mostly assessed by multiple injections of low current it was showed recently that single electroporation pulses are also applicable for reconstruction [17]. We performed *ex vivo* measurement on fresh chicken liver tissue obtained from a slaughterhouse (Perutnina Ptuj, d.d., Ptuj, Slovenia) which operates in accordance to Slovenian law (Ur.l. RS, N. 5/2006). We placed cylindrically shaped tissue samples inside an Oxford 2.35 T horizontal bore superconducting magnet (Oxford instruments, U. K.) and expose it to 1.5 ms long electric pulses with amplitude of 1400 V using an electroporator Jouan GHT 1287 (Jouan, France). *Ex vivo* tissue samples were exposed to electric field with strength ranging from 20 kVm^{-1} up to 250 kVm^{-1} in areas which were distant to, or near, the electrodes respectively. MRI of current induced magnetic field changes inside tissue sample was acquired using the two-shot RARE CDI sequence [17]. Afterwards, we reconstructed electrical conductivity using MREIT J-substitution algorithm which is based on solving iteratively Laplace's equation. More details on the methodology can be found in [17]. Measurements were repeated ten times and each sample was replaced with a fresh one after each electroporation pulse delivery to ensure identical initial conditions.

We start by discussing the simpler case of a single cell (Fig. 1(a)). The results are summarized in Fig. 2. In this figure, two curves are shown for the effective conductivity below (20 kVm^{-1}) or above (100 kVm^{-1}) the EP threshold (40 kVm^{-1}). Below the EP threshold, the results yield superimposable conductivity values (solid and dotted lines) plotted as a function of time. When a perpendicular field is applied above the EP threshold, our simulations predict discrimination compared to the conductivity obtained from the parallel case. These results were also obtained in Ref. 6 and are qualitatively similar to those of Huclova and co-workers [18].
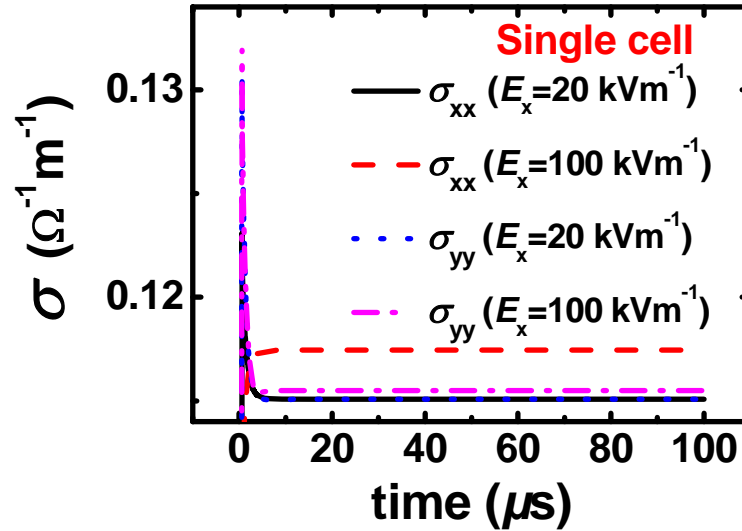
Fig. 2: (a) Simulation results for the electrical conductivity of a single cell as a function of time for the electroporated (solid line) and non-electroporated (dashed line) cell membrane subjected to the applied electric field. (b) Same for the effective conductivity. The field duration is 100 μs

We now concretize these ideas by application to the random ternary CS sphere packings with different spatial scales, as shown in the illustrative case of Fig. 1 (b). We are faced with two serious challenges: firstly, the spatial heterogeneity of the random distribution of cells within the computational domain must be dealt with. Secondly, an ensemble average is taken over many different realizations that have the same boundary conditions. We are, however, able to circumvent these issues by using the analysis described in [4]. The results are summarized in Fig. 3 for the average conductivity of the random ternary core-shell (CS) sphere packings. In Fig. 3, we present data showing the evolution of the average electrical conductivity as a function of time below or above the EP threshold. The anisotropy that we describe in Fig. 3 is a statistical property of an ensemble of realizations, whereas the behavior shown in Fig. 2 is the manifestation of this anisotropy for a single cell. It is also worth observing that the initial spikes observed in Figs. 2 and 3 correspond to the capacitive term of the current. Their amplitude gets more pronounced with shorter rise time of applied electric pulses [19].
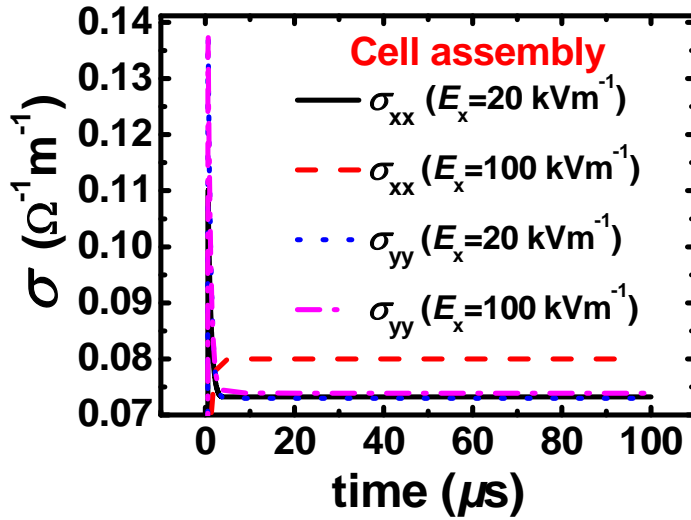
Figure 3: Same as in Fig.2 for the average of five realizations of the random ternary core-shell (CS) sphere packing with different spatial scales modelling a tissue. The volume fraction of cell inside the computational domain is set to 33 vol.%. The field duration is 100 μs.

Fig. 4 further illustrates the effects of raising electric field amplitude on anisotropy ratio of the electrical conductivity defined as $\Delta\sigma = \left(\sigma_{xx} - \sigma_{yy}\right)/\sigma_{xx}$ for our model of tissue. It can be immediately seen that as electric field increases from 40 to 160 kVm[-1], the ratio increases from ≈ 0 to 14 % monotonically with a significant upturn at 60 kVm[-1]. The question that remains now regards the mechanism promoting the field-induced anisotropy, whether it is driven by the anisotropy intrinsic to the individual cell, or that related to the randomness and connectedness of the tissue. The small anisotropy, $\approx 3\%$, observed in Fig. 2 immediately suggests that the electric field dependence of the anisotropy ratio is mainly determined by the collective behavior associated with the cell membrane EP of dense cell suspensions. One additional observation is worthy of note. Fig. 4 shows also the dimensionless parameter $\delta\sigma = \left(\sigma_E - \sigma_{E_0}\right)/\sigma_{E_0}$, which concerns the sole application of an electric field along the x-axis, and where E_0 denotes a reference value for the nonelectroporated state (20 kVm[-1]), and the fraction of electroporated cells p obtained in [4] for cell density of 33 vol.%. We observe that even if all cells are electroporated at a field magnitude of 90 kVm[-1], $\delta\sigma$ still grows in field, indicating the increase of the electroporated cell's area fraction. It is noted that the anisotropy ratio $\Delta\sigma$ observed for electroporated states is significantly smaller than the field ratio $\delta\sigma$.
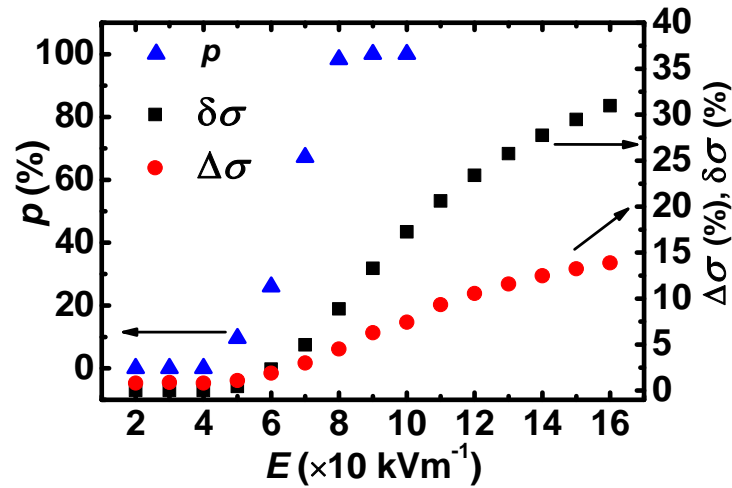
Fig. 4: The anisotropy $\Delta\sigma = \left(\sigma_{xx} - \sigma_{yy}\right)/\sigma_{xx}$ and field $\delta\sigma = \left(\sigma_E - \sigma_{E_0}\right)/\sigma_{E_0}$ ratios of the averaged electrical conductivity tensor components for random ternary core-shell (CS) sphere packing as a function of the applied electric field (left axis). Fraction of electroporated cells p, as a function of electric field magnitude E (right axis, from [4]). The volume fraction of cell inside the computational domain is set to 33 vol.%. $E_0 = 20$ kVm^{-1}. The results are the averages of 5 realizations of the ternary CS tissue model. The field duration is 100 μs.

Fig. 5 shows the measured anisotropy ratio of the electrical conductivity $\Delta\sigma = \left(\sigma_{xx} - \sigma_{yy}\right)/\sigma_{xx}$ for liver tissue in the electric field range between 20 kVm^{-1} and 120 kVm^{-1}. It should be noted that the effect of electric field amplitude on $\Delta\sigma$ can be evaluated and compared with simulation results even though the cylindrical geometry of imaging tissue, the electrode type, and the measurement configuration (4 needle electrodes) introduce conditions which differ from the numerical experiment where the electric field was uniformly applied along either the x- or the y-axis. Remarkably, the electric field dependence of the measured $\Delta\sigma$ shown in Fig. 5 reproduces the simulated one in Fig. 4. Observe that $\Delta\sigma$ remains practically constant below ≈50 kVm^{-1}. In contrast, at higher electric field amplitudes the data show strong scatter. The observed value of ≈50 kVm^{-1} is also similar to the reversible electroporation threshold of rabbit liver determined in an earlier study [18].
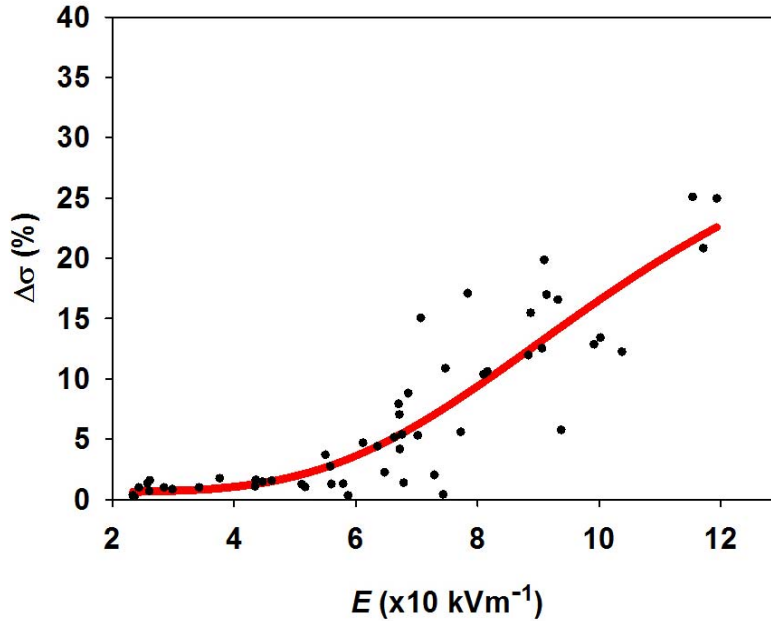
Fig.5: The anisotropy ratio $\Delta\sigma$ of the averaged electrical conductivity tensor components for a chicken liver tissue. The results (full circles) are the averages of measurements on 10 liver samples. The solid (red) line is a guide to the eyes.

Importantly, the presence of anisotropy in the conductivity agrees qualitatively well with conductivity measurements on single cell [6]. Our results are also in qualitative agreement with recent studies of Gilboa *et al.* [5] using microelectrode arrays where they conclude that the tissue conductivity should present a smooth tensor field. More importantly, the analysis method of this work can serve as an opportunity to understand the EP mechanisms of biological tissues.

In summary, the primary motivation in this study was to analyze a particular model of connective biological tissue described as a random assembly of undeformable core-shell and controlled polydisperse spherical structures. We have applied a methodology that circumvents the numerical difficulties of modeling multiscale media by using three cell radii. We note that the anisotropy ratio of the electrical conductivity does not reach substantial amplitude in simulations, except for electric field magnitude which will eventually compromise the viability of the tissue. The conclusions reached here with regards to the EP properties of tissues are consistent with current and previous experimental investigations [5].

While the question of generality of the current modelling approach for a tissue remains open, the present results will both motivate further studies and also serve as an important anchor in future discussions of EP. One immediate extension of our study would be to consider a wider

range of random filling of the computational domain. We certainly acknowledge that there are subtleties due to the randomness of dense sphere packings; for example, the impact of connectedness and clustering of spheres [20]. Nevertheless, the current results suggests that the current model may be a good approximation of biological tissues, and we take this opportunity to remind the reader that extensive discussions of the effective conductivity tensor of random two-component inhomogeneous materials have appeared in the literature [20-21]. In this respect, we expect that the results presented in this Letter will stimulate further work on the applicability of this model to open problems in EP of biological tissues, e.g. relating ITV measurements to the electrophysiological state of cells in the tissue.

Acknowledgments

References

[1] G. Emili, A. Schiavoni, M. Francavilla, L. Roselli, and R. Sorrentino, IEEE Trans. Microwave Theory Tech. **51**, 178 (2003).

[2]] R. Pethig, *Dielectric and Electronic Properties of Biological Materials* (Wiley, New York, 1979); K. R. Foster and H. P. Schwan, Crit. Rev. Biomed. Eng. **17**, 25 (1989).

[3] K. C. Smith, T. R. Gowrishankar, A. T. Esser, D. A. Stewart, and J. C. Weaver, IEEE Trans. Plasma Sci. **34**, 1480 (2006).

[4] M. Essone Mezeme, G. Pucihar, M. Pavlin, C. Brosseau, and D. Miklavčič, Appl. Phys. Lett. **100**, 143701 (2012).

[5] E. Gilboa, P. S. La Rosa, and A. Nehorai, Ann. Biomed. Eng. **40**, DOI: 10.1007/s10439-012-0581-9 (2012). See also C. Gabriel, Dielectric Properties of Biological Materials, in *Bioengineering and Biophysical Aspects of Electromagnetic Fields*, edited by F. S. Barnes and B. Grenebaum, (CRC Press, New York, 2006).

[6] T. Kotnik, F. Bobanović, and D. Miklavčič, Bioelectrochem. Bioenerg. **43**, 285 (1997); M. Pavlin and D. Miklavčič, Biophys. J. **85**, 719 (2003); M. Pavlin, M. Kandušer, M. Reberšek, G. Pucihar, F. X. Hart, R. Magjarević, D. Miklavčič, Biophys. J. **88**, 4378 (2005); T. Kotnik and D. Miklavčič, Biophys. J. **90**, 480, (2006); M. Pavlin, V. Leben, and D. Miklavčič, Biochim. Biophys. Acta **1770**, 12 (2007).

[7] L. Berdondini, K. Imfeld, A. Maccione, M. Tedesco, S. Neukom, M. Koudelka-Hep, and S. Martinoia, Lab. Chip **9**, 2644 (2009); K. Imfeld, S. Neukom, A. Maccione, Y. Bornat, S. Martinoia, P. Farine, M. Koudelka-Hep, and L. Berdondini, IEEE Trans. Biomed. Eng. **55**, 2064 (2008); J. Wtorek, A. Bujnowski, A. Poliński, L. Józefiak, and B. Truyen, Physiol. Meas. **25**, 1249 (2004), P.

Steendijk, G. Mur, E. T. van der Velde, and J. Baan, IEEE Trans. Biomed. Eng. **40**, 1138 (1993), Y. Wang, P. H. Scimpf, D. R. Haynor, and Y. Kim, IEEE Trans. Biomed. Eng. 45, 877 (1998).

[8] D. S. Tuch, V. J. Wedeen, A. M. Dale, J. S. George, and J. W. Belliveau, Proc. Nat. Acad. Sci. **25**, 11697 (2001); D. S. Tuch, V. J. Wedeen, A. M. Dale, and J. W. Belliveau, Ann. NY Acad. Sci. **888**, 314 (1999).

[9] K. A. DeBruin and W. Krassowska, Biophys. J. **77**, 1213 (1999); ibidem, 1225.

[10] H. P. Schwan, Adv. Biol. Med. Phys. **5**, 147 (1957).

[11] G. Pucihar, V, and T. Kotnik, IEEE Trans. Biomed. Eng. **56**, 1491 (2009); G. Pucihar, T. Kotnik, B. Valič, and D. Miklavčič, Ann. Biomed. Eng. **34**, 642-652 (2006); G. Pucihar, D. Miklavčič, T. Kotnik, IEEE Trans. Biomed. Eng. **56**, 1491 (2009); T. Kotnik, G. Pucihar, D. Miklavčič, J. Membrane Biol. 236, 3 (2010).

[12] M. Puc, T. Kotnik, L. M. Mir, and D. Miklavčič, Bioelectrochem. **60**, 1 (2003).

[13] COMSOL MULTIPHYSICS version 3.4.

[14] N. Zhang, Electrical impedance tomography based on current density imaging, MSc Thesis Department of Electrical Engineering, University of Toronto (1992).

[15] E. Degirmenci and B. M. Eyuboglu, Phys. Med. Biol. **52**, 7229 (2007).

[16] J. K. Seo and E. J. Woo, SIAM Rev. **53**, 40 (2011).

[17] M. Kranjc, F. Bajd, I. Sersa, and D. Miklavčič, IEEE Trans. Med. Imaging **30**, 1771 (2011); M. Kranjc, F. Bajd, I. Serša, E. J. Woo, and D. Miklavčič, PLOS One **7**, e45737 (2012).

[18] S. Huclova, D. Erni, and J. Fröhlich, J. Phys. D **43**, 365405 (2010).

[19] D. Cukjati, F. A. Batiuskaite, D. Miklavcic, and L. M. Mir, Bioelectrochem. **70**, 501 (2007); D. Sel, D. Cukjati, D. Batiuskaite, T. Slivnik, L. M. Mir, and D. Miklavčič, IEEE Trans. Biomed. Eng. **52**, 816 (2005).

[20] S. Torquato, *Random Heterogeneous Materials* (Springer, New York, 2001); M. Sahimi, *Heterogeneous Materials* I : *Linear Transport and Optical Properties*, (Springer, New York, 2003).

[21] O. Levy and D Stroud, Phys. Rev. B 56, 8035 (1997); A. Mejdoubi and C. Brosseau, J. Appl. Phys. **99**, 063502 (2006); A. Mejdoubi and C. Brosseau, Phys. Rev. E **74**, 031405 (2006); A. Mejdoubi and C. Brosseau, Phys. Rev. E **73**, 031405 (2006); A. Mejdoubi and C. Brosseau, J. Appl. Phys. **100**, 094103 (2006); V. Myroshnychenko and C. Brosseau, Phys. Rev. E **71**, 016701 (2005); V. Myroshnychenko and C. Brosseau, J. Appl. Phys. **97**, 044101 (2005); C. Brosseau, J. Phys. D **39**, 1277 (2006); C. Fourn and C. Brosseau, Phys. Rev. E 77, 016603 (2008); V. Myroshnychenko and C. Brosseau, J. Phys. D **41**, 095401 (2008); V. Myroshnychenko and C. Brosseau, J. Appl. Phys. **103**, 084112 (2008).

DISCUSSION

The goal of this doctoral dissertation was to investigate current density imaging (CDI) and magnetic resonance electrical impedance tomography (MREIT) using short intense pulses of similar amplitudes as used in electroporation based clinical applications. We investigated experimentally and numerically determination of electric field distribution during electroporation by means of MREIT on homogeneous and heterogeneous phantom with electrical properties similar to human tumor and surrounding tissue. For sensitivity evaluation of the method we exposed phantoms to different pulse sequences. We also investigated feasibility of the MREIT technique to determine electric field distribution during tissue electroporation by means of an *ex vivo* liver tissue experiment. In addition, feasibility of using MREIT to determine electric field distribution during electroporation based treatments was evaluated numerically on a validated 3-D numerical model designed for the purpose of electrochemotherapy (ECT) treatment of deep-seated liver tumors.

AGAR PHANTOMS STUDY

We started evaluation of feasibility to determine electric field distribution using MREIT by performing experiment on agar phantoms. Different number of pulses and of their amplitudes were used in separate experiments to evaluate feasibility of the method to determine electric field distribution during the electroporation. Experimental results were evaluated by comparison to the simulation result obtained by the numerical model. Electric current flowing between the electrodes during pulse sequences was obtained using three different approaches, two experimental and one numerical. Results presented in Table 1 (Article 1, page 25) confirm good agreement between the approaches in both phantoms used and for most of the applied voltages. As shown in Figure 3 (Article 1, page 24) and Figure 4 (Article 1, page 25) a good agreement between experimental and numerical results was obtained when comparing current density and electric field distribution in homogeneous and heterogeneous phantoms. Minor discrepancy was observed between the homogeneous phantom exposed to pulses of 2000 V and the heterogeneous phantom exposed to pulses of 3000 V due to exceedingly high current in agar

of the phantoms, resulting in its deterioration due to excessive heating and consequently increased electrical conductivity. As shown in Figure 5 (Article 1, page 25), experimentally and numerically obtained electric field profiles diagonally across the heterogeneous phantom are in a good agreement. The largest disagreement between experimental and numerical results was observed in areas close to electrodes. Electrodes mainly cause large distortions in the magnetic field and significant susceptibility artefacts. Magnetic field distortion around electrodes however does not represent considerable problem for determination of electric field distribution during electroporation as the area between the electrodes is more critical for efficient electroporation. CDI and MREIT allowed determination of the electric field distribution for all pulse sequences used in our study. As expected, the experiments showed that the electric field intensity increases with applied electric pulse amplitude as shown in Figure 7 (Article 1, page 26) and that electric field intensity and distribution are both independent of the number of pulses as shown in Figure 6 (Article 1, page 25). The main limitation of the agar phantoms study lies in the phantom substance – agar, which became deteriorated after long exposure to high-voltage pulses resulting in numerous measurement failures. Nevertheless, the results confirmed that MREIT can be used to determine electric field distribution during electroporation and next step toward *ex vivo* experiments was designed.

EX VIVO EXPERIMENTS

The aim of *ex vivo* study was to investigate feasibility of the MREIT technique to determine electric field distribution during tissue electroporation by means of an *ex vivo* liver tissue experiment. As shown in Figure 4 (Article 2, page 35) and Figure 6 (Article 2, page 36), electric field and electrical conductivity distributions within liver tissue during application of electroporation pulses were obtained successfully. When examining results and comparing them to our previous findings on agar phantoms, considerable differences were observed. While dielectric properties of agar remained unchanged in spite of applied high electric field, presumably due absence of a cell structure in the agar gel (Essone Mezeme *et al.*, 2012), significant changes of the liver tissue electrical conductivity were observed when tissue was exposed to pulses with an amplitude of 1500 V as shown in Figure 4 (Article 2, page 35). The region with a higher electrical conductivity between electrodes was established as a consequence of tissue changes associated to a high electric field in the region when pulses of 1500 V were applied. Such changes were not detected in tissue exposed to pulses with an amplitude of 1000 V due to lower electric field. Observed tissue changes are thus assumed to be a consequence of local tissue electroporation as electric field in the region between electrodes exceeded reversible threshold value in the case of 1500 V whereas most of this region remained under the threshold value in the case of 1000 V applied voltage. Comparison of electric current

also confirms increment of electrical conductivity as amplitudes value of electric current in liver tissue approximately doubled (from 320 mA to 670 mA) when the voltage was increased for only half of its value (from 1000 V to 1500 V) as shown in Figure 5 (Article 2, page 35). Nonlinear changes of tissue conductivity after electroporation were already observed and have been reported previously (Cukjati *et al.*, 2007; Ivorra *et al.*, 2009). It also needs to be noted that local alterations of conductivity near the boundary of the container and in the region of inactive electrode in Figure 4 (Article 2, page 35) are measurement errors due to noise near the boundary where the lower limit of sensitivity in CDI is met and due to distortions of magnetic field caused by electrodes, respectively

DETECTING ELECTROPORATION INDUCED ANISOTROPY

At this point, there is a lack of knowledge on the anisotropy properties of electrical conductivity in biological tissues. There are only few reported experimental studies of permittivity and electrical tensors of biological tissues (Greenebaum and Barnes, 2006; Gilboa *et al.*, 2012), especially in the case when they are exposed to electroporation pulses (Čorović *et al.*, 2010, 2012; Županic *et al.*, 2010). MREIT was already applied for reconstructing electrical conductivities with anisotropy properties (Seo *et al.*, 2004; Değirmenci and Eyüboğlu, 2007, 2012; Nam and Kwon, 2010) and is a prime candidate for observing induced anisotropy in tissues due to electroporation. As described in Article 3, experimental and numerical investigation on the anisotropy ratio of biological tissue was performed. Whereas numerical model was based on random undeformable spherical cells packing with a core-shell structure (Essone Mezeme *et al.*, 2012), experimental tissue was a chicken liver tissue. Figure 5 (Article 3, page 48) shows the measured anisotropy ratio of the electrical conductivity for liver tissue in the electric field range between 20 kVm^{-1} and 120 kVm^{-1}. It should be noted that the effect of electric field amplitude on anisotropy ratio can be evaluated and compared with simulation results even though the cylindrical geometry of imaging tissue, the electrode type, and the measurement configuration (4 needle electrodes) introduce conditions which differ from the numerical experiment where the electric field was uniformly applied along either the x- or the y-axis. Interestingly, the electric field dependence of the measured anisotropy ratio shown in Figure 5 (Article 3, page 48) agrees with the simulated one in Figure 4 (Article 3, page 47). It can be seen that anisotropy ratio remains almost constant below ≈ 50 kVm^{-1}, whereas at higher electric field amplitudes the data indicates anisotropy ratio higher than one would expect. The observed threshold of electroporation is also similar to the reversible electroporation threshold of rabbit liver determined in an earlier study (Miklavčič *et al.*, 2000; Šel *et al.*, 2005). In addition, results on the anisotropy properties of electrical conductivity in biological tissues reached in this study are also consistent with recent experimental investigations (Gilboa *et al.*, 2012).

Numerical evaluation of determining electric field distribution during electroporation based treatments

We have successfully evaluated a major concern of the MREIT use, namely, whether it is possible to determine an accurate electric field distribution from only one **B** component. By using a 3-D numerical model built for the purpose of ECT treatment of deep-seated tumors in liver (Edhemović *et al.*, 2011). We applied CDI first in order to obtain a current density distribution in a plane of both regions, i.e. in the tumor region and in the tumor-liver region. It should be noted that during the treatment electrodes would need to be directed in parallel to the main magnetic field of MRI in order to obtain accurate current density distribution (Joy *et al.*, 1989). We have successfully obtained electric field in both regions, i.e. in the tumor region and in the tumor-liver region. As shown in Figure 7a and Figure 7b (Article 2, page 36), a good agreement was obtained in both regions. It should be noted that regions with tissues of different conductivities correspond in MREIT to only one current density distribution due to non-uniqueness (Kim *et al.*, 2003). This necessitates application of more than one sequence of pulses in at least two directions in order to determine conductivity and electric field distributions more accurately. This approach is usually done in regular MREIT for diagnostic cases where injected currents are of the order of few mA and dielectric properties of the observed tissue remain unaffected by the current (Seo and Woo, 2011). However, this cannot be done in treatment cases, such as electroporation, where high electric currents affect electrical conductivity of the tissue after each pulse sequence (Cukjati *et al.*, 2007; Ivorra *et al.*, 2009). Even though, results obtained by means of using only a single pulse sequence seem sufficiently accurate to enable determination of electric field and consequently assume tissue electroporation in the target tissue.

Monitoring of electroporation

As already mentioned in the introduction, various methods of monitoring electroporation process were already proposed. Similar to MREIT, EIT was proposed for monitoring electroporation (Davalos *et al.*, 2004) and was already successfully applied *in vivo* (Ivorra and Rubinsky, 2007; Granot *et al.*, 2009). EIT and MREIT are similar as both are used for reconstruction of conductivity images. The difference between them is only in voltage and current measurements, which are in EIT limited only to the boundaries of the imaging object, while in MREIT they cover the entire imaging object. Difficulties associated with the use of EIT to monitor electroporation process are identical to those of using EIT to image tissue in general; numerous additional electrodes are required, sensitivity, spatial resolution and accuracy are low, while noise is high (Holder, 2004). On the other hand, an advantage of EIT is in easier implementation of a typical electroporation treatment procedure, higher temporal resolution and ability to operate with metallic materials. In addition, EIT systems are smaller and less

expensive than MR systems. MRI was also proposed to monitor electroporation process although recent published report on MRI of non-thermal irreversible electroporation in vegetable tissue is limited in observation of only irreversible electroporation where the damage to the cellular membrane and the consequent release of intracellular content can be detected by comparing MRI images of different modalities (T_1-, T_2-weighted, FLAIR or STIR) acquired before and after the application of N-TIRE pulses (Hjouj and Rubinsky, 2010). Similar method of comparing MRI images of different modalities was used to observe irreversible electroporation of liver tissues by detecting local fluid accumulation owing to transient permeabilization of blood vessels, as suggested by authors (Lee *et al.*, 2010; Zhang *et al.*, 2010). Diffusion-weighted magnetic resonance imaging (DW-MRI) has also been proposed as a method to monitor electroporated tissue using the concept of apparent diffusion coefficient (Mahmood *et al.*, 2011). Even though numerical studies reported DW-MRI feasible to monitor reversible electroporation (Imae *et al.*, 2008) preclinical study failed to demonstrate it *in vivo* in rat brains. Ultrasound can also be applied solely to N-TIRE applications (Lee *et al.*, 2007). Main disadvantage of all of the above mentioned methods is the incapability to monitor electroporation during pulse delivery or that they are limited to observing irreversible electroporated areas. This does not apply to the method of current and voltage measurement of delivered pulses described in (Cukjati *et al.*, 2007), although this method inherits the main restrain of conductivity evaluation methods that are based on voltage/current measurements. Namely, monitoring of voltage and current between only one pair of electrodes at a time can led to false conductivity and to an inaccurate electric field distribution calculation due to lack of information on tissue heterogeneity between the electrodes.

We believe that a better evaluation of electroporation process can be accomplished with acquiring current density information and its transformation to the electric field distribution by means of proposed CDI and MREIT method. As the measurement of current density and electrical conductivity is performed during pulse delivery, determined electric field distribution takes into account all changes which occur in tissue due to electroporation. Moreover, single two-shot RARE CDI sequence takes about 20 seconds for acquiring of current density distribution and MREIT J-substitution algorithm additional few seconds for reconstruction of electrical conductivity. This makes CDI and MREIT capable of almost real time monitoring of electroporation as the electric field distribution can then be determined in few tens of seconds after the beginning of pulse delivery.

The main difficulty of using MREIT to determine electric field distribution during electroporation in a clinical environment is associated with the limited capability of MRI scanners for their use in interventional procedures. Although, a recent report on MREIT with an

open MRI scanner (Wang *et al.*, 2010) makes implementation of MREIT feasible in the near future. There is also a limitation with the existing two-shot RARE CDI sequence as it requires an application of at least two electric pulses with a delay of approximately 15 seconds between them in order to deliver complete current density information. This currently puts a frequency limitation on CDI although hopefully future improvements of CDI algorithms and MRI scanners will enable to reduce the required delay between applied pulses. Conductivity changes that occur during the pulse (Ivorra and Rubinsky, 2007) are at the moment also too demanding to asses with MREIT as a function of time. Even though, it is important to be aware that with the CDI technique the accumulative effect of electric current on the MRI signal phase is measured. Therefore, this technique yields a current density distribution, which is a time average of its altering time course so that all the consequences of conductivity alteration, which affect electric current, are not neglected within this distribution.

CONCLUSION

The main focus of the work presented in this doctoral dissertation was to investigate current density imaging and magnetic resonance electrical impedance tomography using short intense pulses of similar amplitudes and directions as used in electroporation based clinical applications and to investigate feasibility of both methods to determine electric field distribution during tissue electroporation It was successfully demonstrated by means of experimental and numerical approach that magnetic resonance electrical impedance tomography together with current density imaging indeed can be used for determination of electric field distribution during electroporation pulse delivery.

Exposure of the treated tissue to a sufficiently large electric field presents one of the most important conditions for successful electroporation. A monitoring method that would allow determination of the electric field would be of great importance for electroporation based applications such as electrochemotherapy and non-thermal irreversible electroporation. Proposed method enables determination of electric field distribution using Ohm's law and magnetic resonance techniques, i.e. current density imaging and magnetic resonance electrical impedance tomography.

Determination of electric field distribution during electroporation pulse delivery by means of current density imaging and magnetic electrical impedance tomography was investigated both experimentally and numerically on homogeneous and heterogeneous phantom tissue with dielectric properties similar to a liver and a tumor. Synchronization of electroporation pulses with the current density imaging sequence enabled acquiring of current density during electroporation. This was followed by reconstruction of the electric field distribution using magnetic resonance electrical impedance tomography *J*-substitution method based on only one component of magnetic flux density obtained by current density imaging and determination of electric field using Ohm's law. A good agreement between experimental and numerical results was obtained, suggesting that current density imaging and magnetic resonance electrical impedance tomography can be used to determine the electric field during electric pulse delivery.

This was also confirmed *ex vivo* by performing experiment on a chicken liver tissue. As expected, alteration of tissue conductivity distribution caused by applied high voltage pulses was detected and measured. In addition, anisotropy of electrical conductivity in a liver tissue was detected when electric field strength exceeded reversible electroporation threshold.

A major concern whether proposed method for determination of electric field distribution can be implemented in electroporation based applications was evaluated by a simulation in the case of a 3-D numerical model designed for the purpose of an electrochemotherapy treatment of deep-seated liver tumors. We demonstrated that it is possible to obtain sufficient information on electric field distribution in the targeted and surrounding tissue by acquiring only one component of magnetic flux density and thus enable detection of areas with insufficient electric field coverage before the end of the treatment, thus increasing and assuring its effectiveness. Nevertheless, there are still some problems that are needed to be addressed in the future such as limited capability of magnetic resonance imaging scanners for their use in interventional procedures and frequency limitation of CDI algorithms.

As there is a lack of tissue specific experimental data on tissue properties for reliable numerical treatment planning and a great need for *in situ* determination of electric field distribution during electroporation pulse delivery, magnetic resonance electrical impedance tomography together with current density imaging could be of significant help in monitoring of electroporation based applications such as electrochemotherapy, non-thermal irreversible electroporation and electroporation based gene transfer. We believe that proposed method and obtained results presented in this doctoral dissertation have demonstrated its great potential in determination of electric field during electroporation and that a next step towards *in vivo* experiments can be taken.

ORIGINAL CONTRIBUTIONS

Based on results in this doctoral dissertation I claim for the recognition of the following original scientific contributions to the research area:

A METHOD OF MONITORING ELECTRIC FIELD DISTRIBUTION

Sufficient electric field coverage presents one of the most important conditions for successful tissue electroporation. We demonstrated that determination of electric field distribution during electroporation pulse delivery can be accomplished by acquiring current density information and electrical conductivity by means of current density imaging and magnetic resonance electrical impedance tomography, respectively. Determination of electric field distribution during tissue electroporation was demonstrated both experimentally and numerically on homogeneous and heterogeneous phantom with electrical properties similar to human tumor and surrounding tissue. Furthermore, determination of electric field distribution during electroporation was also successfully demonstrated on *ex vivo* chicken liver tissue.

AN EVALUATION OF FEASIBILITY TO MONITOR ELECTRIC FIELD DISTRIBUTION DURING ELECTROPORATION AND DETECTION OF ELECTROPORATION INDUCED ANISOTROPY

Electroporation is used for therapeutic purposes and electric pulses can reach up to 3000 V and they can establish electric field distribution with strength up to $150\,\mathrm{kVm^{-1}}$ depending on electrodes geometry and distance between them. As current density imaging and magnetic resonance electrical impedance tomography have been developed for diagnostic purpose and there is a lack of reports where electric pulses that are normally used in electroporation applications would be used we demonstrated that both, current density imaging and resonance electrical impedance tomography, can be applied for obtaining electric field with such high field strength. Electric field distribution was determined in agar phantoms and in *ex vivo* tissue for different pulse sequences, i.e. for different number and amplitude of pulses. Alteration of anisotropy ratio of the conductivity tensor was also detected on *ex vivo* tissue when reversible electroporation threshold was exceeded.

We have also successfully demonstrated that current density imaging and magnetic resonance electrical impedance tomography can be implemented in electroporation based applications by performing numerical evaluation in the case of a 3-D numerical model designed for the purpose of an electrochemotherapy treatment of deep-seated liver tumors.

REFERENCES

Al-Sakere, B., André, F., Bernat, C., Connault, E., Opolon, P., Davalos, R.V., Rubinsky, B., Mir, L.M., 2007. Tumor Ablation with Irreversible Electroporation. PLoS ONE 2.

Andre, F., Gehl, J., Serša, G., Preat, V., Hojman, P., Eriksen, J., Golzio, M., Čemažar, M., Pavšelj, N., Rols, M., Miklavčič, D., Neumann, E., Teissie, J., Mir, L., 2008. Efficiency of High- and Low-Voltage Pulse Combinations for Gene Electrotransfer in Muscle, Liver, Tumor, and Skin. Human Gene Therapy 19, 1261–1271.

Beravs, K., Frangež, R., Demšar, F., 2000. Specific absorption rate study for radiofrequency current density imaging using a two-dimensional finite element model. Magn Reson Med 44, 610–615.

Birgül, O., Eyüboğlu, B.M., Ider, Y.Z., 2003. Experimental results for 2D magnetic resonance electrical impedance tomography (MR-EIT) using magnetic flux density in one direction. Phys Med Biol 48, 3485–3504.

Buhai, B., Binser, T., Kimmich, R., 2007. Electroosmotic flow, ionic currents, and pressure-induced flow in microsystem channel networks: NMR mapping and computational fluid dynamics simulations. Appl. Magn. Reson. 32, 25–49.

Canatella, P.J., Karr, J.F., Petros, J.A., Prausnitz, M.R., 2001. Quantitative study of electroporation-mediated molecular uptake and cell viability. Biophys J 80, 755–764.

Cukjati, D., Batiuskaite, D., André, F., Miklavčič, D., Mir, L.M., 2007. Real time electroporation control for accurate and safe in vivo non-viral gene therapy. Bioelectrochemistry 70, 501–507.

Čemažar, M., Jarm, T., Miklavčič, D., Lebar, A., Ihan, A., Kopitar, N., Serša, G., 1998. Effect of electric-field intensity on electropermeabilization and electrosensitivity of various tumor-cell lines in vitro. Electro- and Magnetobiology 17, 263–272.

Čorović, S., Mir, L.M., Miklavčič, D., 2012. In Vivo Muscle Electroporation Threshold Determination: Realistic Numerical Models and In Vivo Experiments. J Membrane Biol.

Čorović, S., Županic, A., Miklavčič, D., 2008. Numerical Modeling and Optimization of Electric Field Distribution in Subcutaneous Tumor Treated With Electrochemotherapy Using Needle Electrodes. IEEE Trans Plasma Sci IEEE Nucl Plasma Sci Soc 36, 1665–1672.

Čorović, S., Županič, A., Kranjc, S., Al Sakere, B., Leroy-Willig, A., Mir, L.M., Miklavčič, D., 2010. The influence of skeletal muscle anisotropy on electroporation: in vivo study and numerical modeling. Med Biol Eng Comput 48, 637–648.

Daud, A.I., DeConti, R.C., Andrews, S., Urbas, P., Riker, A.I., Sondak, V.K., Munster, P.N., Sullivan, D.M., Ugen, K.E., Messina, J.L., Heller, R., 2008. Phase I Trial of Interleukin-12 Plasmid Electroporation in Patients With Metastatic Melanoma. Journal of Clinical Oncology.

Davalos, R., Huang, Y., Rubinsky, B., 2000. Electroporation: Bio-electrochemical mass transfer at the nano scale. Microscale Thermophys. Eng. 4, 147–159.

Davalos, R.V., Mir, I.L.M., Rubinsky, B., 2005. Tissue ablation with irreversible electroporation. Ann Biomed Eng 33, 223–231.

Davalos, R.V., Otten, D.M., Mir, L.M., Rubinsky, B., 2004. Electrical impedance tomography for imaging tissue electroporation. Biomedical Engineering, IEEE Transactions on 51, 761–767.

Davalos, R.V., Rubinsky, B., Otten, D.M., 2002. A feasibility study for electrical impedance tomography as a means to monitor tissue electroporation for molecular medicine. IEEE Trans Biomed Eng 49, 400–403.

Değirmenci, E., Eyüboğlu, B.M., 2007. Anisotropic conductivity imaging with MREIT using equipotential projection algorithm. Phys Med Biol 52, 7229–7242.

Değirmenci, E., Eyüboğlu, B.M., 2012. Image Reconstruction in Magnetic Resonance Conductivity Tensor Imaging (MRCTI). IEEE Trans. Med. Imaging 31, 525–532.

Delemotte, L., Tarek, M., 2012. Molecular Dynamics Simulations of Lipid Membrane Electroporation. J Membrane Biol.

Edd, J.F., Horowitz, L., Davalos, R.V., Mir, L.M., Rubinsky, B., 2006. In vivo results of a new focal tissue ablation technique: irreversible electroporation. IEEE Trans Biomed Eng 53, 1409–1415.

Edhemović, I., Gadžijev, E.M., Brecelj, E., Miklavčič, D., Kos, B., Županič, A., Mali, B., Jarm, T., Pavliha, D., Marčan, M., Gašljevič, G., Gorjup, V., Mušič, M., Vavpotič, T.P., Čemažar, M., Snoj, M.,

Serša, G., 2011. Electrochemotherapy: a new technological approach in treatment of metastases in the liver. Technol. Cancer Res. Treat. 10, 475–485.

Essone Mezeme, M., Pucihar, G., Pavlin, M., Brosseau, C., Miklavčič, D., 2012. A numerical analysis of multicellular environment for modeling tissue electroporation. Appl Phys Lett 100, 143701.

Eyüboğlu, B.M., Birgül, O., Ider, Y.Z., 2001. A Dual Modality System for High Resolution - True Conductivity Imaging. Proc. XI Int. Conf. Elec. Bioimpedance (ICEBI) 409 – 13.

Gabriel, B., Teissié, J., 1997. Direct observation in the millisecond time range of fluorescent molecule asymmetrical interaction with the electropermeabilized cell membrane. Biophys. J. 73, 2630–2637.

Gamba, H., Delpy, D., 1998. Measurement of electrical current density distribution within the tissues of the head by magnetic resonance imaging. Medical & Biological Engineering & Computing 36, 165–170.

Garcia, P.A., Pancotto, T., Rossmeisl, J.H., Henao-Guerrero, N., Gustafson, N.R., Daniel, G.B., Robertson, J.L., Ellis, T.L., Davalos, R.V., 2011. Non-Thermal Irreversible Electroporation (N-TIRE) and Adjuvant Fractionated Radiotherapeutic Multimodal Therapy for Intracranial Malignant Glioma in a Canine Patient. Technol. Cancer Res. Treat 10, 73–83.

Garcia, P.A., Rossmeisl, J.H., Jr, Robertson, J., Ellis, T.L., Davalos, R.V., 2009. Pilot study of irreversible electroporation for intracranial surgery. Conf Proc IEEE Eng Med Biol Soc 2009, 6513–6516.

Gehl, J., 2003. Electroporation: theory and methods, perspectives for drug delivery, gene therapy and research. Acta Physiol. Scand. 177, 437–447.

Gehl, J., Mir, L.M., 1999. Determination of Optimal Parameters for in Vivo Gene Transfer by Electroporation, Using a Rapid in Vivo Test for Cell Permeabilization. Biochemical and Biophysical Research Communications 261, 377–380.

Gilboa, E., Rosa, P.S., Nehorai, A., 2012. Estimating Electrical Conductivity Tensors of Biological Tissues Using Microelectrode Arrays. Ann Biomed Eng.

Golberg, A., Rubinsky, B., 2012. Towards electroporation based treatment planning considering electric field induced muscle contractions. Technol. Cancer Res. Treat. 11, 189–201.

Granot, Y., Ivorra, A., Maor, E., Rubinsky, B., 2009. In vivo imaging of irreversible electroporation by means of electrical impedance tomography. Phys Med Biol 54, 4927–4943.

Greenebaum, B., Barnes, F.S. (Eds.), 2006. Bioengineering and Biophysical Aspects of Electromagnetic Fields, 3rd ed. CRC Press.

Hamilton, W.A., Sale, A.J.H., 1967. Effects of high electric fields on microorganisms: II. Mechanism of action of the lethal effect. Biochim. Biophys. Acta 148, 789–800.

Heller, L., Heller, R., 2010. Electroporation Gene Therapy Preclinical and Clinical Trials for Melanoma. Current Gene Therapy 10, 312–317.

Heller, R., Gilbert, R., Jaroszeski, M.J., 1999. Clinical applications of electrochemotherapy. Adv Drug Deliver Rev 35, 119–129.

Heller, R., Jaroszeski, M.J., Reintgen, D.S., Puleo, C.A., DeConti, R.C., Gilbert, R.A., Glass, L.F., 1998. Treatment of cutaneous and subcutaneous tumors with electrochemotherapy using intralesional bleomycin. Cancer 83, 148–157.

Hennig, J., Nauerth, A., Friedburg, H., 1986. RARE imaging: a fast imaging method for clinical MR. Magn Reson Med 3, 823–833.

Hjouj, M., Rubinsky, B., 2010. Magnetic Resonance Imaging Characteristics of Nonthermal Irreversible Electroporation in Vegetable Tissue. J Membrane Biol 236, 137–146.

Holder, D.S. (Ed.), 2004. Electrical Impedance Tomography: Methods, History and Applications, 1st ed. Taylor & Francis.

Ider, Y.Z., Onart, S., Lionheart, W.R.B., 2003. Uniqueness and reconstruction in magnetic resonance-electrical impedance tomography (MR-EIT). Physiol Meas 24, 591–604.

Imae, T., Shinohara, H., Sekino, M., Ueno, S., Ohsaki, H., Mima, K., Ootomo, K., 2008. Estimation of cell membrane permeability of the rat brain using diffusion magnetic resonance imaging. J. Appl. Phys. 103, 07A311 –07A311–3.

Ivorra, A., Al-Sakere, B., Rubinsky, B., Mir, L.M., 2009. In vivo electrical conductivity measurements during and after tumor electroporation: conductivity changes reflect the treatment outcome. Phys. Med. Biol. 54, 5949–5963.

Ivorra, A., Rubinsky, B., 2007. In vivo electrical impedance measurements during and after electroporation of rat liver. Bioelectrochemistry 70, 287–295.

Jeong, W.C., Kim, Y.T., Minhas, A.S., Kim, H.J., Woo, E.J., Seo, J.K., 2008. Design of carbon-hydrogel electrode for MREIT, in: Proc. 9th Conf. EIT. Presented at the Conf. EIT, Dartmouth, NH, USA.

Joy, M., Scott, G., Henkelman, M., 1989. In vivo Detection of Applied Electric Currents by Magnetic-Resonance Imaging. Magn Reson Imag 7, 89–94.

Joy, M.L., Lebedev, V.P., Gati, J.S., 1999. Imaging of current density and current pathways in rabbit brain during transcranial electrostimulation. IEEE Trans Biomed Eng 46, 1139–1149.

Kanthou, C., Kranjc, S., Serša, G., Tozer, G., Župančič, A., Čemažar, M., 2006. The endothelial cytoskeleton as a target of electroporation-based therapies. Mol. Cancer Ther. 5, 3145–3152.

Khang, H.S., Lee, B.I., Oh, S.H., Woo, E.J., Lee, S.Y., Cho, M.Y., Kwon, O., Yoon, J.R., Seo, J.K., 2002. J-substitution algorithm in Magnetic Resonance Electrical Impedance Tomography (MREIT): Phantom experiments for static resistivity images. IEEE Trans Med Imaging 21, 695–702.

Kim, H.J., Kim, Y.T., Minhas, A.S., Jeong, W.C., Woo, E.J., Seo, J.K., Kwon, O.J., 2009. In vivo high-resolution conductivity imaging of the human leg using MREIT: the first human experiment. IEEE Trans Med Imaging 28, 1681–1687.

Kim, H.J., Oh, T.I., Kim, Y.T., Lee, B.I., Woo, E.J., Seo, J.K., Lee, S.Y., Kwon, O., Park, C., Kang, B.T., Park, H.M., 2008. In vivo electrical conductivity imaging of a canine brain using a 3 T MREIT system. Physiol Meas 29, 1145–1155.

Kim, S., Kwon, O., Seo, J., Yoon, J., 2003. On a nonlinear partial differential equation arising in magnetic resonance electrical impedance tomography. SIAM J Appl Math 34, 511–526.

Kos, B., Župančič, A., Kotnik, T., Snoj, M., Serša, G., Miklavčič, D., 2010. Robustness of Treatment Planning for Electrochemotherapy of Deep-Seated Tumors. J Membrane Biol 236, 147–153.

Kotnik, T., Bobanović, F., Miklavčič, D., 1997. Sensitivity of transmembrane voltage induced by applied electric fields—A theoretical analysis. Bioelectroch Bioener 43, 285–291.

Kotnik, T., Kramar, P., Pucihar, G., Miklavčič, D., Tarek, M., 2012. Cell membrane electroporation-Part 1: The phenomenon. IEEE electrc insul m 28, 14 –23.

Kotnik, T., Miklavčič, D., 2000. Second-order model of membrane electric field induced by alternating external electric fields. IEEE Trans Biomed Eng 47, 1074–1081.

Kotnik, T., Pucihar, G., Miklavčič, D., 2010. Induced Transmembrane Voltage and Its Correlation with Electroporation-Mediated Molecular Transport. J Membrane Biol 236, 3–13.

Krassowska, W., Filev, P.D., 2007. Modeling electroporation in a single cell. Biophys. J. 92, 404–417.

Kwon, O., Lee, J., Yoon, J., 2002. Equipotential line method for magnetic resonance electrical impedance tomography. Inverse Problems 18, 1089–1100.

Kwon, O., Park, C., Park, E.-J., Seo, J.K., Woo, E.J., 2005. Electrical conductivity imaging using a variational method in Bz-based MREIT. Inverse Probl 21, 969–980.

Kwon, O., Woo, E., Yoon, J., Seo, J., 2002. Magnetic resonance electrical impedance tomography (MREIT): Simulation study of J-substitution algorithm. IEEE Trans Biomed Eng 49, 160–167.

Lavee, J., Onik, G., Mikus, P., Rubinsky, B., 2007. A novel nonthermal energy source for surgical epicardial atrial ablation: irreversible electroporation. Heart Surg Forum 10, E162–167.

Lee, B.I., Park, C., Pyo, H.C., Kwon, O., Woo, E.J., 2006. Phase artefact reduction in magnetic resonance electrical impedance tomography (MREIT). Phys. Med. Biol. 51, 5277–5288.

Lee, E.W., Chen, C., Prieto, V.E., Dry, S.M., Loh, C.T., Kee, S.T., 2010. Advanced Hepatic Ablation Technique for Creating Complete Cell Death: Irreversible Electroporation. Radiology 255, 426–433.

Lee, E.W., Loh, C.T., Kee, S.T., 2007. Imaging guided percutaneous irreversible electroporation: ultrasound and immunohistological correlation. Technol. Cancer Res. Treat. 6, 287–294.

Leveillee, R., Salas, N., Moore, C., Jorda, M., Shields, J., 2009. Preliminary investigations with irreversible electroporation in in-vivo porcine kidneys. J Endourology.

Luxembourg, A., Evans, C.F., Hannaman, D., 2007. Electroporation-based DNA immunisation: translation to the clinic. Expert Opin. Biol. Ther. 7, 1647–1664.

Maček-Lebar, A., Miklavčič, D., 2001. Cell electropermeabilization to small molecules in vitro: control by pulse parameters. Radiology and Oncology 35, 193–202.

Maček-Lebar, A., Troiano, G.C., Tung, L., Miklavčič, D., 2002. Inter-pulse interval between rectangular voltage pulses affects electroporation threshold of artificial lipid bilayers. IEEE Transactions on nanobioscience 1, 116–120.

Mahmood, F., Hansen, R.H., Agerholm-Larsen, B., Jensen, K.S., Iversen, H.K., Gehl, J., 2011. Diffusion-weighted MRI for verification of electroporation-based treatments. J. Membr. Biol 240, 131–138.

Manassen, Y., Shalev, E., Navon, G., 1988. Mapping of electrical circuits using chemical-shift imaging. J. Magn. Reson. 76, 371–374.

Maor, E., Ivorra, A., Leor, J., Rubinsky, B., 2008. Irreversible electroporation attenuates neointimal formation after angioplasty. IEEE Trans Biomed Eng 55, 2268–2274.

Marty, M., Serša, G., Garbay, J.R., Gehl, J., Collins, C.G., Snoj, M., Billard, V., Geertsen, P.F., Larkin, J.O., Miklavčič, D., Pavlović, I., Paulin-Kosir, S.M., Čemažar, M., Morsli, N., Soden, D.M., Rudolf, Z., Robert, C., O'Sullivan, G.C., Mir, L.M., 2006. Electrochemotherapy - An easy, highly effective and safe treatment of cutaneous and subcutaneous metastases: Results of ESOPE (European Standard Operating Procedures of Electrochemotherapy) study. EJC Suppl 4, 3–13.

Maxwell, J.C., 1865. A Dynamical Theory of the Electromagnetic Field. Phil. Trans. R. Soc. Lond. 155, 459–512.

Mikac, U., Demšar, A., Demšar, F., Serša, I., 2007. A study of tablet dissolution by magnetic resonance electric current density imaging. J. Magn. Reson. 185, 103–109.

Mikac, U., Demšar, F., Beravs, K., Serša, I., 2001. Magnetic resonance imaging of alternating electric currents. Magn Reson Imaging 19, 845–856.

Miklavčič, D., Beravs, K., Semrov, D., Čemažar, M., Demšar, F., Serša, G., 1998. The Importance of Electric Field Distribution for Effective in Vivo Electroporation of Tissues. Biophys J 74, 2152–2158.

Miklavčič, D., Čorović, S., Pucihar, G., Pavšelj, N., 2006. Importance of tumour coverage by sufficiently high local electric field for effective electrochemotherapy. European Journal of Cancer Supplements 4, 45–51.

Miklavčič, D., Pavšelj, N., Hart, F.X., 2006. Electric Properties of Tissues, in: Wiley Encyclopedia of Biomedical Engineering. John Wiley & Sons, New York, pp. 3578–3589.

Miklavčič, D., Pucihar, G., Pavlovec, M., Ribarič, S., Mali, M., Maček-Lebar, A., Petkovšek, M., Nastran, J., Kranjc, S., Čemažar, M., Serša, G., 2005. The effect of high frequency electric pulses on muscle contractions and antitumor efficiency in vivo for a potential use in clinical electrochemotherapy. Bioelectrochemistry 65, 121–128.

Miklavčič, D., Snoj, M., Županič, A., Kos, B., Čemažar, M., Kropivnik, M., Bračko, M., Pečnik, T., Gadžijev, E., Serša, G., 2010. Towards treatment planning and treatment of deep-seated solid tumors by electrochemotherapy. Biomed Eng Online 9, 10.

Miklavčič, D., Šemrov, D., Mekid, H., Mir, L.M., 2000. A validated model of in vivo electric field distribution in tissues for electrochemotherapy and for DNA electrotransfer for gene therapy. Biochim. Biophys. Acta 1523, 73–83.

| REFERENCES

Miklavčič, D., Towhidi, L., 2010. Numerical study of the electroporation pulse shape effect on molecular uptake of biological cells. Radiology and Oncology 44, 34–41.

Miller, L., Leor, J., Rubinsky, B., 2005. Cancer cells ablation with irreversible electroporation. Technol. Cancer Res. Treat. 4, 699–705.

Mir, L.M., Banoun, H., Paoletti, C., 1988. Introduction of definite amounts of nonpermeant molecules into living cells after electropermeabilization: direct access to the cytosol. Exp. Cell Res. 175, 15–25.

Mir, L.M., Orlowski, S., 1999. Mechanisms of electrochemotherapy. Adv. Drug Deliv. Rev 35, 107–118.

Muftuler, L., Hamamura, M., Birgul, O., Nalcioglu, O., 2006. In vivo MRI electrical impedance tomography (MREIT) of tumors. Technology in Cancer Research & Treatment 5, 381–387.

Nam, H.S., Kwon, O.I., 2010. Axial Anisotropic Conductivity Imaging Based on Projected Current Density in MREIT. IEEE Trans. Med. Imaging 29, 781–789.

Nam, H.S., Lee, B.I., Choi, J., Park, C., Kwon, O.I., 2007. Conductivity imaging with low level current injection using transversal J-substitution algorithm in MREIT. Phys. Med. Biol. 52, 6717–6730.

Neal, R.E., 2nd, Garcia, P.A., Robertson, J.L., Davalos, R.V., 2012. Experimental characterization and numerical modeling of tissue electrical conductivity during pulsed electric fields for irreversible electroporation treatment planning. IEEE Trans Biomed Eng 59, 1076–1085.

Neal, R.E., 2nd, Rossmeisl, J.H., Jr, Garcia, P.A., Lanz, O.I., Henao-Guerrero, N., Davalos, R.V., 2011. Successful treatment of a large soft tissue sarcoma with irreversible electroporation. J. Clin. Oncol. 29, e372–377.

Nemkov, V., Goldstein, R., 2003. Computer simulation for fundamental study and practical solutions to induction heating problems. Compel-the International Journal for Computation and Mathematics in Electrical and Electronic Engineering 22, 181–191.

Neu, J.C., Krassowska, W., 1999. Asymptotic model of electroporation. Phys. Rev. E 59, 3471.

Neumann, E., Rosenheck, K., 1972. Permeability changes induced by electric impulses in vesicular membranes. J. Membr. Biol. 10, 279–290.

Neumann, E., Schaeferridder, M., Wang, Y., Hofschneider, P., 1982. Gene-Transfer into Mouse Lyoma Cells by Electroporation in High Electric-Fields. EMBO J 1, 841–845.

Neumann, E., Sowers, E.A., Jordan, C.A., 1989. Electroporation and Electrofusion in Cell Biology. Plenum Press, New York.

Oh, S.H., Lee, B.I., Woo, E.J., Lee, S.Y., Cho, M.H., Kwon, O., Seo, J.K., 2003. Conductivity and current density image reconstruction using harmonic Bz algorithm in magnetic resonance electrical impedance tomography. Phys Med Biol 48, 3101–3116.

Oh, S.H., Lee, B.I., Woo, E.J., Lee, S.Y., Kim, T.-S., Kwon, O., Seo, J.K., 2005. Electrical conductivity images of biological tissue phantoms in MREIT. Physiol Meas 26, S279–288.

Okino, M., Mohri, H., 1987. Effects of a high-voltage electrical impulse and an anticancer drug on in vivo growing tumors. Jpn. J. Cancer Res. 78, 1319–1321.

Onik, G., Mikus, P., Rubinsky, B., 2007. Irreversible electroporation: implications for prostate ablation. Technol. Cancer Res. Treat. 6, 295–300.

Orlowski, S., Belehradek, J., Paoletti, C., Mir, L.M., 1988. Transient electropermeabilization of cells in culture. Increase of the cytotoxicity of anticancer drugs. Biochem. Pharmacol 37, 4727–4733.

Park, C., Kwon, O., Woo, E.J., Seo, J.K., 2004. Electrical conductivity imaging using gradient B, decomposition algorithm in magnetic resonance electrical impedance tomography (MREIT). IEEE Trans Med Imaging 23, 388–394.

Park, C., Lee, B.I., Kwon, O.I., 2007. Analysis of recoverable current from one component of magnetic flux density in MREIT and MRCDI. Phys. Med. Biol. 52, 3001–3013.

Park, C., Park, E.-J., Woo, E.J., Kwon, O., Seo, J.K., 2004. Static conductivity imaging using variational gradient Bz algorithm in magnetic resonance electrical impedance tomography. Physiol Meas 25, 257–269.

Patriciu, A., Yoshida, K., Struijk, J.J., DeMonte, T.P., Joy, M.L.G., Stødkilde-Jørgensen, H., 2005. Current density imaging and electrically induced skin burns under surface electrodes. IEEE Trans Biomed Eng 52, 2024–2031.

Pavliha, D., Kos, B., Županič, A., Marčan, M., Serša, G., Miklavčič, D., 2012. Patient-specific treatment planning of electrochemotherapy: Procedure design and possible pitfalls. Bioelectrochemistry 265–273.

Pavlin, M., Pavšelj, N., Miklavčič, D., 2002. Dependence of induced transmembrane potential on cell density, arrangement, and cell position inside a cell system. IEEE Trans. Biomed. Eng. 49, 605–612.

Pavšelj, N., Bregar, Z., Cukjati, D., Batiuskaite, D., Mir, L.M., Miklavčič, D., 2005. The Course of Tissue Permeabilization Studied on a Mathematical Model of a Subcutaneous Tumor in Small Animals. IEEE Trans. Biomed. Eng. 52, 1373–1381.

Pavšelj, N., Miklavčič, D., 2008. Numerical modeling in electroporation-based biomedical applications. Radiology and Oncology 42, 159–168.

Pucihar, G., Kotnik, T., Teissié, J., Miklavčič, D., 2007. Electropermeabilization of dense cell suspensions. Eur. Biophys. J. 36, 173–185.

Pucihar, G., Kotnik, T., Valič, B., Miklavčič, D., 2006. Numerical Determination of Transmembrane Voltage Induced on Irregularly Shaped Cells. Ann Biomed Eng 34, 642–652.

Pucihar, G., Krmelj, J., Reberšek, M., Napotnik, T.B., Miklavčič, D., 2011. Equivalent pulse parameters for electroporation. IEEE Trans Biomed Eng 58, 3279–3288.

Pucihar, G., Mir, L.M., Miklavčič, D., 2002. The effect of pulse repetition frequency on the uptake into electropermeabilization cells in vitro with possible applications in electrochemotherapy. Bioelectrochemistry 57, 167–172.

Rols, M.P., Teissié, J., 1989. Ionic-strength modulation of electrically induced permeabilization and associated fusion of mammalian cells. Eur. J. Biochem. 179, 109–115.

Rols, M.P., Teissié, J., 1990. Electropermeabilization of mammalian cells. Quantitative analysis of the phenomenon. Biophys. J. 58, 1089–1098.

Rols, M.P., Teissié, J., 1992. Experimental evidence for involvment of the cytoskeleton in mammalian cell electropermeabilization. Biochimica et Biophysica Acta 1111, 45–50.

Rubinsky, B., Onik, G., Mikus, P., 2007. Irreversible electroporation: a new ablation modality--clinical implications. Technol. Cancer Res. Treat. 6, 37–48.

Rubinsky, J., Onik, G., Mikus, P., Rubinsky, B., 2008. Optimal parameters for the destruction of prostate cancer using irreversible electroporation. J. Urol 180, 2668–2674.

Sale, A.J.H., Hamilton, W.A., 1967. Effects of high electric fields on microorganisms: I. Killing of bacteria and yeasts. Biochim. Biophys. Acta 148, 781–788.

Sale, A.J.H., Hamilton, W.A., 1968. Effects of high electric fields on micro-organisms: III. Lysis of erythrocytes and protoplasts. Biochim. Biophys. Acta 163, 37–43.

Schwan, H.P., Kay, C.F., 1957. The conductivity of living tissues. Ann. N. Y. Acad. Sci. 65, 1007–1013.

Scott, G., Joy, M., Armstrong, R., Henkelman, R., 1991. Measurement of Nonuniform Current-Density by Magnetic-Resonance. IEEE Transactions on Medical Imaging 10, 362–374.

Scott, G.C., Joy, M.L., Armstrong, R.L., Henkelman, R.M., 1992. RF current density imaging in homogeneous media. Magn Reson Med 28, 186–201.

Seo, J., Kwon, O., Lee, B., Woo, E., 2003. Reconstruction of current density distributions in axially symmetric cylindrical sections using one component of magnetic flux density: computer simulation study. Physiological Measurement 24, 565–577.

Seo, J.K., Pyo, H.C., Park, C., Kwon, O., Woo, E.J., 2004. Image reconstruction of anisotropic conductivity tensor distribution in MREIT: computer simulation study. Phys Med Biol 49, 4371–4382.

Seo, J.K., Woo, E.J., 2011. Magnetic Resonance Electrical Impedance Tomography (MREIT). SIAM Rev 53, 40.

Seo, J.K., Yoon, J.-R., Woo, E.J., Kwon, O., 2003. Reconstruction of conductivity and current density images using only one component of magnetic field measurements. IEEE Trans. Biomed. Eng. 50, 1121–1124.

Serša, G., Čemažar, M., Miklavčič, D., 1995. Antitumor Effectiveness of Electrochemotherapy with cis-Diamminedichloroplatinum(II) in Mice. Cancer Res 55, 3450 –3455.

Serša, G., Čemažar, M., Rudolf, Z., 2003. Electrochemotherapy: advantages and drawbacks in treatment of cancer patients. Cancer Therapy 1, 133–142.

Serša, G., Čufer, T., Paulin, S.M., Čemažar, M., Snoj, M., 2012. Electrochemotherapy of chest wall breast cancer recurrence. Cancer Treat Rev 5, 379–86.

Serša, G., Miklavčič, D., 2008. Electrochemotherapy of Tumours. JoVE.

Serša, I., 2008. Auxiliary phase encoding in multi spin-echo sequences: application to rapid current density imaging. J. Magn. Reson 190, 86–94.

Serša, I., Beravs, K., Dodd, N.J., Zhao, S., Miklavčič, D., Demšar, F., 1997. Electric current density imaging of mice tumors. Magn Reson Med 37, 404–409.

Serša, I., Jarh, O., Demšar, F., 1994. Magnetic Resonance Microscopy of Electric Currents. J Magn Reson 111, 93–99.

Sixou, S., Teissié, J., 1993. Exogenous uptake and release of molecules by electroloaded cells: A digitized videomicroscopy study. Bioelectrochem Bioenerg 31, 237–257.

Stämpfli, E., 1958. Reversible electrical breakdown of the excitable membrane of a Ranvier node. AN ACAD BRAS CIENC 57–63.

Sukhorukov, V.L., Reuss, R., Zimmermann, D., Held, C., Müller, K.J., Kiesel, M., Gessner, P., Steinbach, A., Schenk, W.A., Bamberg, E., Zimmermann, U., 2005. Surviving high-intensity field pulses: strategies for improving robustness and performance of electrotransfection and electrofusion. J. Membr. Biol. 206, 187–201.

Susil, R., Šemrov, D., Miklavčič, D., 1998. Electric field induced transmembrane potential depends on cell density and organization. Electro-and Magnetobiology 17, 391–399.

Šel, D., Cukjati, D., Batiuskaite, D., Slivnik, T., Mir, L.M., Miklavčič, D., 2005. Sequential finite element model of tissue electropermeabilization. IEEE Trans Biomed Eng 52, 816–827.

Šemrov, D., Miklavčič, D., 1998. Calculation of the electrical parameters in electrochemotherapy of solid tumors in mice. Computers in Biology and Medicine 28, 439–448.

Tarek, M., 2005. Membrane electroporation: a molecular dynamics simulation. Biophys. J. 88, 4045–4053.

Thomson, K.R., Cheung, W., Ellis, S.J., Federman, D., Kavnoudias, H., Loader-Oliver, D., Roberts, S., Evans, P., Ball, C., Haydon, A., 2011. Investigation of the safety of irreversible electroporation in humans. J Vasc Interv Radiol 22, 611–621.

Tieleman, D.P., 2004. The molecular basis of electroporation. BMC Biochem 5, 10.

Tieleman, D.P., Leontiadou, H., Mark, A.E., Marrink, S.-J., 2003. Simulation of pore formation in lipid bilayers by mechanical stress and electric fields. J. Am. Chem. Soc. 125, 6382–6383.

Tsong, T., 1991. Electroporation of Cell-Membranes. Biophys J 60, 297–306.

Valič, B., Golzio, M., Pavlin, M., Schatz, A., Faurie, C., Gabriel, B., Teissié, J., Rols, M.-P., Miklavčič, D., 2003. Effect of electric field induced transmembrane potential on spheroidal cells: theory and experiment. Eur. Biophys. J. 32, 519–528.

Wang, H., Wang, Y., Yang, W., Wang, Z., Hu, L., 2010. Conductivity Image Reconstruction of Oblique Slice With C-Shaped Open Permanent Magnet MRI Systems. IEEE Trans. Appl. Supercond. 20, 814–817.

Weaver, J.C., Chizmadzhev, Y.A., 1996. Theory of electroporation: A review. Bioelectrochemistry and Bioenergetics 41, 135–160.

Weber, M., Kimmich, R., 2002. Maps of electric current density and hydrodynamic flow in porous media: NMR experiments and numerical simulations. Phys Rev E Stat Nonlin Soft Matter Phys 66, 026306.

Webster, J.G. (Ed.), 1990. Electrical Impedance Tomography,, 1st ed. Taylor & Francis.

Woo, E., Seo, J., 2008. Magnetic resonance electrical impedance tomography (MREIT) for high-resolution conductivity imaging. Physiological Measurement 29, R1–R26.

Woo, E.J., Lee, S.Y., Mun, C.W., 1994. Impedance tomography using internal current density distribution measured by nuclear magnetic resonance. SPIE, 2299 377 – 385.

Zhang, L., Widera, G., Rabussay, D., 2004. Enhancement of the effectiveness of electroporation-augmented cutaneous DNA vaccination by a particulate adjuvant. Bioelectrochemistry 63, 369–373.

Zhang, Y., Guo, Y., Ragin, A.B., Lewandowski, R.J., Yang, G.-Y., Nijm, G.M., Sahakian, A.V., Omary, R.A., Larson, A.C., 2010. MR Imaging to Assess Immediate Response to Irreversible Electroporation for Targeted Ablation of Liver Tissues: Preclinical Feasibility Studies in a Rodent Model1. Radiology 256, 424 –432.

Zimmermann, U., 1982. Electric field-mediated fusion and related electrical phenomena. Biochim. Biophys. Acta 694, 227–277.

Zimmermann, U., Pilwat, G., Riemann, F., 1974. Dielectric Breakdown of Cell Membranes. Biophys J 14, 881–899.

Županic, A., Čorovic, S., Miklavčič, D., Pavlin, M., 2010. Numerical optimization of gene electrotransfer into muscle tissue. Biomed Eng Online 9, 66.

Župančič, A., 2010. Treatment planning in biomedical applications of electroporation (PhD Thesis).

DECLARATION

The author hereby declares that the content of the thesis is a result of his own research work supervised by prof. Damijan Miklavčič. The results, which were collected in collaboration with other colleagues, are published in the presented papers. The assistance from other colleagues is stated in the Acknowledgements. The published results of other authors are presented in the literature.

Matej Kranjc

IZJAVA

Izjavljam, da sem doktorsko disertacijo izdelal sam, pod mentorstvom prof. dr. Damijana Miklavčiča. Rezultati, ki so nastali v sodelovanju z drugimi sodelavci, so bili objavljeni v predstavljenih člankih. Izkazano pomoč ostalih sodelavcev sem v celoti navedel v zahvali. Že objavljeni dosežki drugih avtorjev so navedeni v spisku literature.

Matej Kranjc